PULL-THROUGH FAILURE OF BOLTED COMPOSITE JOINTS

Zao Chen

Department of Mechanical Engineering

McGill University

Montreal, Canada

March 2013

A thesis submitted to McGill University
in partial fulfillment of the requirements for the degree of
Master of Engineering

© Zao Chen 2013

Abstract

The design and certification of composite aircraft structures requires extensive and costly testing of bolted joints since no robust predictive tools are available. The majority of investigations in this field focus on the shear loading of bolted carbon fibre-reinforced polymer matrix composites while studies on the behaviour of pull-through are limited. Thus, this work presents an extensive investigation of the factors affecting bolted composite panels subjected to out-of-plane loading with the objective to develop a semi-empirical predictive model.

First, an experimental investigation is presented where the influence of fastener size and laminate thickness was systematically studied. The effect of the laminate layup and fastener clamping torque was also examined. Specimens manufactured from out-of-autoclave carbon-epoxy prepregs were transversely loaded in an electromechanical testing machine. The load-displacement response was measured and the failure mechanisms were examined by optical microscopy. Relatively thick specimens were used to ensure that the head depth of the countersink fasteners did not exceed seventy percent of the laminate thickness. Second, numerical analysis was conducted to predict joint failure by using a simplified axisymmetric 3-D finite element approach. Contact elements were used under the region of the fastener head and the failure was predicted using the maximum principal strain criterion.

The experimental results showed that failures were dominated by inter-ply delamination and through-thickness shear failure of the laminate. A conical damage zone was found under the fastener head with damage radially dispersed from the fastener hole. The opening angles of the cones varied with the fastener head geometry. The load-displacement behaviour was affected by the fastener type. The finite element analysis showed that a concentrated shear stress area under the fastener head caused the cone damage initiation. Maximum fibre direction stresses and out-of-plane shear were both found near the fastener hole on the opposite side of the loading face. Transverse deformation and inter-laminar shear caused the final failure in the form of inter-ply delamination. The numerical analysis also indicated that the pull-through load resistance was more sensitive to the contact area under the fastener head and the head geometry than to the fastener shank size. Finally, a semi-empirical equation for the prediction of the pull-through resistance that includes the joint characteristic factors was developed.

Résumé

La conception et la certification des structures aéronautiques en matériaux composites avec assemblages boulonnés nécessitent un important programme de tests très coûteuxcar il n’existe pas d’outils de prédiction robuste de la rupture des joints boulonnés. La majorité des études dans ce domaine portent sur la résistance en cisaillement des boulons alors que les études sur le comportement hors plan des assemblages boulonnés sont très limitées. Ainsi, cette thèse présente une étude approfondie des facteurs affectant les assemblages boulonnés en matériau composite soumis à des charges hors plan avec l’objectif de développer un modèle semi-empirique de la charge de rupture du joint.

Premièrement, une étude expérimentale est présentée où l’influence du diamètre du boulon et de l’épaisseur du laminé est menée de façon systématique. L’effet de la configuration du laminé et du couple de serrage a aussi été étudié. Des échantillons fabriqués hors-autoclave composés de fibres de carbone pré-imprégnées d’une matrice époxy ont été chargés transversalement dans la machine d’essai électromécanique. La courbe force–déplacement a été mesurée et les mécanismes de rupture ont été examinés par microscope optique. Des échantillons relativement épais ont été utilisés pour s’assurer que l’épaisseur de la tête du boulon n’excède pas soixante-dix pourcent de l’épaisseur du laminé. Deuxièmement, des simulations numériques par la méthode des éléments finis ont été effectuées afin de prédire la rupture de l’assemblage en utilisant un modèle 3-D axisymétrique simplifié. Des éléments de contact ont été utilisés sous la région de la tête de vis et la rupture a été prédite en utilisant le critère de déformation principale maximale.

Les résultats expérimentaux ont montré que les mécanismes de rupture comportent un délaminage inter-pli et un cisaillement à travers l'épaisseur du laminé. Une zone d'endommagement conique a été observée sous la tête du boulon avec des fissures réparties radialement autour du trou. Les angles d'ouverture des cônes varient selon la géométrie de la tête de vis. Le comportement charge-déplacement variait en fonction du type de boulon. L'analyse par éléments finis a démontré qu'une concentration de contraintes de cisaillement située sous la tête du boulon causait l'initiation des dommages conique. Les contraintes de tension maximale et de cisaillement hors- plan ont été observées près du trou, du côté opposé de la charge. La déformation transversale et le cisaillement inter-laminaire causent la rupture finale sous forme de délaminage inter-pli. Le modèle numérique indique également que la résistance au chargement hors plan est plus sensible à la région de contact sous la tête du boulon et sa géométrie. Finalement, une équation semi-empirique pour prédire la résistance hors plan des joints boulonnés a été développée.

Acknowledgement

First and foremost, I would like to express my sincere gratitude to my supervisor Prof. Pascal Hubert and Dr. Isabelle Paris from Bombardier Aerospace for their continuous support, patience and dedicated help during the course of this work.

I would like to thank Mr. Khassan Mourtazov from Bombardier Aerospace for providing the testing materials. I would also like to thank Prof. Steve Yue from Department of Material and Mining Engineering, McGill University, for his kindness in providing the access to the testing instrument.

I am grateful to Natural Sciences and Engineering Research Council of Canada (NSERC) and Consortium for Research and Innovation in Aerospace in Quebec (CRIAQ) for their generous financial support.

Last but not least, I am so thankful for working with people from Structures and Composites Laboratory and Micro/Nano Structures Laboratory, McGill University. Their kindness and generousness enriched my life and knowledge.

TABLE OF CONTENT

Chapter1 Introduction 19

1.1. JOINING OF COMPOSITE STRUCTURES 20

1.1.1. Adhesive bonding 20

1.1.2. Welding 22

1.2. MECHANICAL JOINING 24

1.3 OBJECTIVES AND STRUCTURE OF THESIS 28

1.3.1 Objectives 28

1.3.2 Structure of Thesis 28

Chapter 2 Literature Review on Bolted Composite Joint under Pull-Through Loading 29

2.1 EXPERIMENTAL DESIGN AND RESULTS 31

2.1.1 Experimental Design 31

2.1.2. Experimental Results 34

2.1.3 Specimen Inspection 38

2.2 NUMERICAL MODELLING 45

2.3 SUMMARY 50

Chapter 3 Methodology 51

3.1 EXPERIMENTAL DESIGN 53

3.1.1 Sample Preparation 53

3.1.2 Test Matrix 55

3.1.3 Testing instrumentation 57

3.1.4 Testing Procedure 58

3.2 NUMERICAL MODELS 59

Chapter 4 Results and Discussion..65

4.1 EXPERIMENTAL RESULTS 67

4.1.1 Load-Displacement Behaviour of Specimens..69

4.2 FINITE ELEMENT ANALYSIS 74

4.2.1 Fibre direction Stress σ_{11}..77

4.2.2 Transverse Stress σ_{22}..79

4.2.3 Interlaminar Shear Stress 82

4.2.4 Maximum Principal Stress..85

4.3 FAILURE MODE ANALYSIS 88

4.3.1 Specimen Inspection 88

4.3.2 Numerical Analysis..95

4.4 EVALUATION OF THE FACTORS INFLUENCING LAMINATE PULL-THROUGH STRENGTH..99

4.5 SEMI-EMPIRICAL EQUATION OF FASTENER PULL-THROUGH STRENGTH..102

4.5.1 Failure load prediction for t/D > 0.5 102

4.5.2 Failure Load Prediction of Specimens with “t/D” = 0.5 106

4.5.3 Failure Load Prediction of Specimens with t/D < 0.5 107

4.6 SUMMARY 109

Chapter 5 Conclusion and Future Work 111

5.1 CONCLUSIONS..113

5.2 RECOMMANDATIONS FOR FUTURE WORK 114

Reference 117

LIST OF FIGURES

Figure 1.1: Single (a) and double (b) lap joint..21

Figure 1.2: Scarf joint (a) and double sided scarf joint (b)..21

Figure 1.3: Single (a) and double (b) strap joint...22

Figure 1.4: Layup with welding thermoplastic film 23

Figure 1.5: Welded joint..23

Figure 1.6: Bolted composite structure and mechanical fastener 24

Figure 1.7: Failure modes of composite mechanical joints 26

Figure 2.1: Schematic of clamped testing arrangement...33

Figure 2.2: Schematic of simply-supported testing arrangement 33

Figure 2.3: Typical idealized load-displacement behaviour of fastener pull-through 34

Figure 2.4: Load-displacement behaviour of a 16-ply protruding head pull-through specimen 35

Figure 2.5: Load-displacement curves for (a) epoxy quasi-isotropic laminate (Test ID 10); (b) vinylester quasi-isotropic laminate (Test ID 13)..................................40

Figure 2.6: Propagation of failure for both thin and thick specimen (Test ID 10 to 15) 40

Figure 2.7: Micrograph of thin epoxy specimen loaded to 50% of the failure load...40

Figure 2.8: Micrograph of thick specimen (40 mm opening restraining plate) loaded to 50% of the failure load...41

Figure 2.9: Propagation of failure for both thin and thick specimen (Test ID 1 to 9) 42

Figure 2.10: Micrograph of thin specimens unloaded instantaneously after failure load..42

Figure 2.11: Complete through-thickness damage of thick specimen, unloaded instantaneously after failure load...43

Figure 2.12: Baseline finite element model setup...46

Figure 2.13: Contour plot of fibre direction stresses for the baseline specimen configuration 46

Figure 2.14: Contour plot of through thickness stresses for the baseline specimen configuration 47

Figure 2.15: Interlaminar shear stresses distribution for the baseline specimen configuration 48

Figure 2.16: Map of stress distribution 49

Figure 3.1: Bagging arrangement 53

Figure 3.2: Cure cycle for panel manufacturing; in figure: RT (room temperature), FCT (final curing temperature) 54

Figure 3.3: Three-level factorial design matrix containing two factors: specimen thickness and fastener shank diameter 56

Figure 3.4: Fastener pull-through testing fixture for MTS 100kN servo-hydraulic machine 57

Figure 3.5: Numerical model setup including fixture, laminate and fastener 60

Figure 3.6: Schematic of contact pairs (in an X-Z cross section through center of the fastener); master surfaces are in red; slave surfaces are in blue 62

Figure 4.1: Typical idealized load-displacement behaviour of fastener pull-through 66

Figure 4.2: Type I load-displacement behaviour of a thick specimen (P0.19-24LT).. 68

Figure 4.3: Type II load-displacement behaviour of an 8-ply specimen (P0.3-8LT), the pull-through failure characterized by a succession of small load drops 69

Figure 4.4: Type III load-displacement behaviour of a 16-ply specimen (P0.25-16LT), the pull-through failure characterized by a change in the slopes of the load-displacement curve 70

Figure 4.5: Comparison of load-displacement behaviour for specimens with different t/D 72

Figure 4.6: Load-displacement behaviour of three specimens for Test ID 5 (P0.25-16LT) of *t/D = 0.5* 72

Figure 4.7: Typical flexure deformation plot (scaled) of the laminate under fastener pull-through load. Area 1 and 2 show two flexure detected and Point A indicates the location of the global maximum compressive stress 75

Figure 4.8: Important stress components for the pull-through behaviour: the fibre direction (σ_{11}), transverse (σ_{22}) and transverse shear (τ_{13}) stresses, showed in a 3-D stress element diagram..77

Figure 4.9: Contour plot of σ_{11} stress for specimen P0.19-8NT with *t/D = 0.34*. Unites of stress MPa 78

Figure 4.10: Contour plot of σ_{11} stress for specimen P0.25-16NT with *t/D = 0.5*. Unites of stress MPa 78

Figure 4.11: Contour plot of σ_{11} stress for specimen P0.25-24NT with *t/D = 0.76*. Unites of stress MPa 79

Figure 4.12: Contour plot of σ_{22} stress for specimen P0.19-8NT with *t/D = 0.34*. Unites of stress MPa 81

Figure 4.13: Contour plot of σ_{22} stress for specimen P0.25-16NT with *t/D = 0.5*. Unites of stress MPa 81

Figure 4.14: Contour plot of σ_{22} stress for specimen P0.25-24NT with *t/D = 0.76*. Unites of stress MPa 82

Figure 4.15: Contour plot of the interlaminar shear stress for specimen with *t/D = 0.34*. Unites of stress MPa 83

Figure 4.16: Contour plot of the interlaminar shear stress for specimen with *t/D = 0.5*. Unites of stress MPa 83

Figure 4.17: Contour plot of the interlaminar shear stress for specimen with *t/D = 0.76*. Unites of stress MPa 84

Figure 4.18: Contour plot of the maximum principle stress distribution for specimen with *t/D = 0.34*. Unites of stress MPa 85

Figure 4.19: Contour plot of the maximum principle stress distribution for specimen with *t/D = 0.5*. Unites of stress MPa 8

Figure 4.20: Contour plot of the maximum principle stress distribution for specimen with *t/D = 0.76*. Unites of stress MPa 86

Figure 4.21: Points selected along the load-displacement curve (P0.19-24LT) for interrupted pull-through tests and specimen damage inspection 88

Figure 4.22: Photos of surface damage of selected points from specimen series P0.3-24LT, contact area under fastener head (top) and damage near fastener hole on the opposite side of the contact surface (bottom) 89

Figure 4.23: Voids at and near fastener hole boundary, right hand side of the fastener hole 90

Figure 4.24: (Top) Micrograph scratch of specimen (test ID “3”) unloaded prior to the failure force (point A in Figure 4.22). (Bottom) A schematic description of the damage at point A 92

Figure 4.25: (Top) Micrograph of specimens (P0.19-24LT) unloaded right after the initial failure load (point B in Figure 4.22). (Bottom) A schematic description of the damage at point B 92

Figure 4.26: (Top) Micrograph of specimen (P0.3-16LT) unloaded after maximum failure load (point C in Figure 4.23). (Bottom) A schematic description of the damage at point C 93

Figure 4.27: “Staircase” interlaminar shear stress distribution 94

Figure 4.28: (Top) Micrograph of specimen (P0.3-24LT) unloaded from where load dropped 30% after maximum failure load (point D in Figure 22). (Bottom) A schematic description of the damage at point D 94

Figure 4.29: Comparison between the maximum fibre direction stresses from numerical models and the corresponding experimentally determined strength of the specimens 95

Figure 4.30: Comparison between the maximum transverse stresses from numerical models and the corresponding experimentally determined strength of the specimens 95

Figure 4.31: Comparison between the maximum interlaminar shear stresses of numerical models and the corresponding experimentally determined strength of the specimens 96

Figure 4.32: Effect of specimen thickness and fastener shank diameter on pull-through failure load 100

Figure 4.33: Effect of specimen thickness and fastener shank diameter on pull-through maximum load 100

Figure 4.34: Effect of fastener clamping torque on pull-through failure load 101

Figure 4.35: Effect of fastener clamping torque on pull-through maximum load 101

Figure 4.36: Calculation of shear stress distribution in the laminate cross section 102

Figure 4.37: Second order polynomial fit of function “F (t/D)”. F (tD) is the ratio of pull-through strengths from experimental results over numerical models 104

Figure 4.38: Comparison between the pull-through failure load semi-empirical model prediction and the experimental data 106

Figure 4.39: Stresses induced by bulging effect near the fastener hole boundary (CourtesyCourtesy of Federal Aviation Administration) 108

Figure 5.1: Summary of load-displacement behaviours and failure modes depend on *t/D* 113

LIST OF NOMENCLATURE

P_i = Initial sub-critical failure load of the load-displacement behaviour

P_f = Failure load of the load-displacement behaviour

P_m = Maximum load of the load-displacement behaviour

δ_f = Displacement at failure load

δ_m = Displacement at maximum load

t = Specimen laminate thickness

D = Fastener shank diameter

$D_{\text{fastener head}}$ = Fastener head diameter

P = Fastener pull-through failure load

σ_{11} = fibre direction stress

σ_{22} = Transverse stress

τ_{13} = Shear stress

τ_{max} = Shear stress from short beam test

Chapter1

Introduction

In this chapter, a general background of composite structure joining and a brief description of mechanical fastener joint are presented. Then the disadvantages of the fastened joint are discussed and the organization of the thesis is presented.

Because of their excellent mechanical properties, fibre reinforced polymer matrix composites are shaping the world by replacing conventional materials such as metal in many applications. Their light weight, high strength, environment resistance and eco-friendly nature enable the manufacturing of more robust and durable products.

1.1. JOINING OF COMPOSITE STRUCTURES

Fibre reinforced polymer matrix composites are composed of fibre tows embedded in a polymer resin matrix. Composites are non-homogeneous and have orthotropic properties. Composites enable the manufacturing of large complex structures with fewer components. Nevertheless, composites structures still need to be joined and this operation can be critical to the structural integrity of the final assembly. Three joining methods are typically used with composites: adhesive bonding, welding, and mechanical joining. Brief introductions will be given for the first two methods and the mechanical joining will be discussed in more details in Section 1.2.

1.1.1. Adhesive bonding

Adhesive bonding consists of joining two or more composite parts by co-curing, co-bonding or secondary bonding using adhesives. Co-curing is typically used for sandwich structures where the composite parts and adhesives are cured simultaneously during the composite curing process. Co-bonding involves the curing of two or more composite parts where at least one part is cured and at least one part is uncured. This method needs surface treatment on the cured part(s) and possibly involves adding some additional adhesives at the interface. Secondary bonding is consisted of joining two or more cured composite parts with an adhesive that is cured during the bonding process. Careful bonding surfaces treatment and well-designed fixture to align the parts are mandatory for this process. The control of the part temperature is also critical in order to avoid the composite degradation during the bonding process.

There are three types of lay-out patterns for bonded joints:

1. Single and double lap joints are the most common and easy-to-manufacture joints (Figure 1.1).

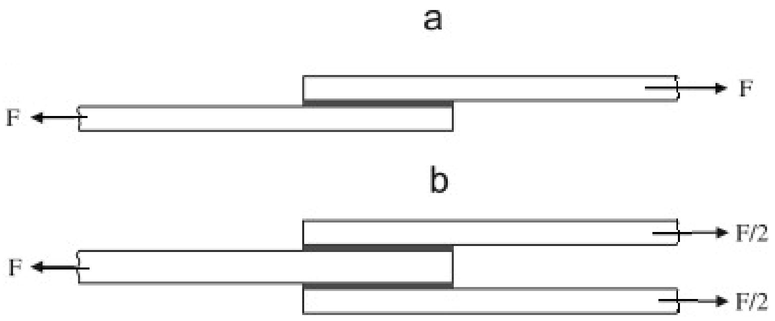

Figure 1.1: Single (a) and double (b) lap joint [20]

2. Scarf joints provide better surface contact but are more labour intensive (Figure 1.2).

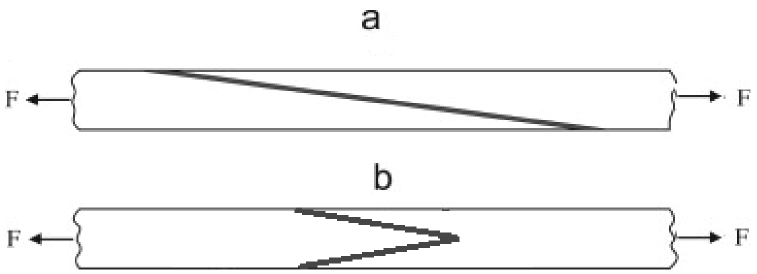

Figure 1.2: Scarf joint (a) and double sided scarf joint (b) [20]

3. Strap joints are relatively easy to apply. The ease of assembly and flush surface make them desirable if the total thickness is allowed (Figure 1.3).

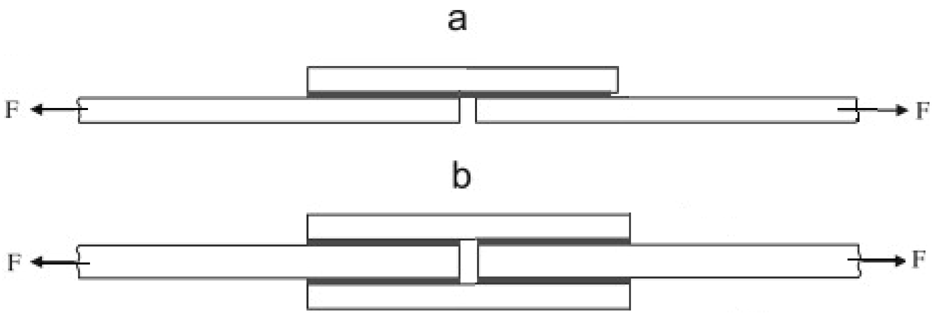

Figure 1.3: Single (a) and double (b) strap joint [20]

Adhesive bonding offers excellent performance but has several drawbacks. First, the autoclave or oven curing requires additional tooling to align and hold the parts during the bonding operation. Second, a careful surface treatment is mandatory as any surface contaminations could cause a drop in mechanical properties.

1.1.2. Welding

Composite welding is a relatively new technology for joining advanced composite components for aerospace application. Thermoplastic composite parts can be welded together by utilizing heat energy to melt the matrix at the bond line. Thermoset composite parts can also be welded together by adding thermoplastic material during layup and can be co-cured with the composite laminates (Figure 1.4). Commonly used welding techniques include resistance welding, ultrasonic welding and induction welding. A welded composite structure is shown in Figure 1.5.

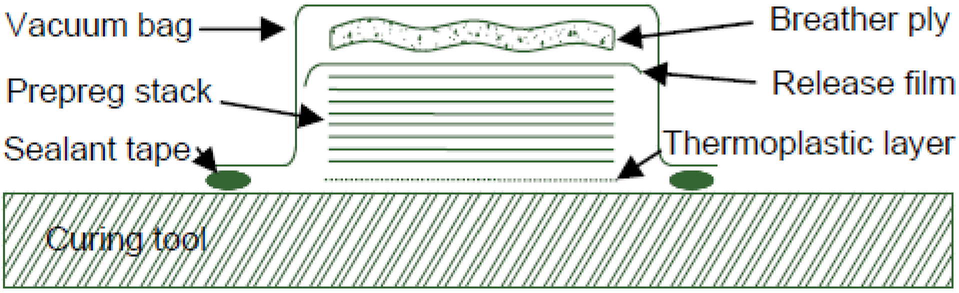
Vacuum bag
Prepreg stack
Sealant tape
Breather ply
Release film
Thermoplastic layer
Curing tool

Figure 1.4: Layup including thermoplastic film for thermoset composite welding [21]

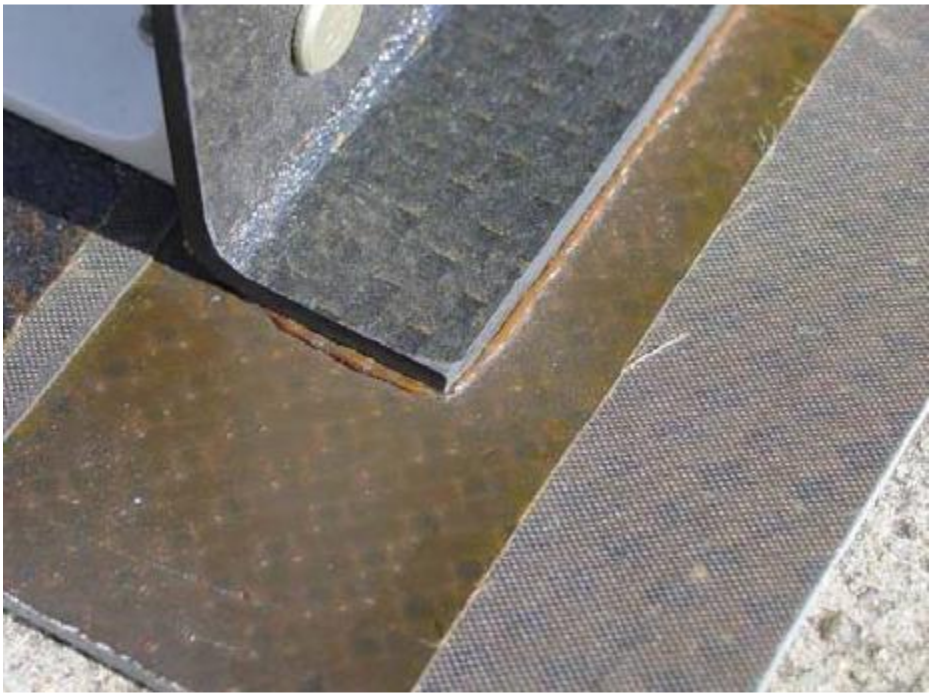

Figure 1.5: Welded joint [21]

1.2. MECHANICAL JOINING

Mechanical joining is the most widely used method for joining composite structures in the aerospace industry. An example of bolted composite laminates and fasteners is shown in Figure 1.6.

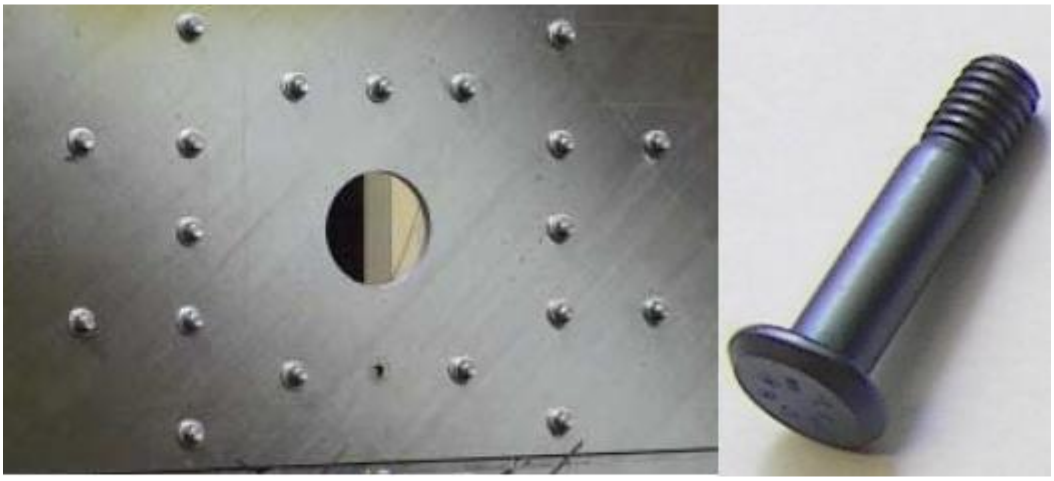

Figure 1.6: Bolted composite structure and mechanical fastener [22]

Metallic mechanical fasteners have to be environmentally compatible with the laminate material to avoid galvanic corrosion [9]. Therefore, they are typically made of titanium alloy and used in heavily loaded structures. Non-metallic fasteners are generally made of composite materials and used in lightly loaded structures to reduce weight, avoid corrosion, reduce radar signature and avoid lightning strikes [9].

The use of mechanical fasteners has several advantages. First, as opposed to adhesive bonding joints, there are no specific tools and techniques required to work with mechanical fasteners. Second, there is little or no need for part surface treatment and cleaning [9]. Third, since using mechanical joints is a mature technique, the structural and fastener reliability are assured. Last but not least, the use of mechanical fasteners allows repeated assembly and disassembly for joint inspection, parts replacement and composite parts reparation [9].

Nevertheless, mechanical joining has several drawbacks. First, the orthotropic composite materials are brittle in nature, lacking the ductility required to relieve local stress concentration. Second, the notch effect created by mechanical fastener holes may reduce the strength of the composite laminate. To compensate it, thicker laminates are required and thus result in an increase in weight. Finally, the increased number of operations and required machining raise the cost of composite structures.

Common types of failure of fastener composite joints are shown in Figure 1.7. Composite parts with mostly on-axis plies (0 degree direction) have the tendency to fail (Figure 1.7 (a)) because the laminate is weakened by the fastener hole regardless of the distance from the edge. Tension failure and bearing failure are related to each other. Cutting holes reduces the cross section area and, therefore, increases the risk of having net tensile failure (Figure 1.7 (b)). Large spacing between fastener holes offsets the stresses but results in bearing strength reduction (Figure 1.7 (c)), where the laminate is compressed by excessive pressure caused by a small bearing area. Cleavage failure is a mixed mode failure involving tension and bearing (Figure 1.7 (d)). Fastener and fastener pull-through failure are shown in Figure 1.7 (e) and (f). Fastener failure results from using fasteners which are too weak to carry the load. Fastener pull-through failure is a through thickness type of failure characterized by fastener head penetrating into the laminate surface.

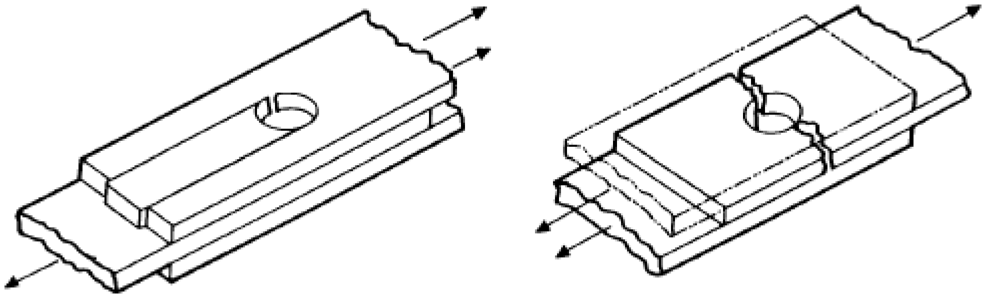

(a) Shearout failure (b) Tension failure

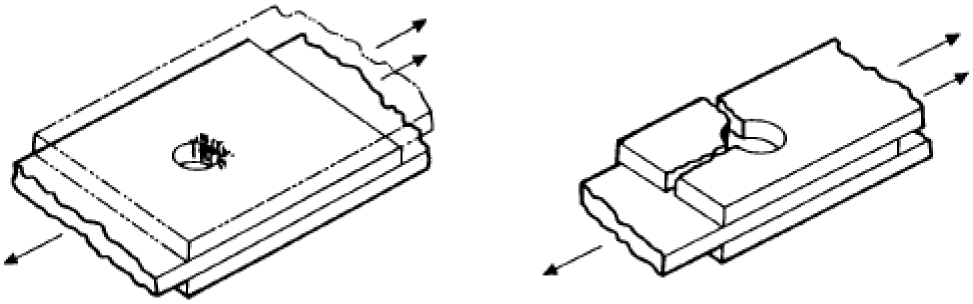

(c) Bearing failure (d) Cleavage - tension failure

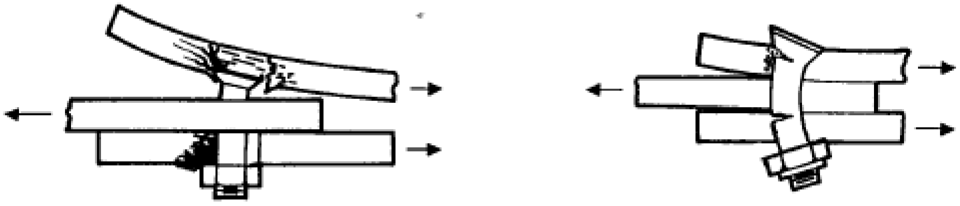

(e) Fastener pull-through failure (f) Bolt failure

Figure 1.7: Failure modes of composite mechanical joints [18].

There is no universal joining technique available. It is essential to choose the joining method based on the on-site scenario. Advantages and limitations of each joining technique are summarized in Table 1.1.

Method		**Advantages**	**Limitations**
Adhesive bonding	**Co-bonding**	• Reduce fastener count • Reduce weight • Complex shape	• Moderate risk • Cure cycle required • Additional tooling
	Secondary bonding		
	Co-curing	• Homogeneous joint • Low risk	• Limited part size • Limited shape complexity
Welding	**Resistance**	• Can use automated process • Continuous welding • Reduce weight	• Moderate risk • Need both side access
	Ultrasonic	• Can use automated process • Possible continuous welding • Reduce weight	• Moderate risk • Need both side access
	Induction	• Can use automated process • One side access only • Continuous welding • Reduce weight	• High risk • Needs magnetic subsector
Mechanical joining		• Reliable • Accessibility • No additional tooling required	• Limited part shape • Corrosion • Weight

Table 1.1: Summary of joining techniques [18, 20, 21, and 22]

1.3 OBJECTIVES AND THESIS ORGANIZATION

1.3.1 Objectives

Mechanical fasteners are designed to carry shear loads while through thickness loads are generally avoided. Thus, a large number of studies were performed on the shear load failure while the through thickness mode of failure has received less attention. This work presents an extensive investigation of the factors affecting bolted composite panels subjected to out-of-plane loading. The completion of this study is accomplished by the following objectives:

i. Examine factors affect pull-through strength
ii. Investigate the failure mechanism of pull-through failure
iii. Develop a predictive semi-empirical model for the pull-through failure load

1.3.2 Thesis organization

This thesis includes five chapters. Chapter 1 provides a general description of mechanical fastener joining techniques and introduces the objectives of the research. Chapter 2 presents a detailed summary of the literature. Chapter 3 describes the methodology used in this research including the description of both experimental design and modelling parameter settings. Chapter 4 presents and discusses the results. Chapter 5 summarizes the outcomes of this study and presents a general guideline for future work.

Chapter 2

Literature Review on Bolted Composite Joint under Pull-Through Loading

This chapter presents and discusses the relevant literature about the pull-through failure of composite bolted joints.

Design guidelines tend to avoid through thickness load in composite structures. However, an increased number of components have to carry such load under certain circumstances. A good example is the joint between the wing spar and the skin. The flexure of the wings induces out-of-plane loads at the joints. Hence, understanding the fastener pull-through failure is essential when designing composite structures.

Few studies were conducted on this subject where a limited number of parameters were investigated. In general, the pull-through strength was found to be influenced by laminate thickness [3, 5], stacking sequence [3, 4], resin system [3], laminate size [3], fastener head diameter [2] environmental condition [12] and friction [4].

2.1 EXPERIMENTAL DESIGN AND RESULTS

2.1.1 Experimental Design

A wide range of experimental designs were used in the past as no standard was introduced for the fastener pull-through test until recent years.

In references 2 and 6, laminates were manufactured from two types of fibre systems and two resin systems. The non-crimp fabric and epoxy matrix (T700/Shell Epicote LV828) composite was manufactured using the resin transfer moulding process. The same fibre system was then embedded with vinylester matrix (T700/Jotun 9100) and manufactured using vacuum infusion. The third and fourth types of laminates were manufactured from plain weave prepregs (T650-35/ W4G282 F584-108) and unidirectional tape prepreg (T650-35/T7G145 F584-9).

The effect of specimen size, titanium fastener head geometry and diameter was taken into consideration. A list of laminate configurations and corresponding fasteners is presented in Table 2.1. Specimens were arranged from 4 plies to 24 plies and mainly quasi-isotropic layup except two cross ply (Test ID 6 and 14) were studied. Specimens from Test ID 10 to 15 were loaded via a protruding fastener with a Ø 12 mm washer inserted at the interface between fastener head and laminate (Figure 2.2).

Various testing fixtures were designed to reproduce the pull-through load scenario. They could be categorized into two types: clamped (Figure 2.1) and simply-supported (Figure 2.2). In both cases, the load was applied through a loading yoke which was attached to the crosshead of the Instron tension/compression machine. The fixture was fixed to the machine, and the specimen was restrained by the edge of the opening hole in the restraining plate. The clamped fixture had a constant opening size of 32 mm in diameter in the restraining plate. All tested specimens were in circular disk shape with a constant diameter of 45.7 mm. It was used to investigate the effect of laminate thickness and fastener head geometry. The simply-supported fixture had interchangeable restraining plates with openings of 40, 80 and 120 mm in diameter with the purpose of investigating the effect of the specimen size. Fastener was finger tightened for all specimens to exclude the effect of clamping torque on pull-through strength.

Test ID	**Fibre type**	**No. of plies**	**Stacking sequence**	**Laminate thickness [mm]**	**Resin type**	**Fastener type**	**Fastener head diameter [mm]**
1	Plain weave	16	$[0,90/\pm45]_{2s}$	3.5	Epoxy	Protruding	3.99
2	Plain weave	16	$[0,90/\pm45]_{2s}$	3.5	Epoxy	Protruding	3.62
3	Plain weave	16	$[0,90/\pm45]_{2s}$	3.5	Epoxy	Protruding	4.94
4	Plain weave	16	$[0,90/\pm45]_{2s}$	3.5	Epoxy	Countersunk	4.17
5	Plain weave	24	$[0,90/\pm45]_{3s}$	5.24	Epoxy	Protruding	3.99
6	Plain weave	16	$[0,90]_{4s}$	3.5	Epoxy	Protruding	3.99
7	Tape	16	$[0,90/\pm45]_{2s}$	2.4	Epoxy	Protruding	3.99
8	Plain weave	4	$[0,90/\pm45]$	0.87	Epoxy	Protruding	3.99
9	Plain weave	8	$[0,90/\pm45]_{s}$	1.75	Epoxy	Protruding	3.99
10	Non-crimp	8	$[0/45/90/-45]_{s}$	1.68	Epoxy	Protruding	12 (w)
11	Non-crimp	16	$[0/45/90/-45]_{s2}$	3.42	Epoxy	Protruding	12 (w)
12	Non-crimp	8	$[0/45/90/-45]_{s}$	1.48	Epoxy	Protruding	12 (w)
13	Non-crimp	8	$[0/45/90/-45]_{s}$	2.42	Vinylester	Protruding	12 (w)
14	Non-crimp	8	$[0/90]_{s2}$	2.42	Vinylester	Protruding	12 (w)
15	Non-crimp	16	$[0/45/90/-45]_{s2}$	4.68	Vinylester	Protruding	12 (w)

Table 2.1: List of specimen configurations [2, 6]

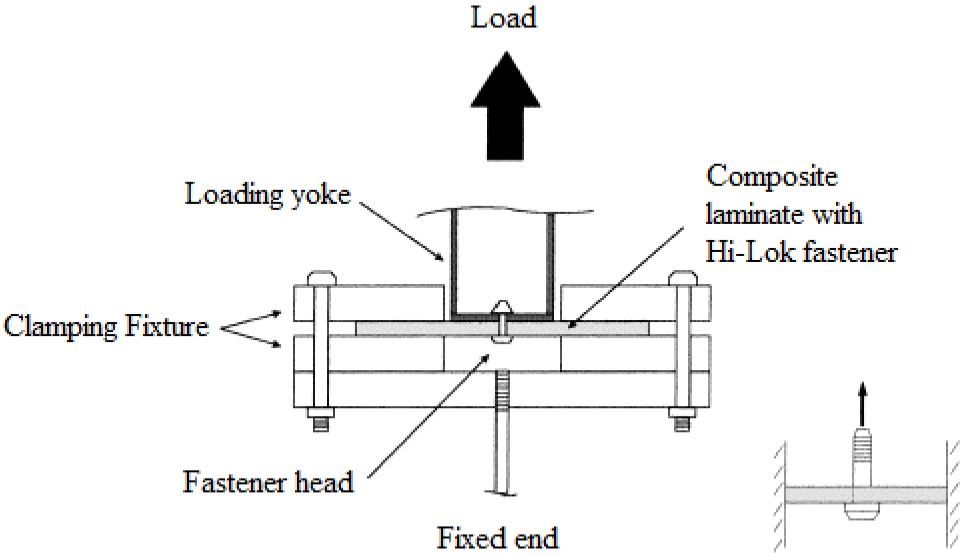

Figure 2.1: Schematic of clamped testing arrangement [2]

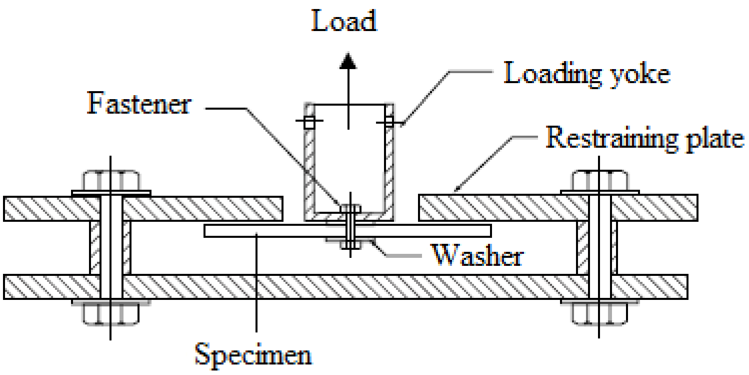

Figure 2.2: Schematic of simply-supported testing arrangement [6]

2.1.2. Experimental Results

A typical idealized load-displacement curve for a pull-through test is shown in Figure 2.3 [1]. After an initial non-linearity in the curve, the load-displacement curve is relatively linear until the initial sub-critical failure load “P_i”, which is characterized by a small load drop (< 10% of the failure force) or a slope change. Then the load continues to increase until the failure load “P_f” at a displacement “δ_f”. This point is typically characterized by a large drop in load (≥10% of the failure force). Finally, a maximum load “P_m” at a displacement “δ_m” is reached, which is characterized by a significant load drop before the complete fracture of the specimen.

The average failure load and maximum load results for Tests ID 1 to 9 are summarized in Table 2.2. The highest pull-through failure load “P_f” was 11 kN with a standard deviation of 0.15 kN for specimen Test ID 5 and the lowest was 1.53 kN with a standard deviation of 0.04 kN for specimen Test ID 8. The accurate experimental results were not provided in the literature for Test ID 10 to 15

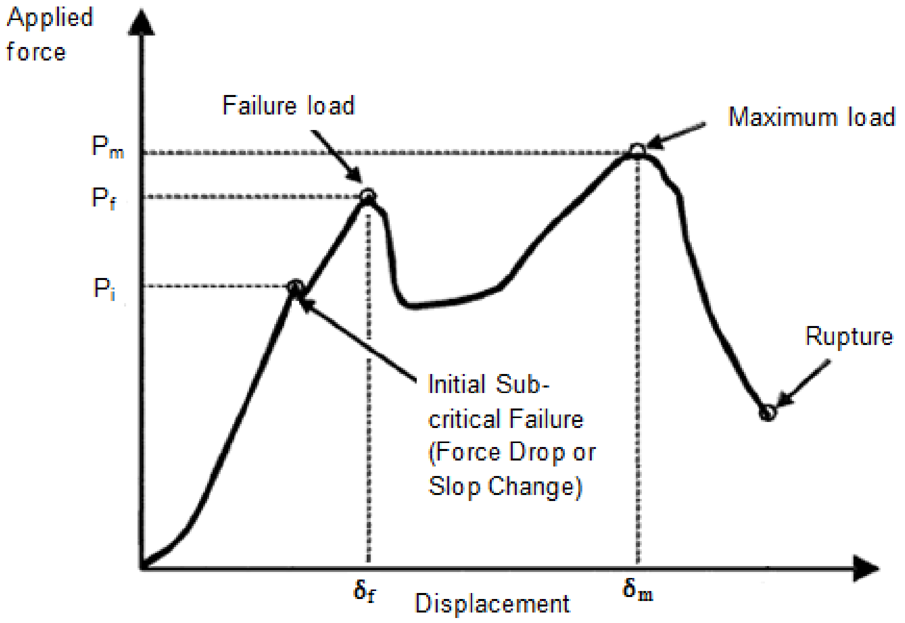
Applied force
Failure load
Maximum load
P_m
P_f
P_i
Rupture
Initial Sub-critical Failure (Force Drop or Slop Change)
δ_f
Displacement
δ_m

Figure 2.3: Typical idealized load-displacement behaviour of fastener pull-through [1]

Test ID	**No. of plies**	**Stacking sequence**	**Laminate thickness [mm]**	**Failure load (kN)**	**Standard deviation of failure load**	**Maximum load (kN)**
1	16	$[0,90/\pm45]_{2s}$	3.5	6.88	0.18	8.12
2	16	$[0,90/\pm45]_{2s}$	3.5	6.46	0.12	7.70
3	16	$[0,90/\pm45]_{2s}$	3.5	8.31	0.33	N/A
4	16	$[0,90/\pm45]_{2s}$	3.5	7.17	0.12	N/A
5	24	$[0,90/\pm45]_{3s}$	5.24	11.0	0.15	N/A
6	16	$[0,90]_{4s}$	3.5	6.51	0.12	7.15
7	16	$[0,90/\pm45]_{2s}$	2.4	4.35	0.09	4.63
8	4	$[0,90/\pm45]$	0.87	1.53	0.04	1.57
9	8	$[0,90/\pm45]_{s}$	1.75	3.12	0.09	3.82

Table 2.2: Average measured pull-through failure loads and maximum loads [2, 6]

The actual load-displacement behaviour was found to depend on the specimen configuration. Figure 2.4 shows the typical load-displacement curve for Test ID 1 to 7. The load-displacement behaviour of specimens of reduced thickness (Test ID 8 and 9) differed from what was presented in Figure 2.4 in one significant way, that there were no major load drops detected at point B. Instead, the slope preceding the first load drop contained a number of relatively minor load drops. No slope changes found following such drops indicated the fact that the failures responsible for the minor drops did not appreciably degrade the laminate [2].

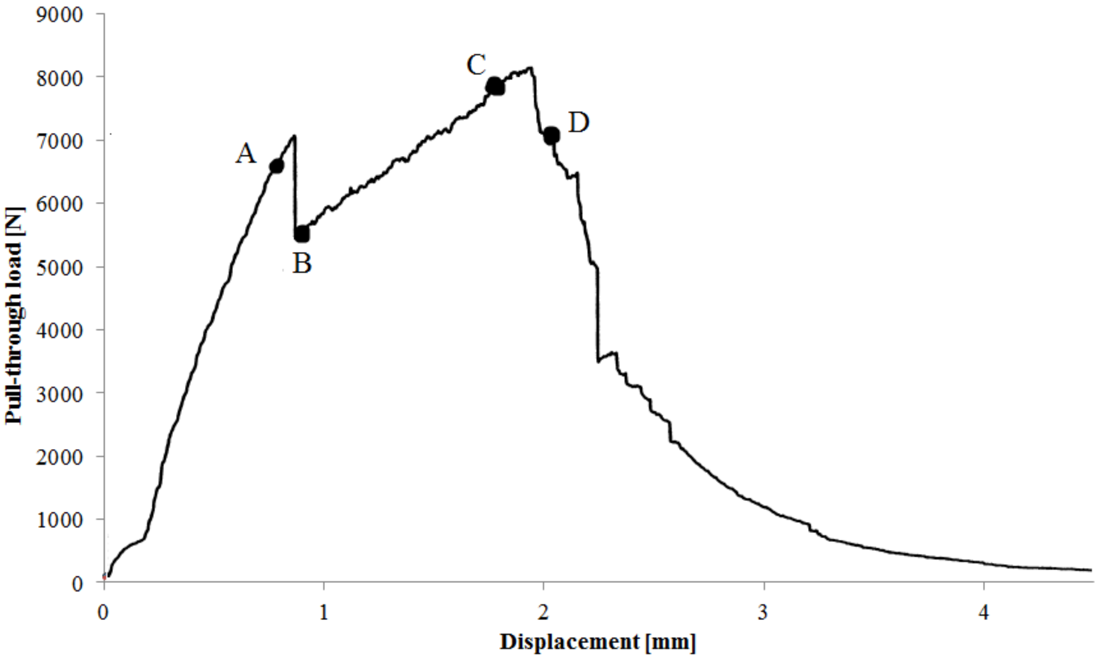

Figure 2.4: Load-displacement behaviour of a 16-ply protruding head pull-through specimen [2]

The load-displacement behaviour (Figure 2.5) of 8-ply non-crimp fabric laminates (Test ID 10, 12, 13 and 14) was different from the plain weave and tape prepregs specimens (Test ID 1 to 9). The load-displacement curves started with a linear region until the first peak which represents the failure load, and then followed by a sudden load drop with no second peak observed. This failure load was much larger than the load for specimens bolted with smaller fastener head (Test ID 6). Similar load-displacement behaviour was found in the 16-ply specimens (Test ID 11 and 15), but there was a distinct reduction in slope at approximately half of its failure load when using Φ 40 mm opening restraining plate. The reduction in the slope was not observed in specimens restrained with Φ 80 mm and 120 mm opening restraining plate.

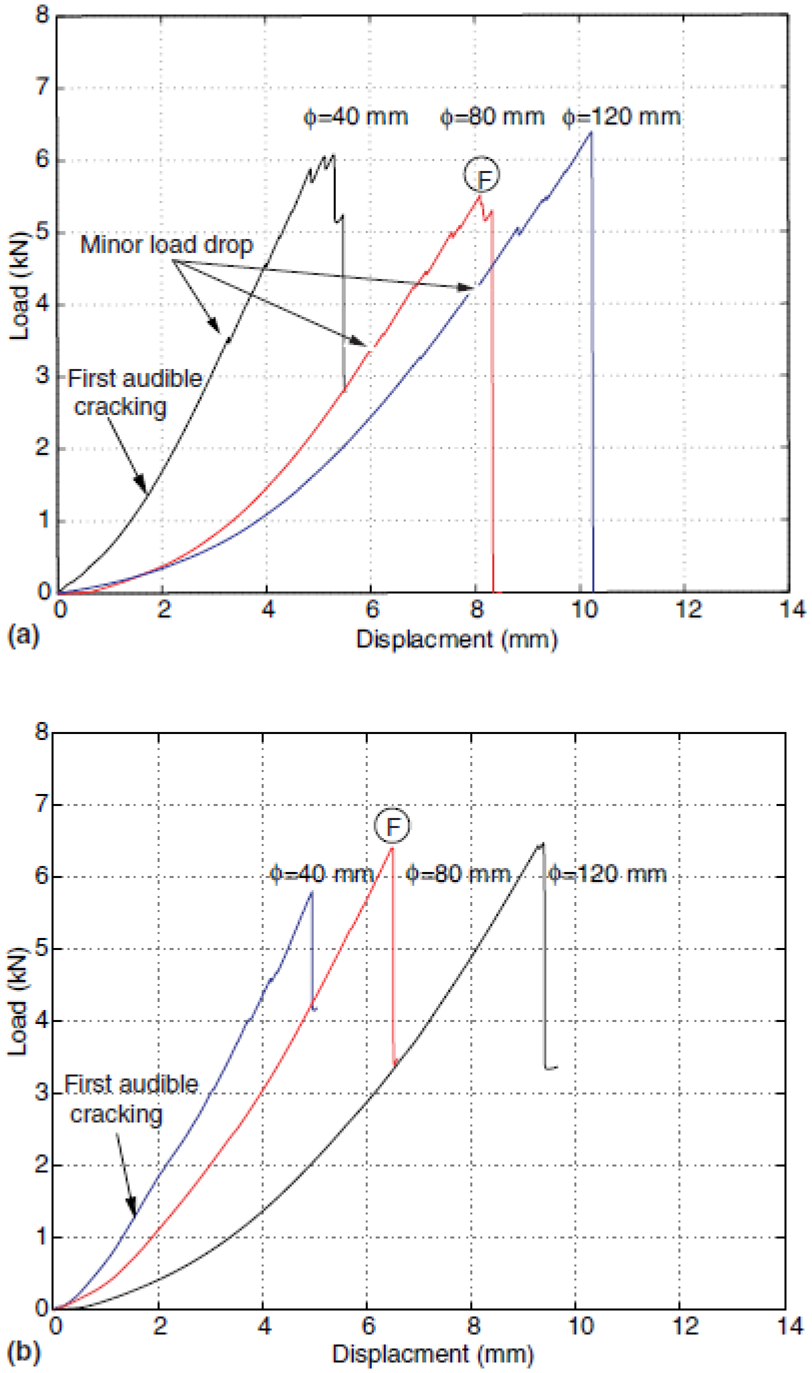

Figure 2.5: Load-displacement curves for (a) epoxy quasi-isotropic laminate (Test ID 10); (b) vinylester quasi-isotropic laminate (Test ID 13) [6]

In summary, the load-displacement behaviour of pull-through loading followed the following trends:

1) The increase in fastener head diameter and specimen thickness leads to an increase in both failure load and maximum load.

2) The post-failure load behaviour depends on the laminate thickness.

3) The specimen manufactured from tape prepreg experiences a larger drop in load succeeding failure load.

4) The increase of the restraining plate opening size leads to the reduction in laminate flexure stiffness, but the failure load remains unaffected.

2.1.3 Specimen Inspection

Four locations along the load-displacement curve were selected by two criteria and the specimens were unloaded accordingly during the test. For the first criterion, specimens were unloaded from various load levels: 25%, 50% and 90% of the failure load and instantaneously after the failure load. This pattern was designed specifically for the epoxy and vinylester reinforced with non-crimp fabric fibre (Test ID 10 to 15) since only one peak load was found in the load-displacement curve. Unloading points selected for Test ID 1 to 9 according to the second criterion were critical locations along the load-displacement curve: prior to failure load, instantaneously after failure load, before maximum load and after maximum load corresponding to point A, B, C and D in Figure 2.4.

Figure 2.6 presents a map of damage propagation for the specimens made from non-crimp fabric fibres embedded in epoxy and vinylester resin. No considerable differences of damage propagation pattern were found between the specimens of the two resin systems. For the thin specimen, there was no clear indication of damages at 25% of the failure load. At 50% of the failure load, a transverse tensile failure at top plies appeared (Figure 2.7), but no visible evidence was noticed at the load-displacement curve. When the load increased to 90% of the failure load, interlaminar shear cracking had propagated along the interface between the on and off-axis in the mid-plies. Fibre kinking and matrix intralaminar shear cracking were found directly under the edge of the washer. The final failure was characterized by fastener head embedded in the laminate [6].

The damage propagation of thick specimens behaved differently. The initial damage occurred in a form of intralaminar shear cracking under the washer edge. At half of the failure load, a network of intralaminar and interlaminar shear cracking was dominating the cross sections for specimens restrained by the 40 mm opening restraining plate (Figure 2.8). Such network had only appeared at 90% of the failure load for the specimens restrained by the 80 and 120 mm opening restraining plates. The final failure of these specimens was found in the same manner as the thin specimens' [6].

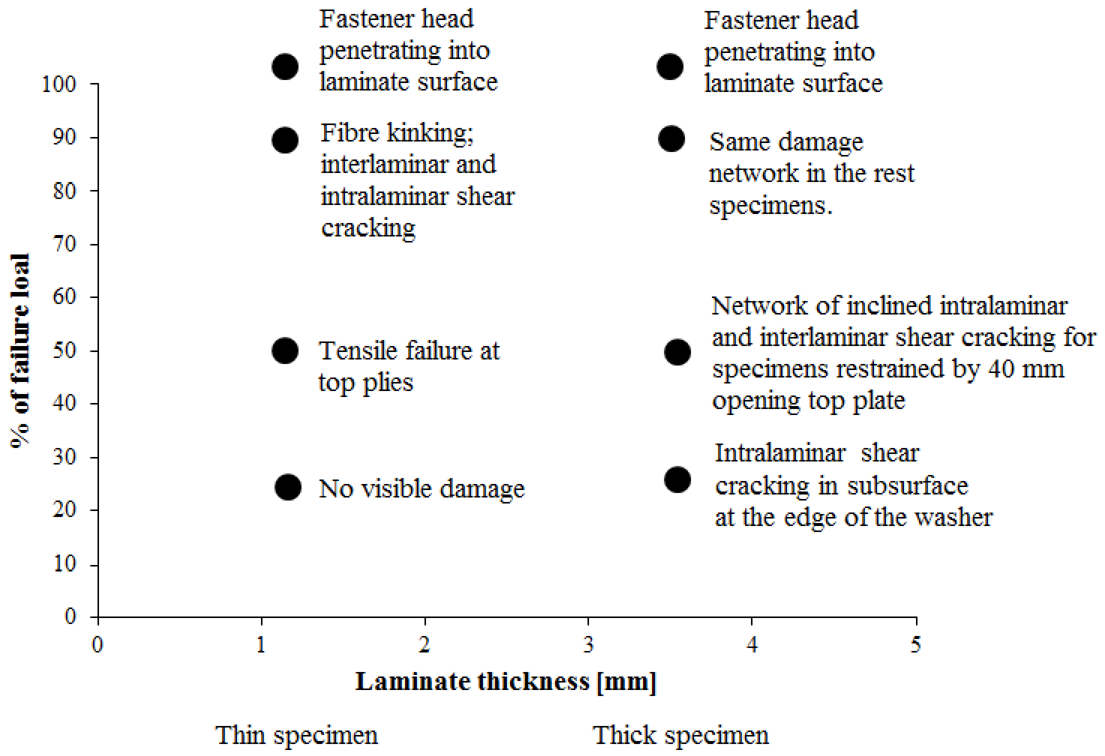

Figure 2.6: Propagation of failure for both thin and thick specimen (Test ID 10 to 15) [6]

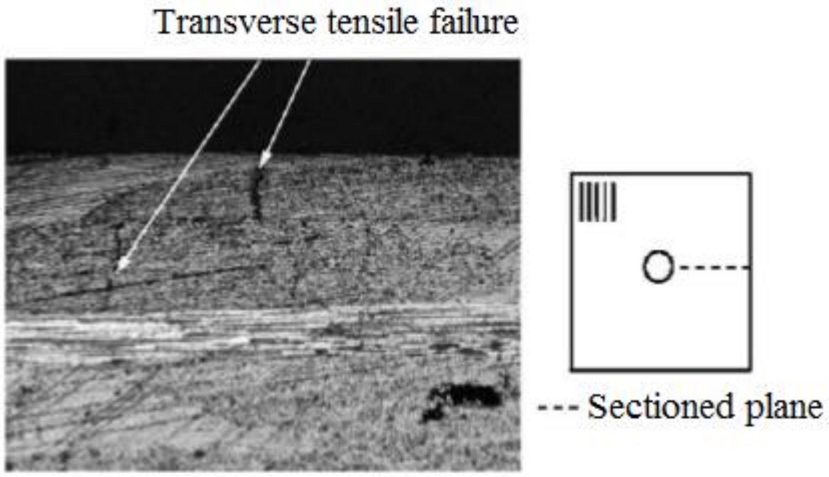
Transverse tensile failure
--- Sectioned plane

Figure 2.7: Micrograph of thin epoxy specimen loaded to 50% of the failure load [6]

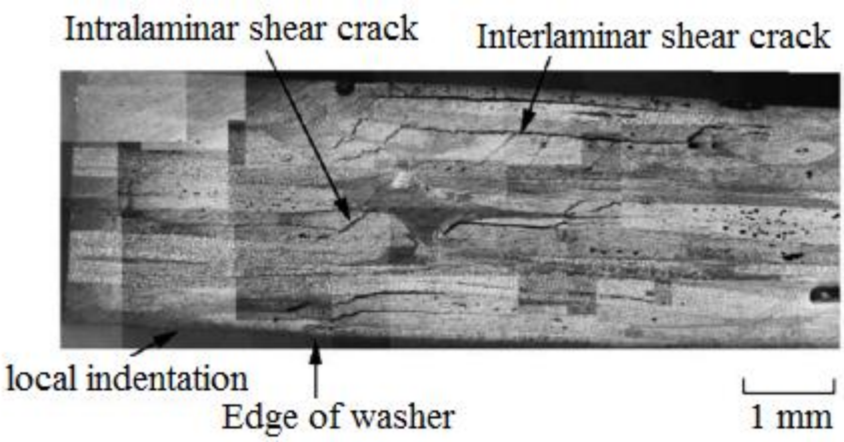
Intralaminar shear crack
Interlaminar shear crack
local indentation
Edge of washer
1 mm

Figure 2.8: Micrograph of thick specimen (40 mm opening restraining plate) loaded to 50% of the failure load [6]

The prepreg specimens (Test ID 1 to 9) had a similar damage propagation pattern (Figure 2.9) to the non-crimp fabric specimens. Because the selected unloading points were the critical points along the load-displacement curve, a better understanding of the failure mechanism was observed. The failure mode of fastener pull-through for thin and thick specimens was described with bold texts in Figure 2.9 and the corresponding micrographs are shown in Figure 2.10 and Figure 2.11.

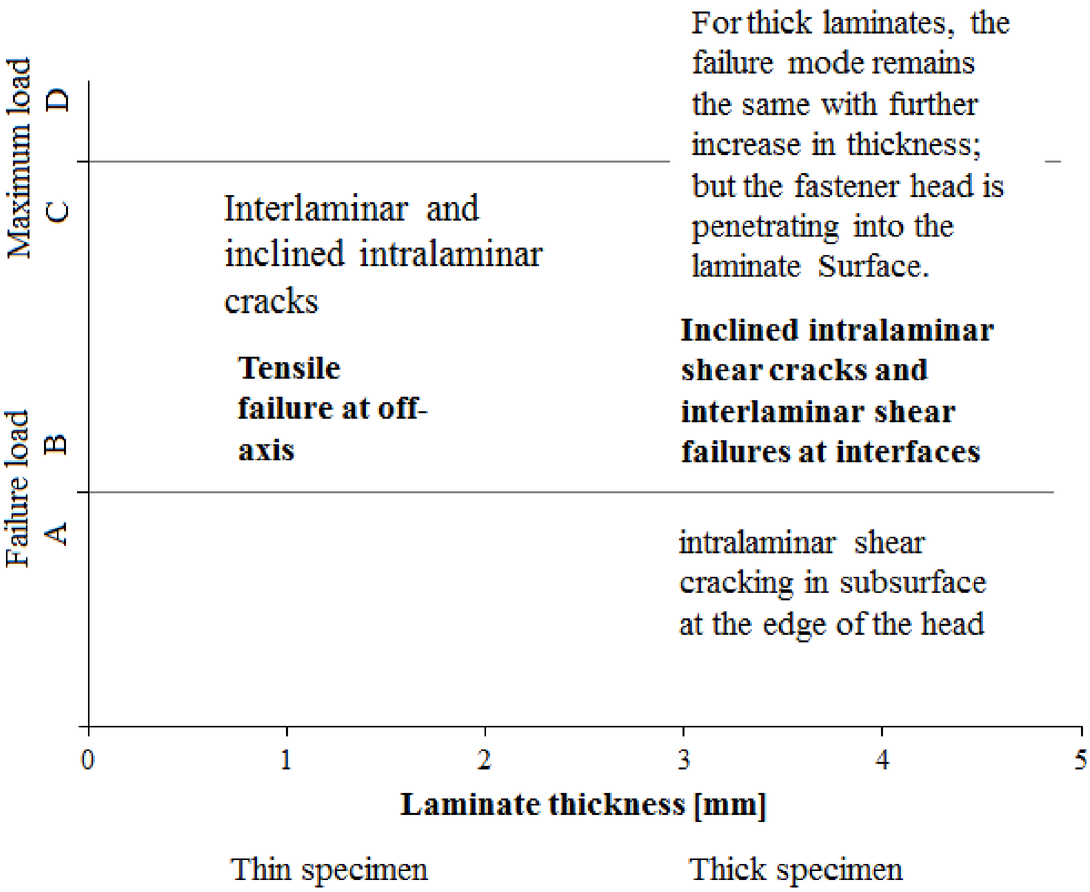
Maximum load
Failure load
D
C
B
A
For thick laminates, the failure mode remains the same with further increase in thickness; but the fastener head is penetrating into the laminate Surface.
Interlaminar and inclined intralaminar cracks
Tensile failure at off-axis
Inclined intralaminar shear cracks and interlaminar shear failures at interfaces
intralaminar shear cracking in subsurface at the edge of the head
0
1
2
3
4
5
Laminate thickness [mm]
Thin specimen
Thick specimen

Figure 2.9: Propagation of failure for both thin and thick specimen (Test ID 1 to 9) [2]

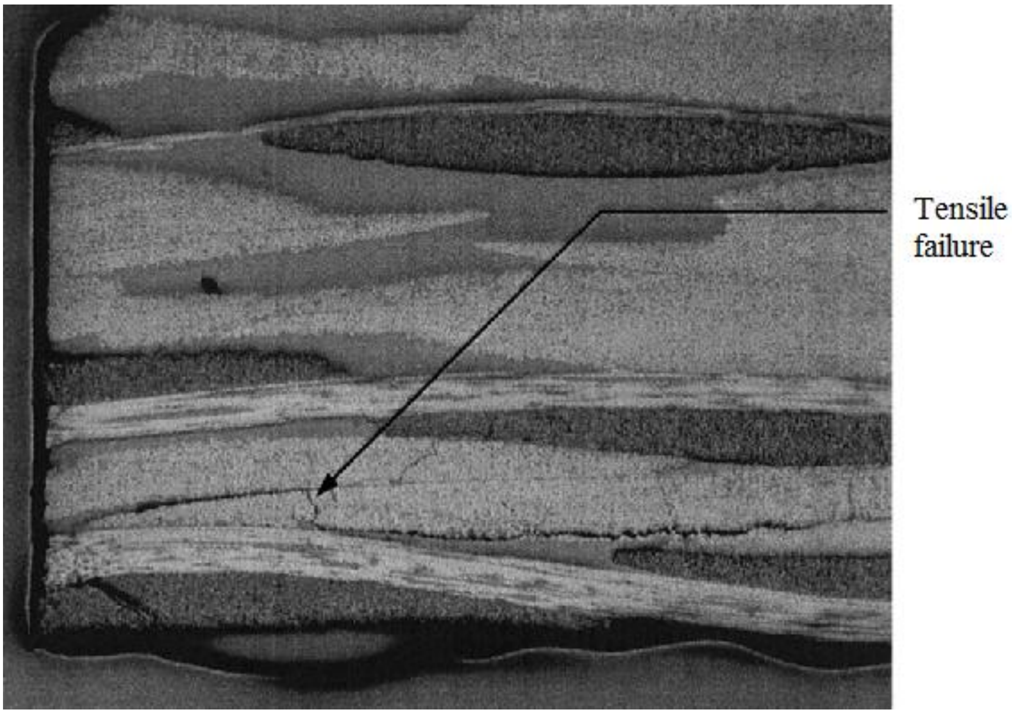
Tensile failure

Figure 2.10: Micrograph of thin specimens unloaded instantaneously after failure load [2]

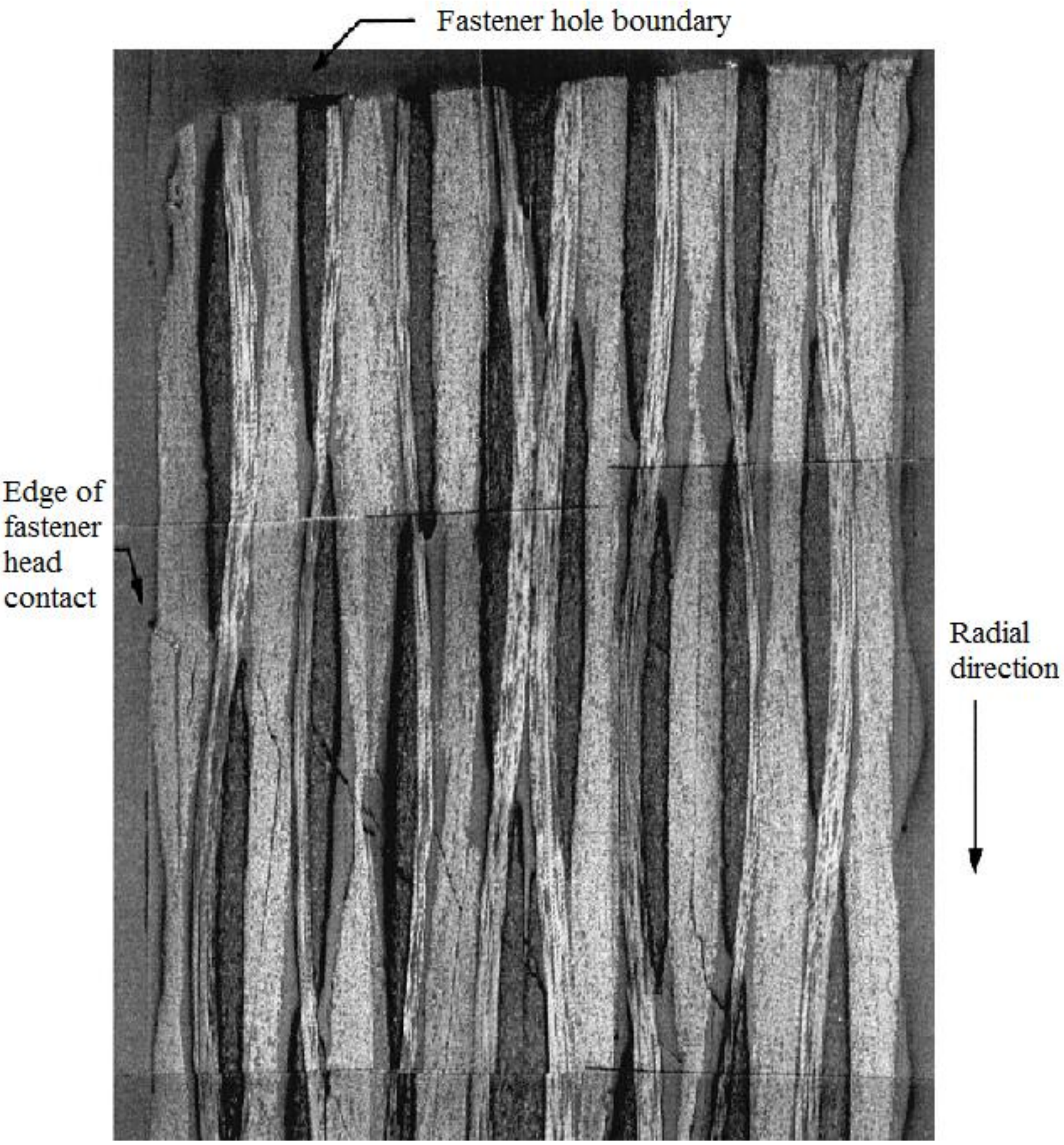
Fastener hole boundary
Edge of fastener head contact
Radial direction

Figure 2.11: Complete through-thickness damage of thick specimen, unloaded instantaneously after failure load [2]

The specimen inspection showed that the failure mechanism and damage propagation patterns were similar between the two literatures [2 (Test ID 1 to 9) and 6 (Test ID 10 to 15)]. The fastener head diameter, the laminate thickness and the specimen mounting method only influenced the failure load magnitude and load-displacement behaviour. Thin specimens failed due to tensile stresses but intralaminar and interlaminar shear cracking were introduced by further loading the specimen. The failure of relatively thick specimens was characterized by a global network of interlaminar shear cracking which was connected by the inclined intralaminar shear cracking.

2.2 NUMERICAL MODELLING

Through the experimental results, a basic understanding of the fastener pull-through load-displacement behaviour and failure mechanism was provided. Detailed stress/strain distribution could help to determine and confirm the stresses responsible for each failure mechanism and thus predict the failure. A numerical simulation using finite element software is necessary. Most researchers used Abaqus and Nastran as the former is better in solving non-linear problems and the latter is the world's most widely used Finite Element Analysis (FEA) solver. The simulation solutions of the finite element models displayed in this section was performed using MSC-Nastran version 69.

The finite element models were meshed with 8-nodes isoparametric solid element. Each ply was modelled by one element through the thickness. Contact elements between the fastener and laminate surfaces were used to simulate the friction and clearance. A model setup of the baseline specimen configuration is shown in Figure 2.12.

An increase in contact area between the fastener head and the laminate surface resulted in higher pull-through strength [2, 3]. Stiffer laminates also led to an increase in higher pull-through strength [16, 17]. Hence, an increase in contact area and laminate stiffness improved the pull-through strength. Changing these two parameters would also change the stress/strain distribution.

The through thickness load generated flexure of the laminate which induced fibre direction stresses (Figure 2.13). The maximum tension and compression were found in the bottom plies and plies under the fastener head. Flexure stresses thus did not contribute to the formation of matrix cracking adjacent to the fastener head [2]. The level of the in-plane stresses increased with the reduction of the laminate thickness.

The through thickness stress distribution is shown in Figure 2.14. The critical region is under the fastener head, and the magnitude of the stress decreases in radial direction.

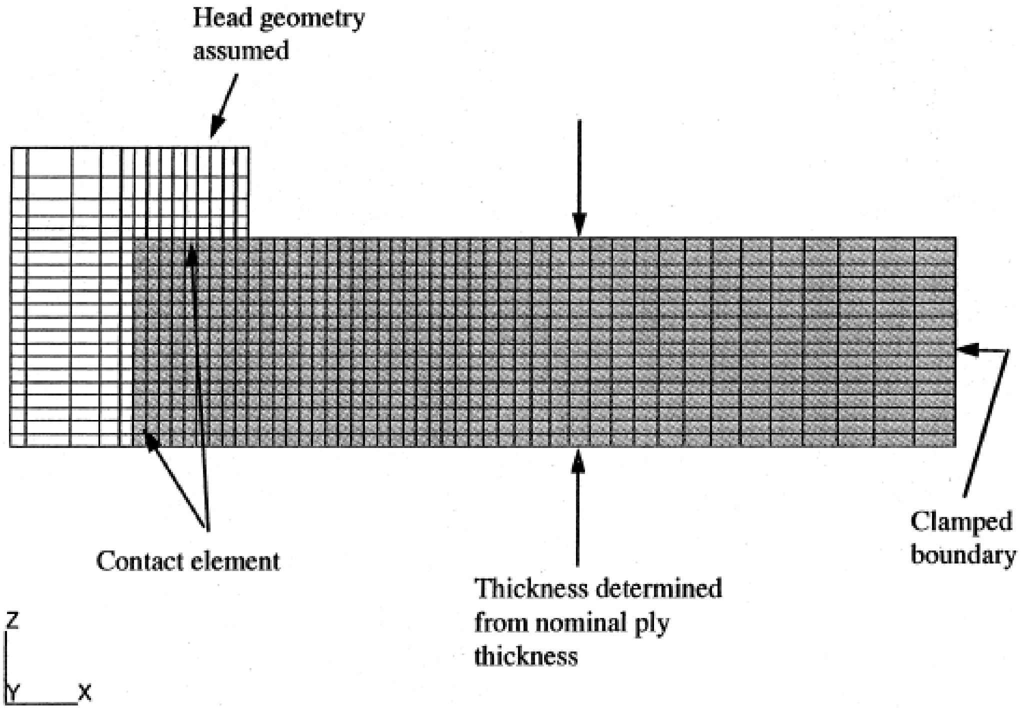
Head geometry assumed
Contact element
Thickness determined from nominal ply thickness
Clamped boundary
Z
Y
X

Figure 2.12: Baseline finite element model setup [19]

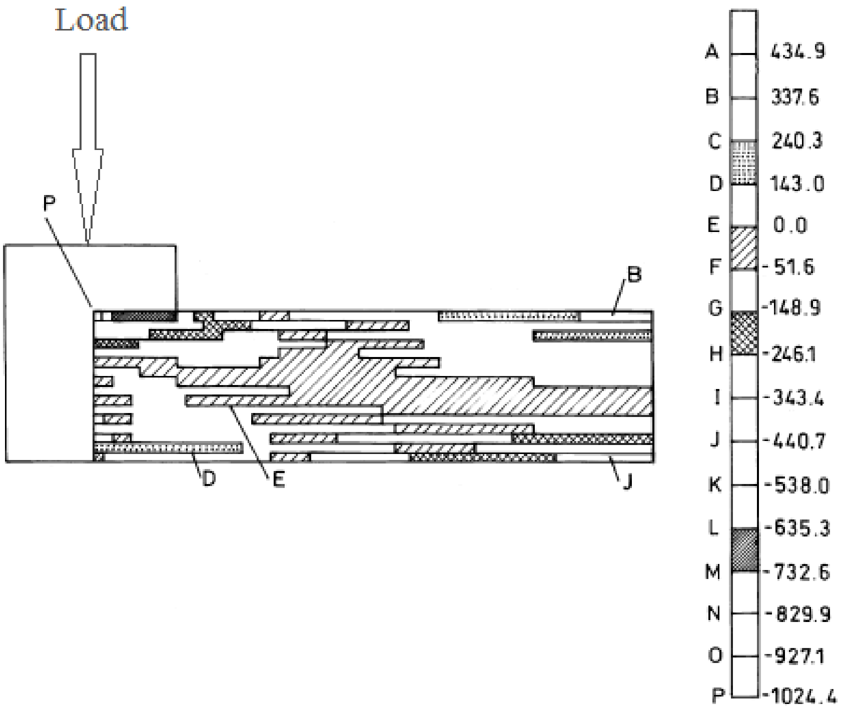

.

Figure 2.13: Contour plot of in-plane stresses for the baseline specimen configuration [19]

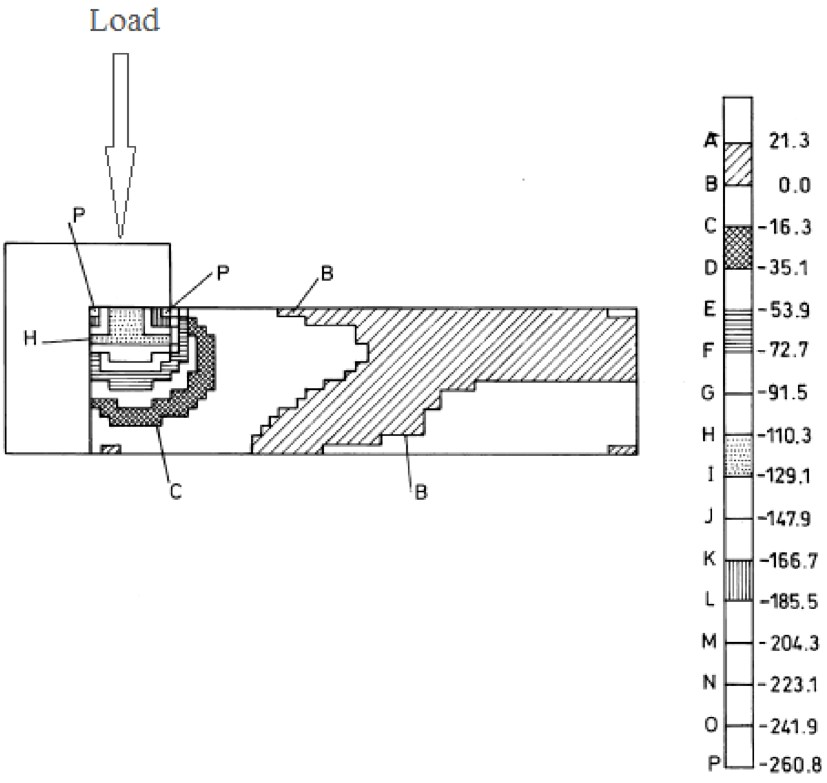

Figure 2.14: Contour plot of through thickness stresses for the baseline specimen configuration [19]

The interlaminar shear stresses (Figure 2.15) exhibited a parabolic distribution originating from the fastener head. Maximum shear stress was observed under the edge of the fastener head and gradually dispersed towards the mid-plies with a decreased magnitude at an angle of approximately 45 degree with the laminate surface. The distribution of the interlaminar shear stresses was consistent with the failure mechanisms discussed in the previous experimental results [2, 3, and 6]

To summarize the finding discussed above, Figure 2.16 shows the prominent stresses at each region of the specimen's cross section. The 2-D stress elements represented the type, direction and magnitude of the local stresses in the cross section of the laminate.

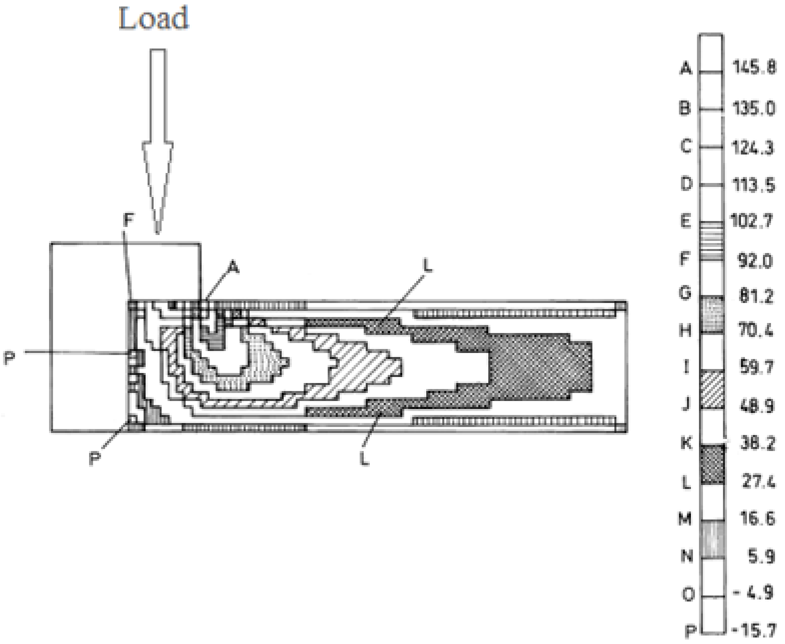

Figure 2.15: Interlaminar shear stresses distribution for the baseline specimen configuration [2]

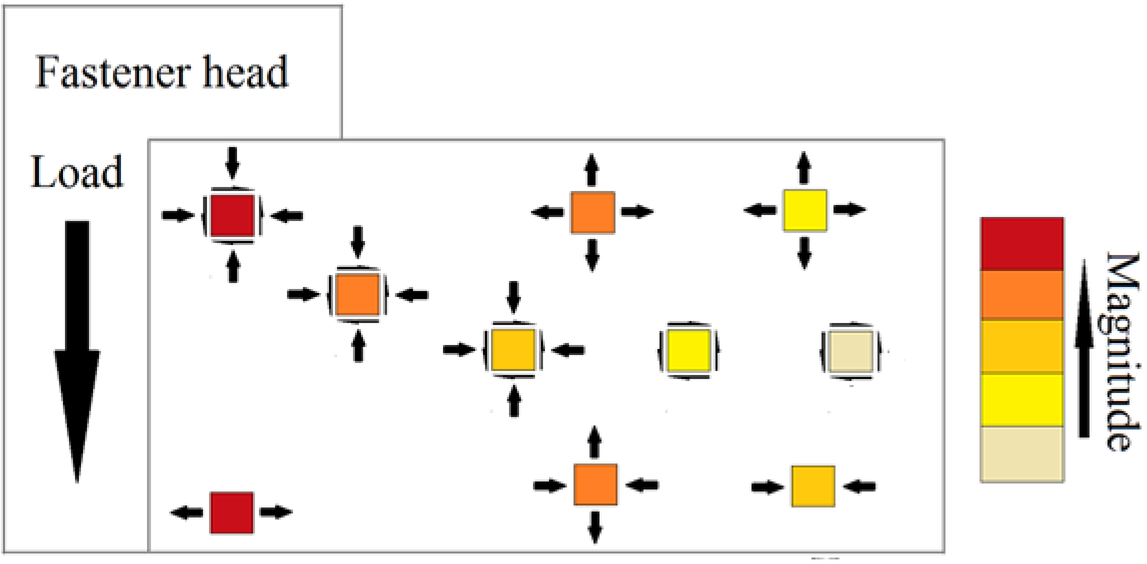
Fastener head
Load
Magnitude

Figure 2.16: Map of stress distribution

THIS DOCUMENT PROVIDED BY THE ABBOTT AEROSPACE TECHNICAL LIBRARY ABBOTTAEROSPACE.COM

2.3 SUMMARY

This literature review provided a general understanding of the fastener pull-through failure mechanism and damage propagation. Parameters such as, fastener head diameter, laminate thickness, restrain boundary size and fastener type were considered. Results indicated that an increase in laminate thickness and fastener head diameter could improve the pull-through strength. Laminate flexure stiffness was inversely proportional to the restrain boundary size. The failure mode of thin specimens was in-plane tensile failure and the failure mode of thick specimens was matrix cracking and delamination. Numerical models confirmed that the delamination failure mode was initiated by the combination of through thickness tensile stress and interlaminar shear stress.

The following issues were raised from the literature review:

1) No unique standard was followed for the experimental investigations leading to inconsistency in the data interpretation.

2) The various parameters affecting pull-through failure were not examined systematically. Although the effect of individual parameter was clearly identified, the cross effect of two or more parameters combined was unclear.

3) The general knowledge of the pull-through failure provided guidance for composite structure designers. Nevertheless, the most practical benefit to the designers is a method that can reduce the large number of costly tests required to obtain the failure load magnitude.

Chapter 3

Methodology

The methodology used to investigate the pull-through failure is presented in this chapter. First, the experimental investigation based on the ASTM standard D 7332/D 7332M – 07 [1] is described. Second, the modelling approach and assumptions of the pull-through loading is described.

3.1 EXPERIMENTAL DESIGN

In this section, the specimen manufacturing method, the testing instrumentation, the testing matrix and procedure are described. Only SI units were used except for the fastener dimensions defined in inches.

3.1.1 Sample Preparation

The prepreg chosen for this study, manufactured by CYTEC Engineered Materials, was the CYCOM 5320 epoxy resin reinforced with a plain weave T650-3K carbon fibre which has a fibre areal weight of 196g/cm^2 and a resin content of 36% wt. The specimen layup was $[45/0/-45/90]_{ns}$ (n=1 or 2 or 3). Side breather and non-perforated release film were used for the vacuum bagging (Figure 3.1). Panels were cured in a convection oven using a two ramp and two dwell cure cycle with a long debulk at room temperature (Figure 3.2).

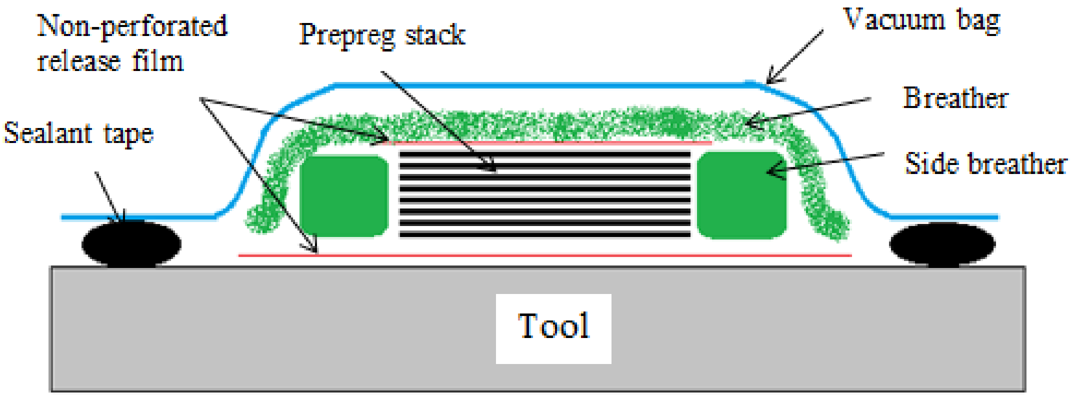
Non-perforated release film
Prepreg stack
Vacuum bag
Breather
Sealant tape
Side breather
Tool

Figure 3.1: Bagging arrangement

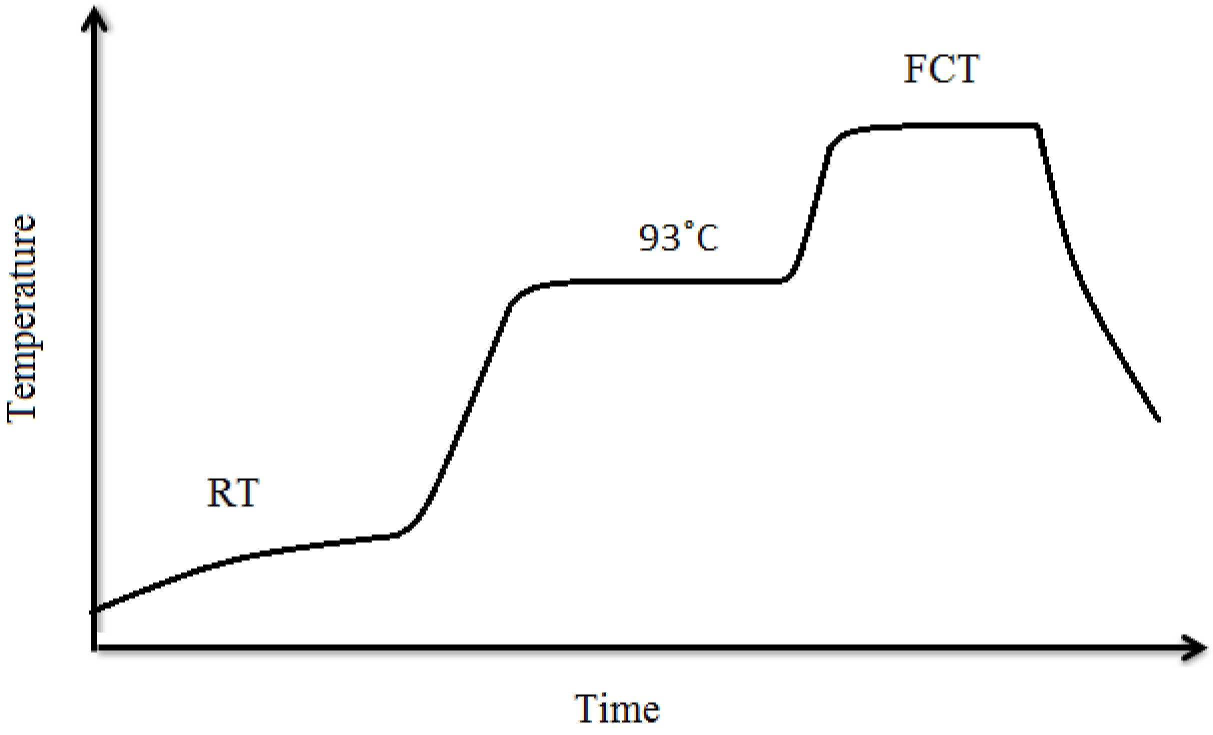

Figure 3.2: Cure cycle for panel manufacturing; in figure: RT (room temperature), FCT (final curing temperature)

The cured panels were then cut into 4”×4” (100 mm × 100 mm) rectangular samples using a water-cooling diamond coated circular saw. A fastener hole was drilled through the centre of the sample using brad-point drill bits. Since friction between the fastener shank and hole can change the specimen behaviour in strength, both the hole and fastener diameters were accurately measured in order to achieve the tolerance on fastener-hole clearance which is +0.08/-0.00 mm [1].

Voids can increase local stress concentration factor and thus reduce the specimen’s pull-through strength. Voids content was measured by optical microscopy and image analysis using ImageJ, which was a java-based image processing software. Under magnification of 50, small sections of the laminate cross-section were captured as grey-scale micrographs. Then, the micrographs were collaged and converted to a binary image. The void area was visible in the binary image. To find the fraction of the void area, two methods were used. First method, the void area was automatically detected by the software based on the intensity of the threshold binary image. The second method was to manually select the voids in the binary image. Results were average values from both methods and showed that the void content was below 2% for all manufactured panels.

Titanium sulphuric acid anodized protruding head fasteners HST12 and self-locking nuts were used (Table. 3.1). The first letter indicates the head type ("P" for protruding) and the number indicates the shank diameter in inches. The shank diameter and the head diameter of the fasteners along with their corresponding installation clamping torque level are shown in Table 3.1.

Fastener code	Type	Shank diameter Inch [mm]	Head diameter Inch [mm]	Torque Nm
P0.19	Protruding	0.190 [4.76]	0.360 [9.14]	1.13
P0.25	Protruding	0.250 [6.35]	0.420 [10.67]	2.26
P0.3	Protruding	0.313 [7.94]	0.480 [12.09]	4.00

Table 3.1: Fastener types, dimensions and corresponding low torque values

3.1.2 Test Matrix

A 2-factor, 3-level testing matrix was designed to evaluate the effect of fastener size and specimen thickness on the pull-through failure load (Figure 3.3). Three protruding fastener sizes (P0.19, P0.25 and P0.3 in Table 3.1) and three specimen thicknesses (0.063

[1.6], 0.126 [3.2] and 0.19 [4.8] inch [mm]) were tested (Test ID 1 to 9). The clamping torque was set to a low torque value according to the fastener size as shown in Table. 3.1. The effect of the clamping torque magnitude was investigated in a separate test plan (Test ID 12 to 17). Sixteen and twenty four plies laminates with P0.3 fasteners were tested at four levels of clamping torques: 0 Nm, 4 Nm, 8 Nm and 12 Nm. The following nomenclature was used to define a particular testing condition: started with the sample type (P for protruding), followed by the shank diameter, then the laminate number of plies and finally, the torque setting (NT for no torque, LT for low torque, MT for medium torque and HT for high torque). For example "P0.19-24LT" represents a protruding head fastener with a shank diameter of 0.19 inch bolted to a 24 plies laminate and then fastened with a low torque setting. A total of five samples were tested under each condition.

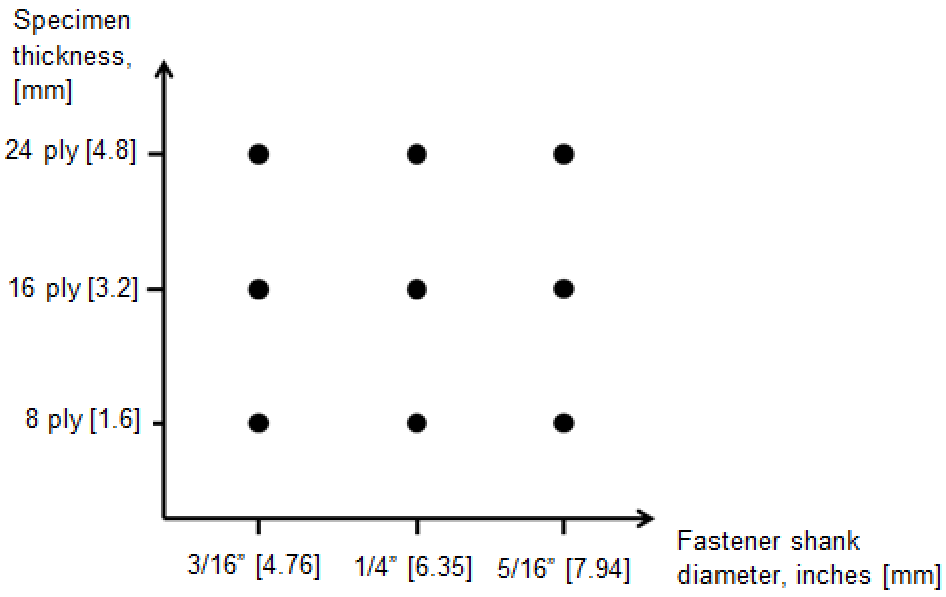

Figure 3.3: Three-level factorial design matrix containing two factors: specimen thickness and fastener shank diameter

3.1.3 Testing instrumentation

The tests were performed using a MTS Systems Corporation 100kN servo-hydraulic machine. The testing fixture (Figure 3.4) was designed to fit the testing machine configuration. The top and bottom plates of the fixture were spaced by four beams and fastened together. The top plate contained a clearance hole to load the fastener. Three different sizes of clearance holes in the top plate were used for different fastener sizes (Table 3.2). The clearance between the edges of specimens and the fixture beams was 12 mm. The specimen was simply-supported under the top plate and loaded via a fastener bolted to the loading yoke connected to the testing machine crosshead. All parts were machined from cold rolled 1020 carbon steel.

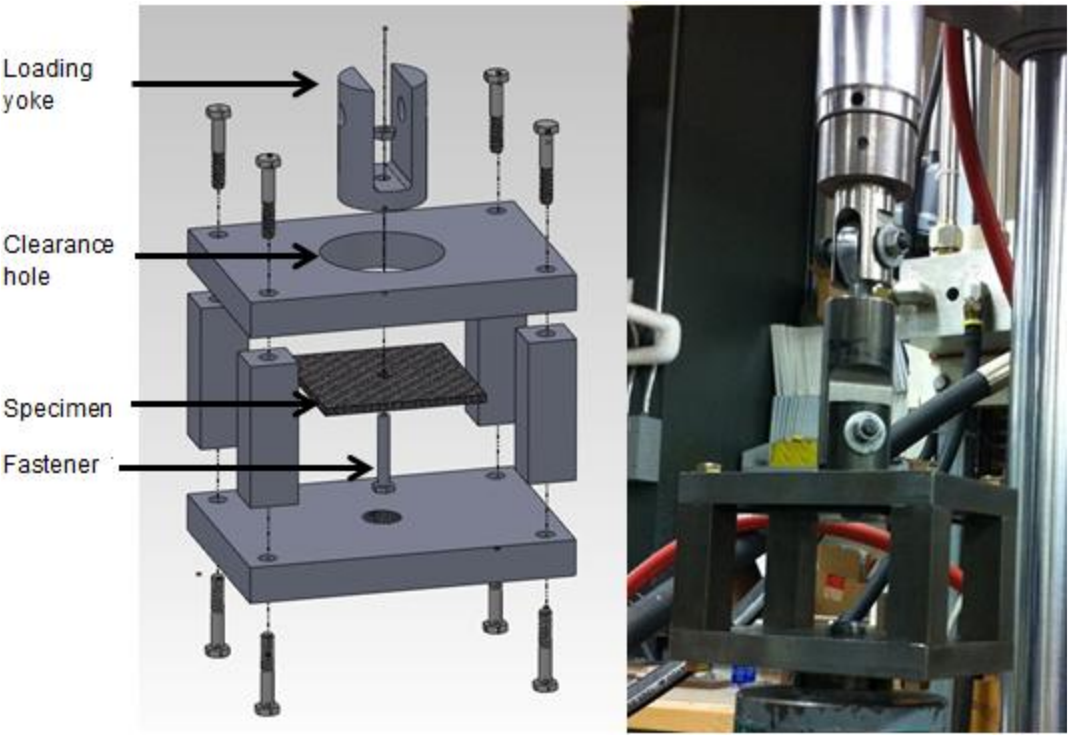

Figure 3.4: Fastener pull-through testing fixture for MTS 100kN servo-hydraulic machine

Shank diameter, in [mm]	Min Specimen Length/Width, mm	Clearance Hole Diameter, mm
0.190 [4.76]	72	38
0.250 [6.35]	84	50
0.313 [7.94]	96	63

Table 3.2: Minimum specimen length/width and fixture clearance dimensions corresponding to the fastener shank diameter

3.1.4 Testing Procedure

The test procedure was designed according to ASTM Standard D 7332/D 7332M – 07 [1]. The load-displacement readings were recorded every 0.2 second throughout each test. Certain specimens may be interrupted and unloaded during the test in order to examine the damage at a specific damage level. The following procedure was used for each test:

1. Install specimen with fastener by using calibrated torque wrench to a specific clamping torque level[1];

2. Apply a 125 N tensile preload to ensure that the fixture and the specimen are aligned and to minimize errors in the measurement of the pull-through displacement;

3. Reset the displacement to zero;

4. Start loading at a crosshead speed of 0.5 mm/min;

5. Unload the specimen when the load dropped by 50% from the maximum load;

---

[1] Specimens with zero clamping torque level should be figure tightened.

3.2 NUMERICAL MODELS

The numerical models were developed using ABAQUS 6.10. The non-linear contact was taken into consideration. 3-D model geometry simplification, material properties, meshing, contact properties, boundary conditions and load case were detailed in the following paragraphs.

There are three regions in the finite element models: the laminate, the fastener with the nut and the testing fixture (Figure 3.5). The laminate was built using the actual test dimensions. The fastener and the nut assembly were simplified as a one-piece dumbbell shaped part. The “handle” of the dumbbell shaped part represented the fastener shank. The thicker “weight disk” represented the fastener head (Figure 3.5: section A-A) and the thinner “weight disk” on the other end of the “handle” represented the nut. The fixture was simplified as a cylindrical shell representing the edge of the opening due to the fact that the only contact region between the fixture and the specimen was the edge of the fixture opening when specimens were subjected to the pull-through load.

Three materials were defined to represent steel, titanium and composite in the numerical models. The steel Young’s modulus and Poisson’s ratio were 200 GPa and 0.29 respectively. The titanium Young’s modulus and Poisson’s ratio were 110 GPa and 0.28 respectively. Instead of using the default composite elements in Abaqus, solid elements with orthotropic material properties were assigned. Table 3.3 shows the orthotropic material properties of the composite laminate. The Elastic properties D_{1111}, D_{2222}, D_{1122} and D_{1133} were provided by the material manufacturer. They were experimentally determined according to ASTM standard D 3039, D3039, D3518 and D 2344, respectively. Elastic properties D_{3333}, D_{2233}, D_{1212}, D_{1313} and D_{2323} were estimated values.

D_{1111}	D_{2222}	D_{3333}	D_{1122}	D_{1133}	D_{2233}	D_{1212}	D_{1313}	D_{2323}
68000	65000	6000	5800	4000	4000	5800	4000	4000

Table 3.3: Elastic properties of composite laminate, unit in MPa

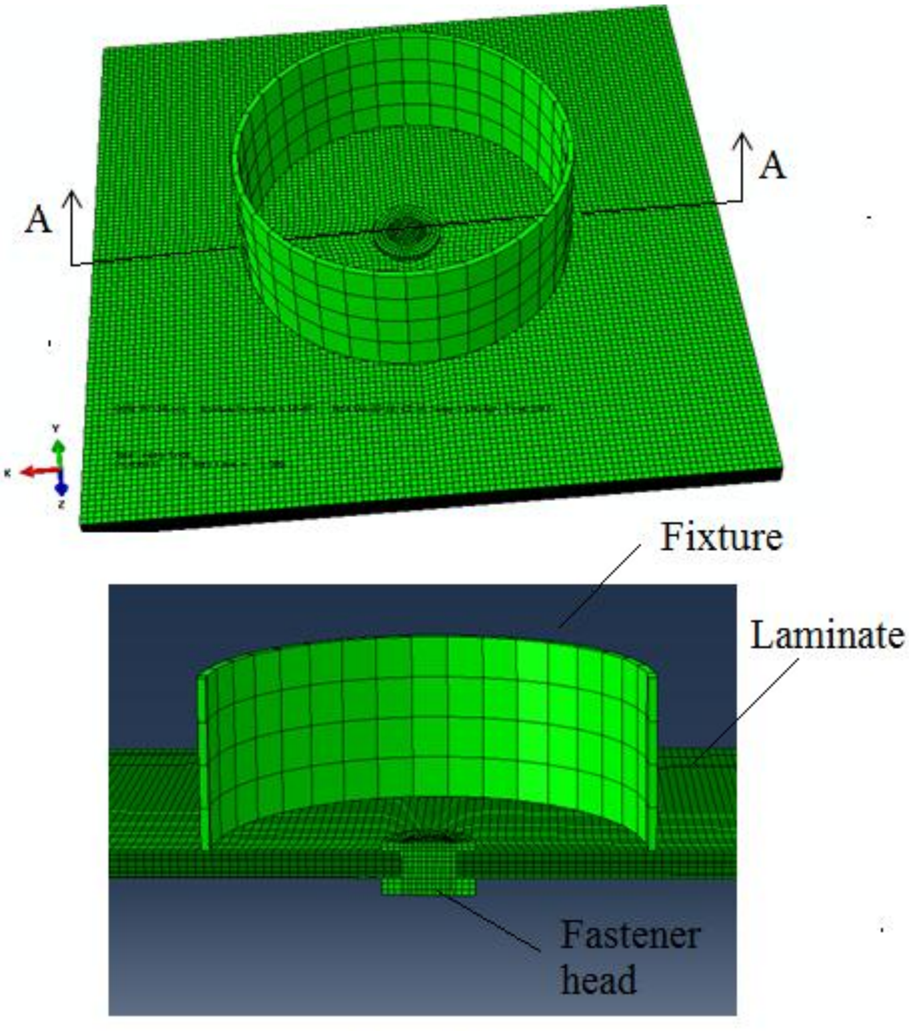

Section A-A

Figure 3.5: Numerical model setup including fixture, laminate and fastener

All parts were meshed using 8-node hex elements. Relatively coarse mesh was assigned to the fastener and fixture whereas the laminate was assigned with a fine mesh. In order to ensure a balance between accurate results and reasonable solution time, mesh convergence studies were performed. In the through thickness direction, the laminate ply was modeled with one element. Cell partition technique was performed to ensure an axi-symmetric mesh.

Normal and tangential contacts interaction properties were defined. The normal contact behaviour was defined as a "hard contact" and allowed separation after contact. The tangential behaviour was assumed to be a small isotropic friction with an estimated friction coefficient of 0.2. The assembled model contained four "surface to surface" contact pairs. Three of the four contact pairs were between the fastener/nut and the laminate. Figure 3.6 shows the Schematic of the four contact pairs. The red color represents the master surfaces and the blue color represents the slave surfaces. The master surfaces were the fastener head bottom surface, the fastener shank and the top surface of the nut. The slave surfaces were the top and bottom surface of the laminate and the interior surface of the fastener hole. The fourth pair of "surface to surface" contact was between the laminate bottom surface (master) and the fixture edge (slave). It was crucial to allow small sliding for "surface to surface" contact. Small sliding would result in more robust convergence behaviour. For the same purpose, the slave surface was set to be "adjusted only to remove the overclosure" [17].

During pull-through test, the specimen was loaded through a fastener constrained by the testing fixture top plate. The fixture top plate was considered as stationary part and the loading yoke traveled in the through thickness direction only. Therefore, the fixture top plate was restrained from displacement along X; Y and Z axes in the global coordinate (Figure 3.6). Fastener was allowed to move in the Z axis direction only.

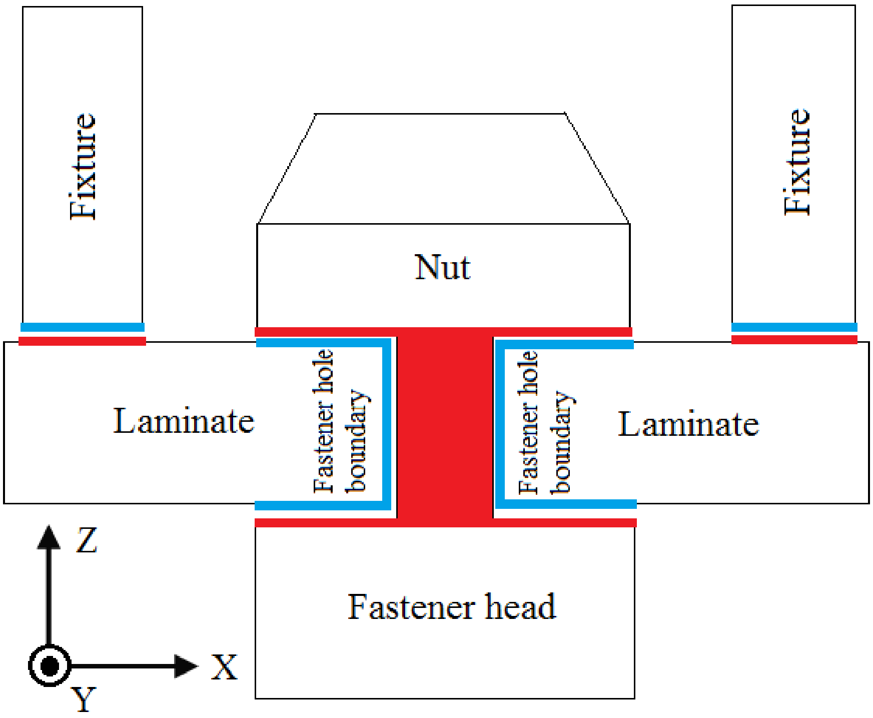
Fixture
Fixture
Nut
Laminate
Fastener hole boundary
Fastener hole boundary
Laminate
Z
X
Y
Fastener head

Figure 3.6: Schematic of contact pairs (in an X-Z cross section through center of the fastener); master surfaces are in red; slave surfaces are in blue

The load-displacement behaviour of the fastener pull-through test results from literatures [1, 2, and 3] show that there are two load peaks along the load-displacement curve. The first peak, which is called the "failure load", was selected to be the load case in the numerical models as the load-displacement curve had a sudden drop after it. The load case was simulated by adding uniformly distributed pressure onto the fastener head. The pressure was determined by the average load from the experimental testing results divided by the correspondent fastener head surface area.

3.3 SUMMARY

The investigation of the fastener pull-through failure of bolted composite joint was performed by two approaches: experimental testing and numerical simulation. The experimental testing methodology involves examining three factors that potentially affect the fastener pull-through strength: fastener size, laminate thickness and the fastener clamping torque. The effect of fastener size and laminate thickness was examined systematically according to a 2-factor, 3-level testing matrix. The clamping torque was examined individually. The numerical simulation involves building 3-D models using finite element software ABAQUS 6.10 based on the actual testing configuration. Frictions and non-linear contact between surfaces are taken into consideration. Both results from experimental testing and numerical simulation will be presented and discussed in the following section.

Chapter 4

Results and Discussion

This chapter discusses the results of the experimental testing and the finite element model simulations. The testing results discuss particularly the fastener pull-through load-displacement behaviour and the effect of factors considered on the pull-through failure. Then a detailed analysis of the failure modes is presented and the results are linked to the findings of the finite element analysis. Finally, a predictive semi-empirical equation for the pull-through failure load is presented.

4.1 EXPERIMENTAL RESULTS

A typical idealized load-displacement curve for a pull-through test is shown in Figure 4.1 [1]. After an initial non-linearity, the load-displacement curve is relatively linear until the initial sub-critical failure load "P_i", which is characterized by a 10% load drop or a slope change. Then the load continues to increase until the failure force "P_f" at a displacement "δ_f". This point is typically characterized by a large drop in load (≥10% of the failure force). Finally, a maximum force "P_m" at a displacement "δ_m" is reached, which is characterized by a major load drop before the complete fracture of the specimen.

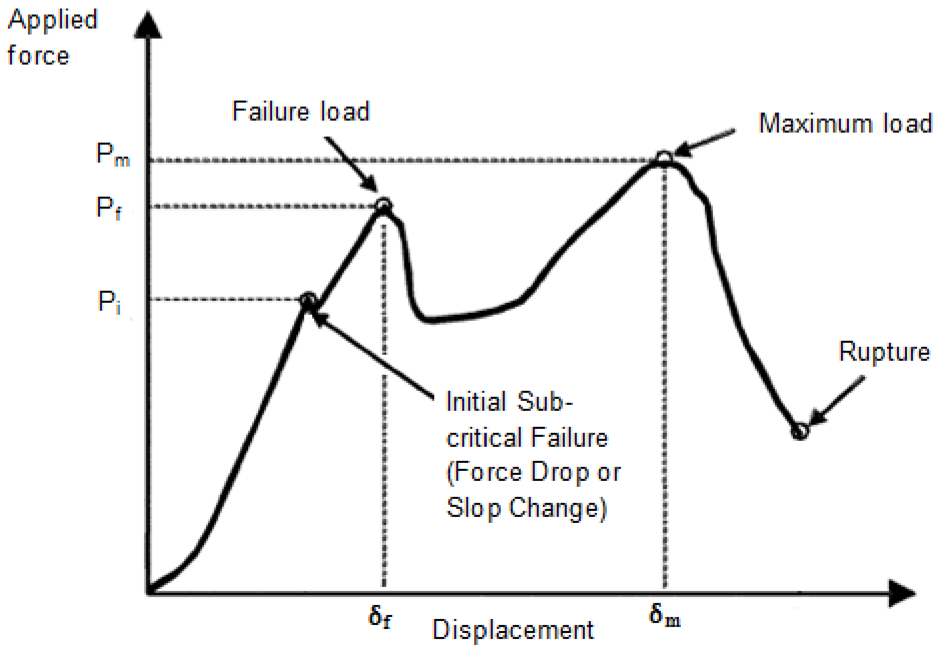

Figure 4.1: Typical idealized load-displacement behaviour of fastener pull-through [1]

The average failure load and displacement results for Tests ID 1 to 9 are summarized in Table 4.1. The failure load and displacement values were the average from five repeats.

The highest pull-through failure load “P_f” was 11,825 N with a standard deviation of 175 N for specimen P0.25-24LT (Test ID 6) and the lowest pull-through load was 2702 N with a standard deviation of 132 N for specimen P0.19-8LT (Test ID 1). For Test ID 10 to 15, the highest pull-through failure load “P_f” was 11,868 N with a standard deviation of 151 N for specimen P0.3-24HT (Test ID 15) and the lowest pull-through load was 6566 N with a standard deviation of 165 N for specimen P0.3-16HT (Test ID 12)

Test ID	Fastener shank diameter in [mm]	Laminate thickness [mm]	Clamping torque [Nm]	t/D	Pull-trough failure load “P_f” (Standard deviation) [N]	Pull-through failure load displacement “δ_f” (Standard deviation) [mm]
1	0.19 [4.76]	1.6	4	0.3	2702 (132)	2.14 (0.12)
2	0.19 [4.76]	3.2	4	0.7	6640 (212)	1.72 (0.02)
3	0.19 [4.76]	4.8	4	1.0	11476 (107)	1.77 (0.09)
4	0.25 [6.35]	1.6	4	0.3	3198 (131)	3.08 (0.35)
5	0.25 [6.35]	3.2	4	0.5	6700 (258)	2.35 (0.09)
6	0.25 [6.35]	4.8	4	0.8	11825 (175)	2.02 (0.05)
7	0.313 [7.94]	1.6	4	0.2	3407 (76)	3.41 (0.06)
8	0.313 [7.94]	3.2	4	0.4	6673 (119)	3.22 (0.09)
9	0.313 [7.94]	4.8	4	0.6	11650 (118)	2.57 (0.03)
10	0.313 [7.94]	3.2	0	0.4	6703 (105)	3.46 (0.07)
11	0.313 [7.94]	3.2	8	0.4	6720 (92)	3.12 (0.03)
12	0.313 [7.94]	3.2	12	0.4	6566 (165)	2.96 (0.05)
13	0.313 [7.94]	4.8	0	0.6	11465 (190)	2.65 (0.11)
14	0.313 [7.94]	4.8	8	0.6	11631 (165)	2.44 (0.09)
15	0.313 [7.94]	4.8	12	0.6	11868 (151)	2.37 (0.07)

Table 4.1: Average measured pull-through failure loads and displacements for the effect of: fastener diameter and laminate thickness (Test ID 1-9) and clamping torque (Test ID 10-15)

4.1.1 Load-Displacement Behaviour of Specimens

Different types of load-displacement behaviours were observed:

- Type I: Relatively thick specimens (Test ID 2, 3, 6, and 9 to 15) followed the typical load-displacement behaviour (Figure 4.2).
- Type II: 8-ply specimens and some of the 16-ply specimens (Test ID 1, 4, 7, 8) had a pull-through failure characterized by a succession of distinct minor load drops (<10% drop in load) and slope increasing (stiffening) before the minor load drops (Figure 4.3).
- Type III: Specimens of the 16-ply laminate bolted with the 0.25 inch shank diameter fastener (Test ID 5) had a pull-through failure characterized by a change in the load-displacement slope (Figure 4.4).

The failure load in Type I located at displacement "δ_f" according to ASTM standard. The location of the failure load in Type II and Type III was defined be the point where the slope changed.

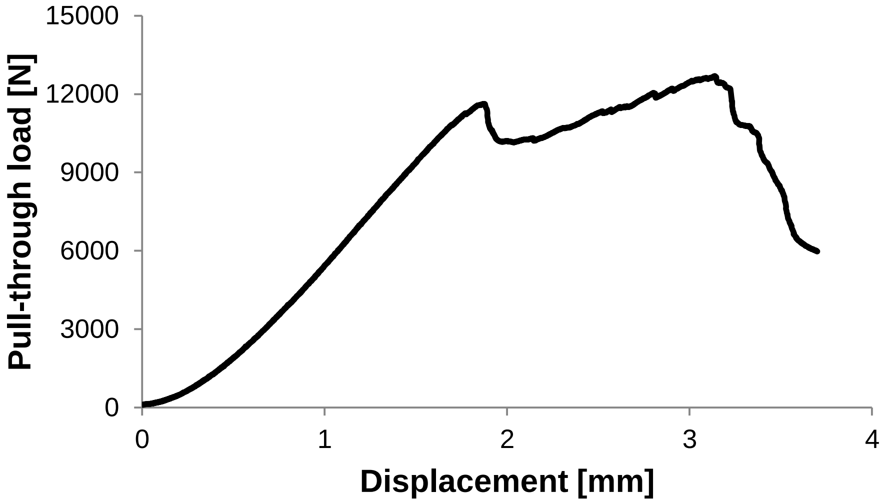

Figure 4.2: Type I load-displacement behaviour of a thick specimen (P0.19-24LT)

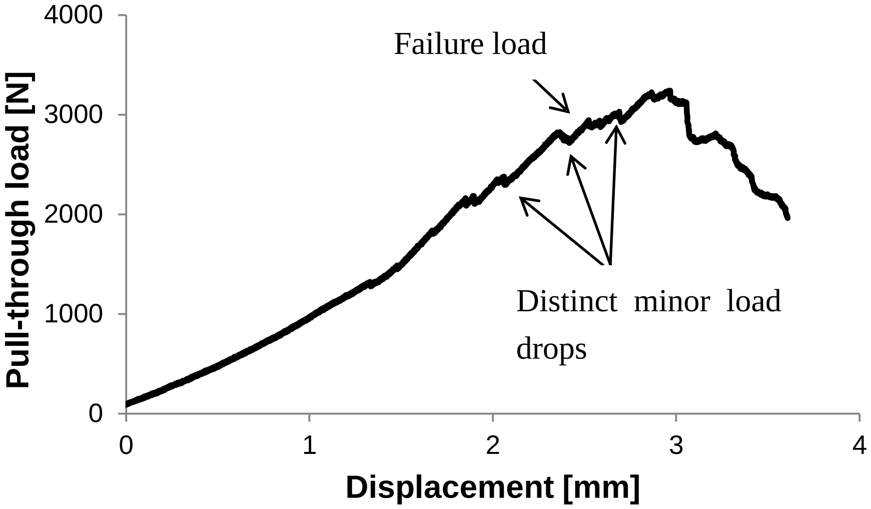

Figure 4.3: Type II load-displacement behaviour of an 8-ply specimen (P0.3-8LT), the pull-through failure characterized by a succession of small load drops

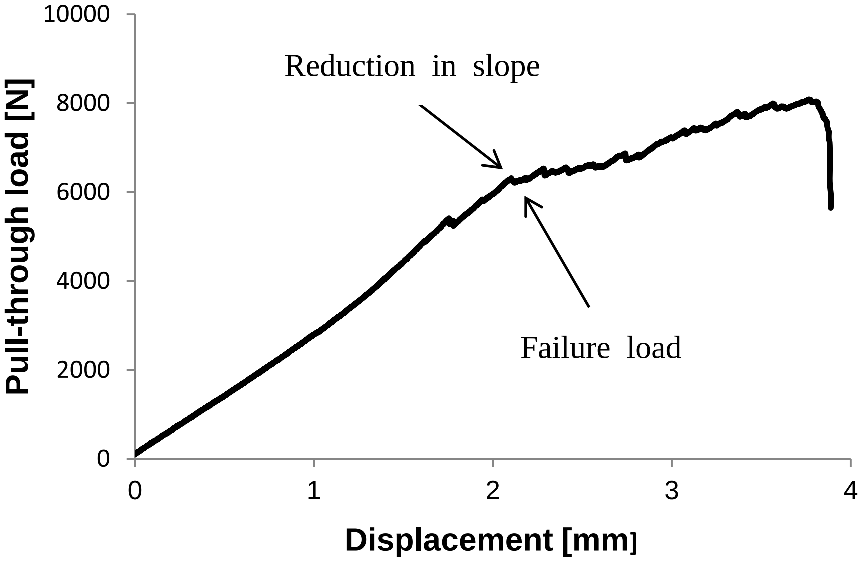

Figure 4.4: Type III load-displacement behaviour of a 16-ply specimen (P0.25-16LT), the pull-through failure characterized by a change in the slopes of the load-displacement curve

To describe the trend of the change in load-displacement curves, parameter "*t/D*" was introduced, which was the laminate thickness to fastener shank diameter ratio. This ratio ranged from 0.2 to 1.0 for the specimens tested in this work (Table 4.2). For $t/D > 0.5$, the load-displacement behaviours followed Type I as shown in Figure 4.2. For $t/D < 0.5$, the load-displacement behaviours followed Type II as show in Figure 4.3. The load-displacement behaviours followed Type III when ratio t/D equalled to 0.5, Figure 4.5 demonstrated the changes of the load-displacement curves for specimens of different *t/D* ratio.

D / t	0.19”	0.25”	0.313”
8-Ply	0.34	0.25	0.20
16-Ply	0.67	0.50	0.40
24-Ply	1.0	0.76	0.60

Table 4.2: *t/D* ratio of each specimen configuration

The reproducibility of the load-displacement behaviour was good except for the Type III specimens (Figure 4.6). The “*t/D*” ratio was 0.5 and the standard deviation of the average failure load was the highest (258 N). The stiffness of Sample 3 was reduced at displacement of 2.1 mm without any distinct drops in load whereas sample 4 consisted of smaller decaying peeks. There was a different behaviour for Sample 5 that a major drop (>10% drop in load) occurred at displacement of 2.8 mm after the slope reduction (at displacement of 2.1 mm). In another word, the behaviour of this specimen combined three types of load-displacement behaviours. Thus, the transition point of the three types of load-displacement behaviour is at $t/D = 0.5$.

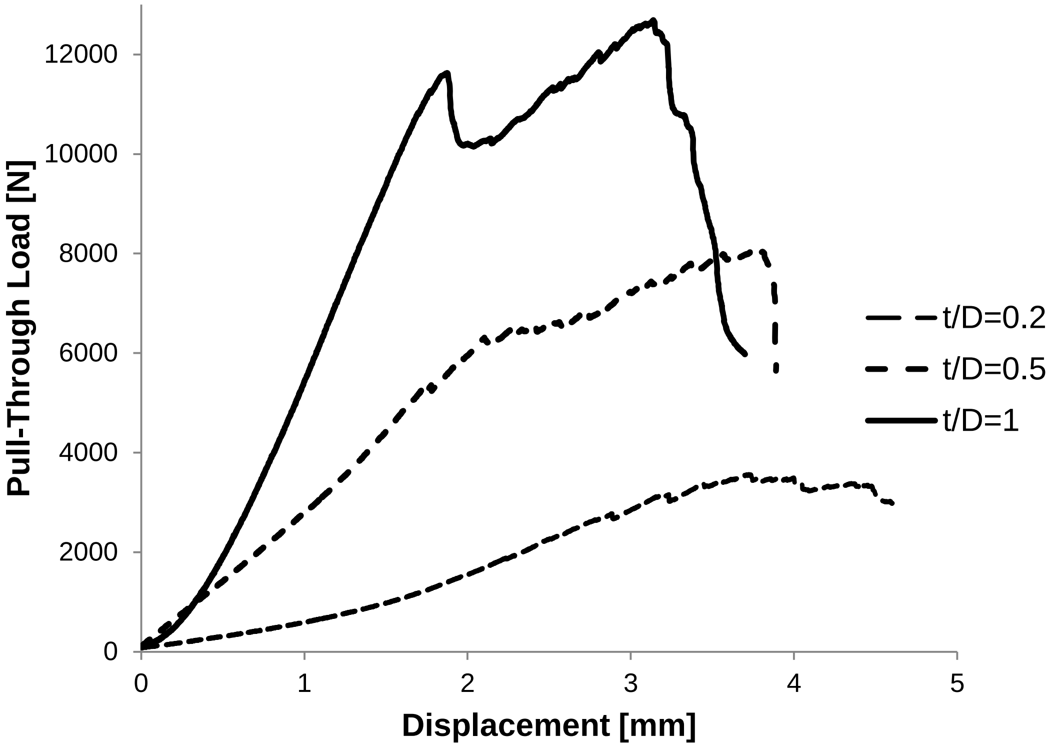

Figure 4.5: Comparison of load-displacement behaviour for specimens with different t/D

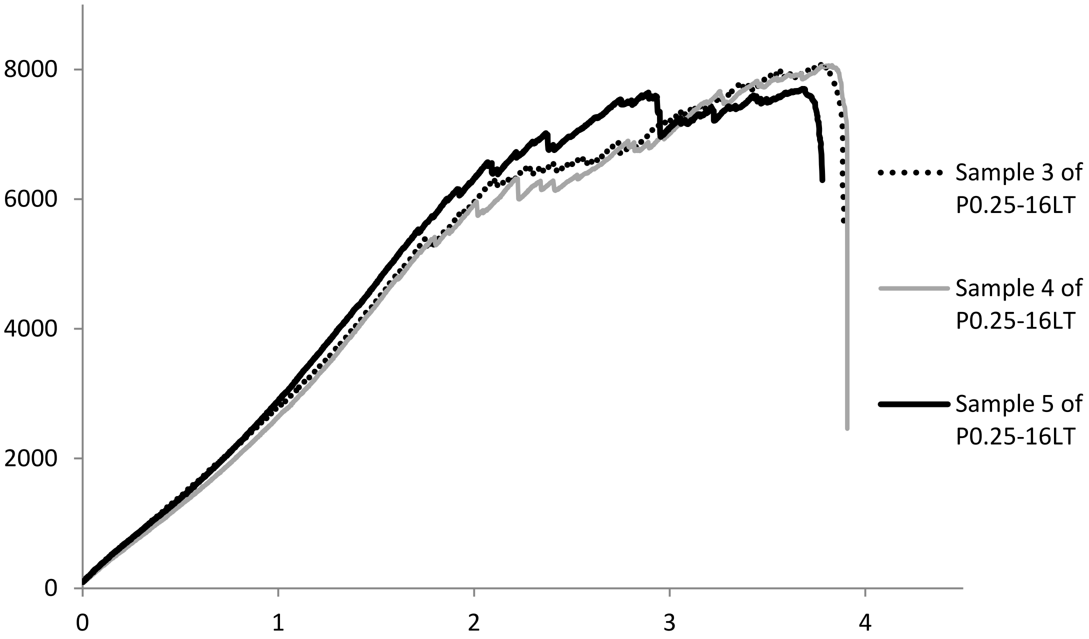

Figure 4.6: Load-displacement behaviour of three specimens for Test ID 5 (P0.25-16LT) of *t/D = 0.5*

In this section, the experimentally obtained fastener pull-through strength were presented A new parameter *t/D* was introduced to categorize the types of the load-displacement behaviour. In order to understand the causes of the load-displacement behaviours and the failure mode for each type, the results of numerical modelling will be discussed in the following section.

4.2 FINITE ELEMENT ANALYSIS

The finite element models showed that two flexure deformations were generated in the cross-section of the laminate by the pull-through force. Figure 4.7 shows a typical flexure deformation plot using specimen P0.3-8LT as an example. The first flexure was found under the edge of the fastener head (Area 1). The second flexure was located to the left of the fixture support of the laminate (Area 2). The curvature of the flexure at Area 1 is much larger than the curvature of the flexure at Area 2. In addition, all the numerical models showed that the local maximum tension or compression at Area 1 was larger than the local maximum tension or compression at Area 2 by approximately 100%. For this reason, this study focused on Area 1 only. However, it is important to note that due to the flexures, the bottom-left corner of the laminate (Point A in Figure 4.8) was moving toward the fastener shank and generated the global maximum compressive stress at Point A.

This thesis focused on three important stress components for the pull-through behaviour [19] in Area 1: the fibre direction (σ_{11}), transverse (σ_{22}) and transverse shear (τ_{13}) stresses (Figure 4.8).

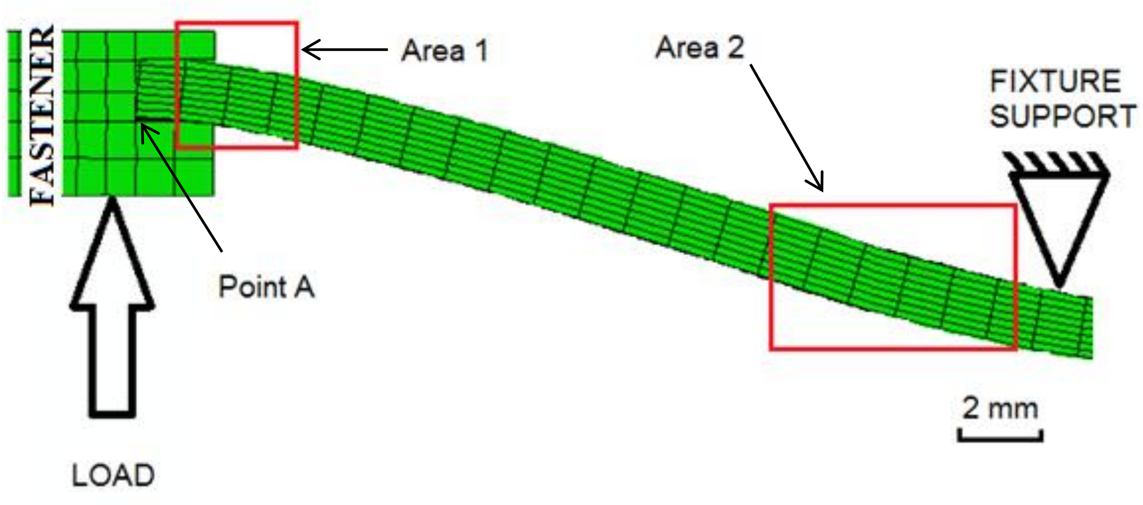

Figure 4.7: Typical flexure deformation plot (scaled) of the laminate under fastener pull-through load. Area 1 and 2 show two flexure detected and Point A indicates the location of the global maximum compressive stress

The maximum compressive and tensile stresses of σ_{11} and σ_{22}, and the maximum shear stress τ_{13} in Area 1 were drawn from each finite element model. Summarized results are presented in Table 4.2. The highest compressive and tensile fibre direction stresses σ_{11} and the highest compressive and tensile transverse stresses σ_{22} were found in the same specimen P0.3-08nt. The highest compressive fibre direction stress σ_{11} was 1351 MPa. The highest tensile fibre direction stress σ_{11} was 1217 MPa. The highest compressive transverse stress σ_{22} was 1319 MPa. The highest tensile stress σ_{22} was 1428 MPa. The highest shear stress τ_{13} was 98 MPa for specimen P0.19-24NT.

The distribution of the three stress components σ_{11} and σ_{22} and τ_{13} was discussed in the following section using examples of each *t/D* range. Specimens P0.19-8NT (*t/D = 0.34*), P0.25-16NT (*t/D = 0.5*) and P0.25-24NT (*t/D = 0.76*) were chosen to represent the three *t/D* ranges (three types of load-displacement behaviour).

Model ID	Specimen Name	t/D	σ_{11} (MPa)		σ_{22} (MPa)		τ_{13} (MPa)
			Maximum Compression	Maximum Tension	Maximum Compression	Maximum Tension	
1	P0.3-08NT	0.20	1351	1217	1319	1428	83
2	P0.25-08NT	0.25	1160	1070	1126	1240	88
3	P0.19-08NT	0.34	990	986	962	914	81
4	P0.3-16NT	0.40	784	834	755	986	78
5	P0.25-16NT	0.50	821	787	797	937	86
6	P0.3-24NT	0.60	814	700	694	890	92
7	P0.19-16NT	0.67	790	732	600	863	94
8	P0.25-24NT	0.76	517	637	584	750	94
9	P0.19-24NT	1.0	522	566	589	674	98

Table 4.3 Maximum compressive and tensile stresses of σ11 and σ22, and maximum interlaminar shear stress τ13 of numerical models. Unites of stress MPa

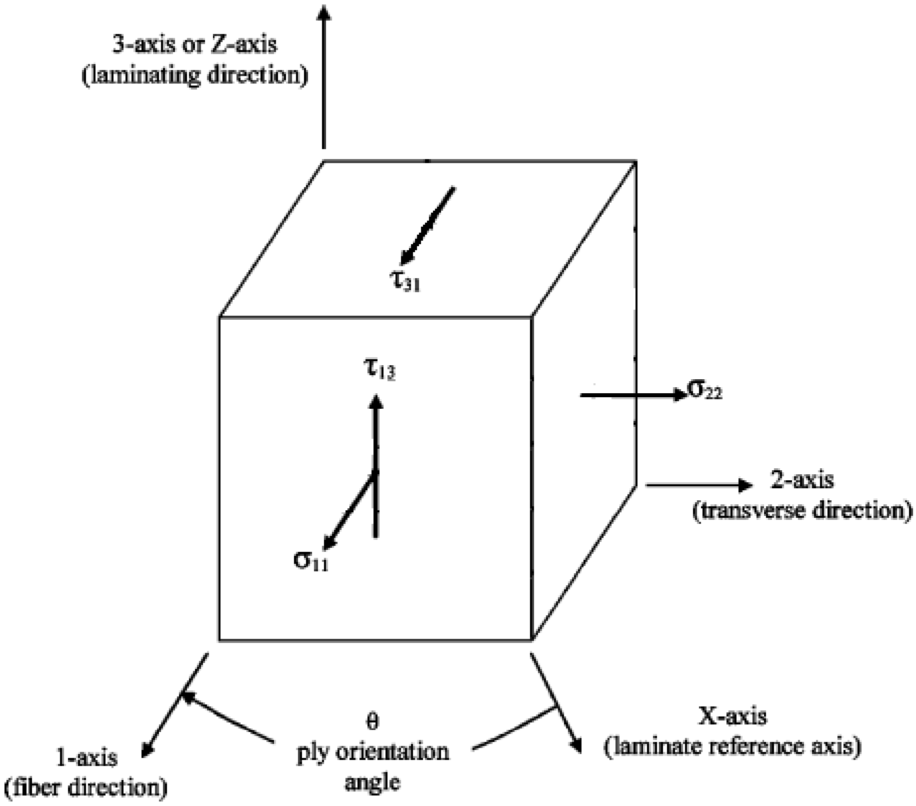
3-axis or Z-axis
(laminating direction)
τ_{31}
τ_{13}
σ_{22}
2-axis
(transverse direction)
σ_{11}
θ
ply orientation
angle
X-axis
(laminate reference axis)
1-axis
(fiber direction)

Figure 4.8: Important stress components for the pull-through behaviour: the fibre direction (σ_{11}), transverse (σ_{22}) and transverse shear (τ_{13}) stresses, showed in a 3-D stress element diagram

4.2.1 Fibre direction Stress σ_{11}

The flexure at Area 1 generated fibre direction compressive and tensile stresses. Plies near the fastener head (bottom plies in Figure 4.9, 4.10 and 4.11) were subjected to compression and plies near the nut side (top plies in Figure 4.9, 4.10 and 4.11) were subjected to tension. The maximum compressive stress at Area 1 for specimen P0.19-8NT ($t/D=0.34$), P0.25-16NT ($t/D=0.50$) and P0.25-24NT ($t/D=0.76$) was 990 MPa, 821 MPa and 517 MPa, respectively. The maximum tensile stress at Area 1 for specimens P0.19-8NT ($t/D=0.34$), P0.25-16NT ($t/D=0.50$) and P0.25-24NT ($t/D=0.76$) was 986 MPa, 788 MPa and 638 MPa, respectively. Compressive stresses were found to have larger magnitude compared to tensile stresses, as the plies in compression were also subjected to the fibre direction compression from the fastener shank. The results also showed a trend that the magnitude of the fibre direction stress σ_{11} decreased as the thickness of the specimen laminates increased. Therefore, thinner specimens had a higher risk of fibre direction compressive and/or tensile failure. Figures 4.9, 4.10 and 4.11 show the fibre direction stress contour for specimens P0.19-8LT, P0.25-16LT and P0.25-24LT.

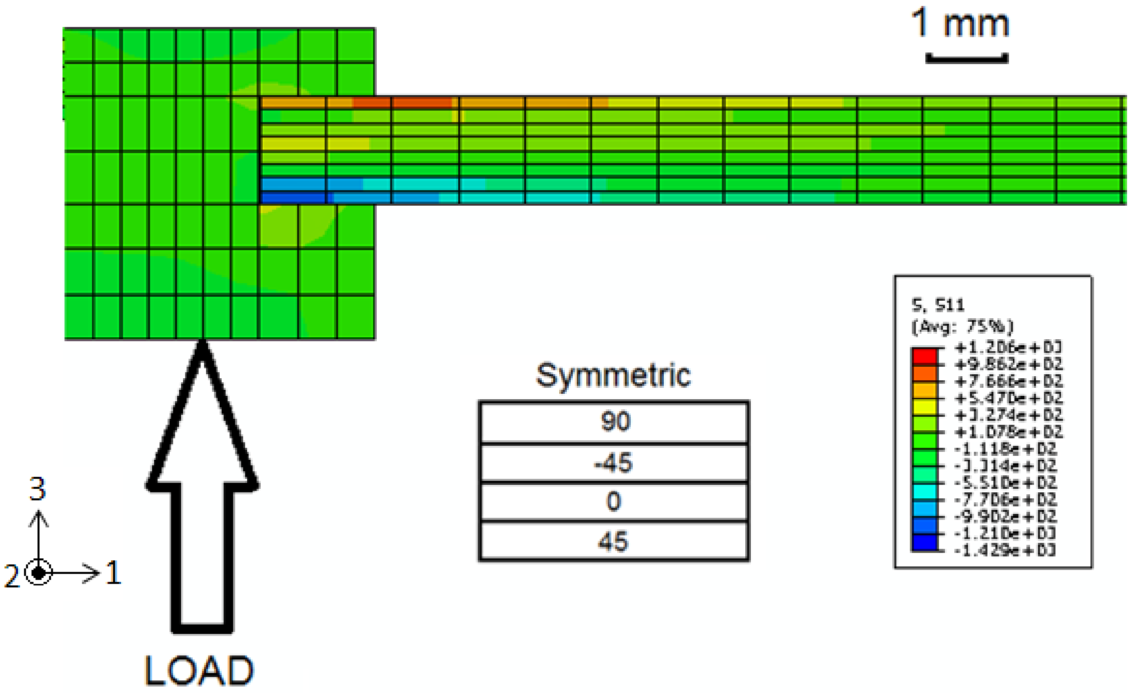

Figure 4.9: Contour plot of σ_{11} stress for specimen P0.19-8NT with *t/D = 0.34*. Unites of stress MPa

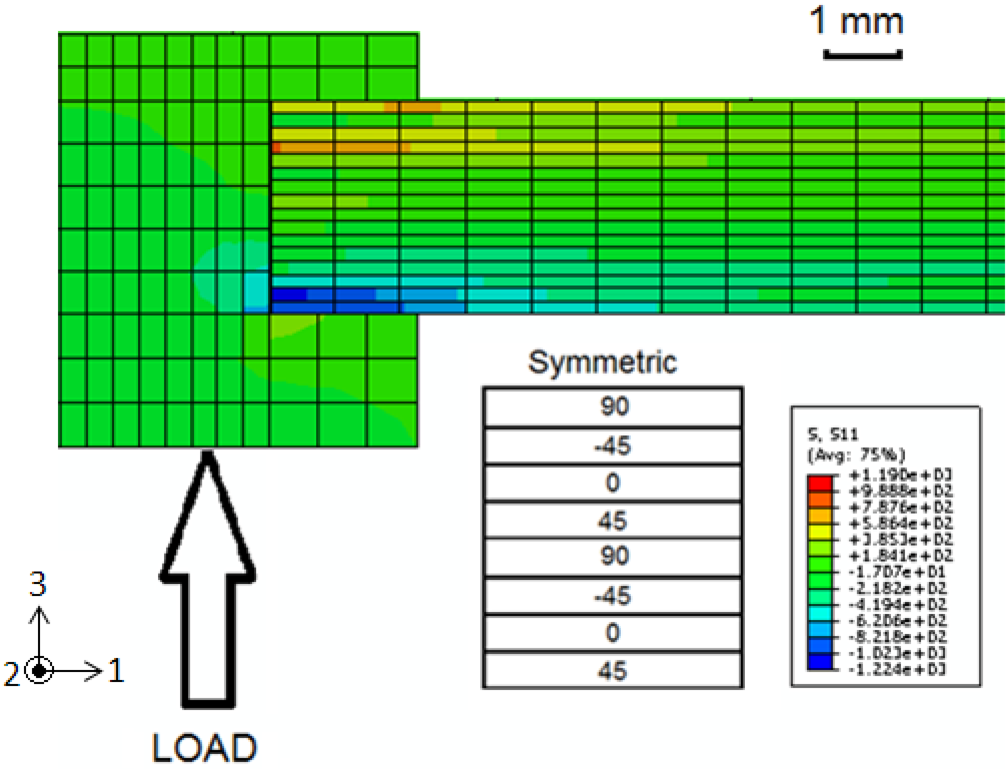

Figure 4.10: Contour plot of σ_{11} stress for specimen P0.25-16NT with *t/D = 0.5*. Unites of stress MPa

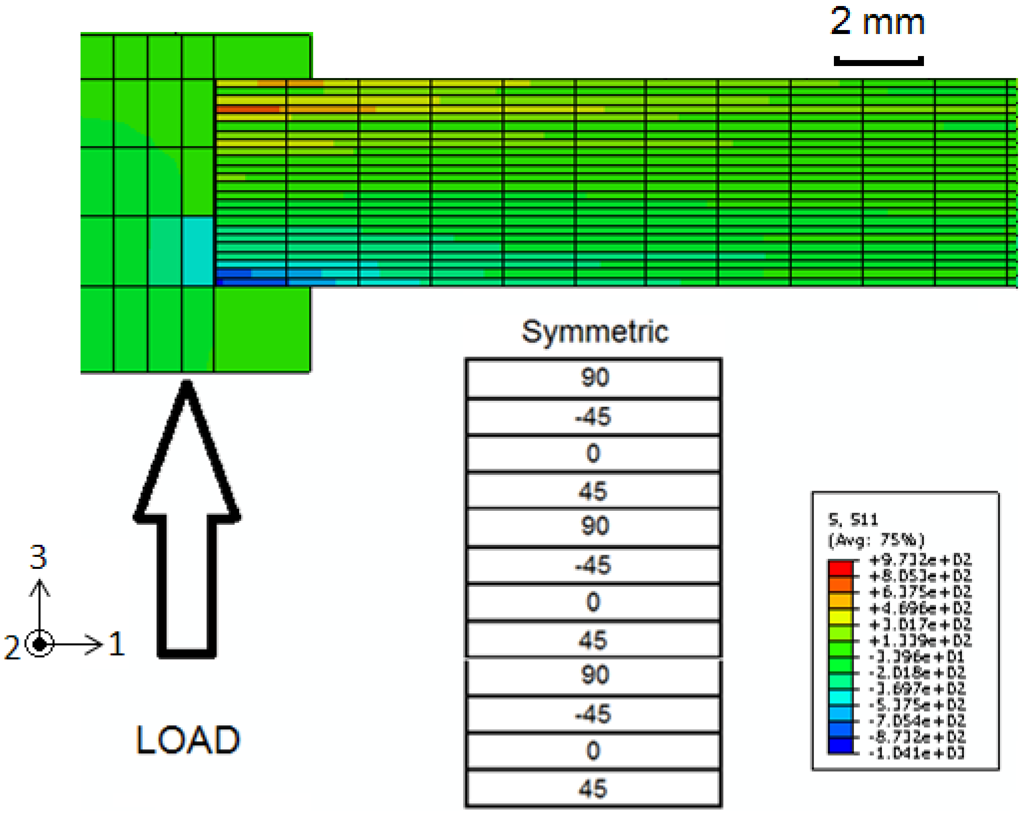

Figure 4.11: Contour plot of σ_{11} stress for specimen P0.25-24NT with *t/D = 0.76*. Unites of stress MPa

4.2.2 Transverse Stress σ_{22}

Figure 4.12, 4.13 and 4.14 show the transverse stress contour for specimens with *t/D* = 0.34, 0.5 and 0.76. The results of transverse stress distribution showed that plies near the fastener head (bottom plies in Figure 4.12, 4.13 and 4.14) were subjected to compression and plies near the nut side (top plies in Figure 4.12, 4.13 and 4.14) were subjected to tension. The maximum compressive stress at Area 1 for specimen P0.19-8NT (*t/D=0.34*), P0.25-16NT (*t/D=0.50*) and P0.25-24NT (*t/D=0.76*) was 962 MPa, 797 MPa and 584 MPa, respectively. The maximum tensile stress at Area 1 for specimen P0.19-8NT (*t/D=0.34*), P0.25-16NT (*t/D=0.50*) and P0.25-24NT (*t/D=0.76*) was 914 MPa, 937MPa and 750 MPa, respectively. The distribution of the transverse stress σ_{22} was different from the fibre direction stress σ_{11} in two ways. First, the average magnitude of the maximum tensile stress σ_{22} of all models was larger by 17% than that of the in-plan stress $\sigma_{11;}$ whereas the average magnitude of the maximum compressive stress σ_{22} of all models was smaller by 4% than that of the in-plan stress σ_{11}. Second, it was observed in Figures 4.12, 4.13 and 4.14, the area under tension for transverse stress σ_{22} in Area 1 was larger than that of the fibre direction stress σ_{11}; whereas the area under compression for transverse stress σ_{22} in Area 1 was smaller than that of the fibre direction stress σ_{11}. Therefore, the neutral axis of the flexure stresses was shifted towards the plies in compression, particularly for thin specimens ($t \leq 1.6$ mm). The differences in stress magnitude and distribution between the transverse stress σ_{22} and the fibre direction stress σ_{11} can be explained by the bulging effect of the specimen caused by the out-of-plane load. The bulge on the specimen surface induced additional tensile stress in the tangential direction around the fastener hole. Therefore, both magnitude of the tensile stress and the area under tension were increased [35].

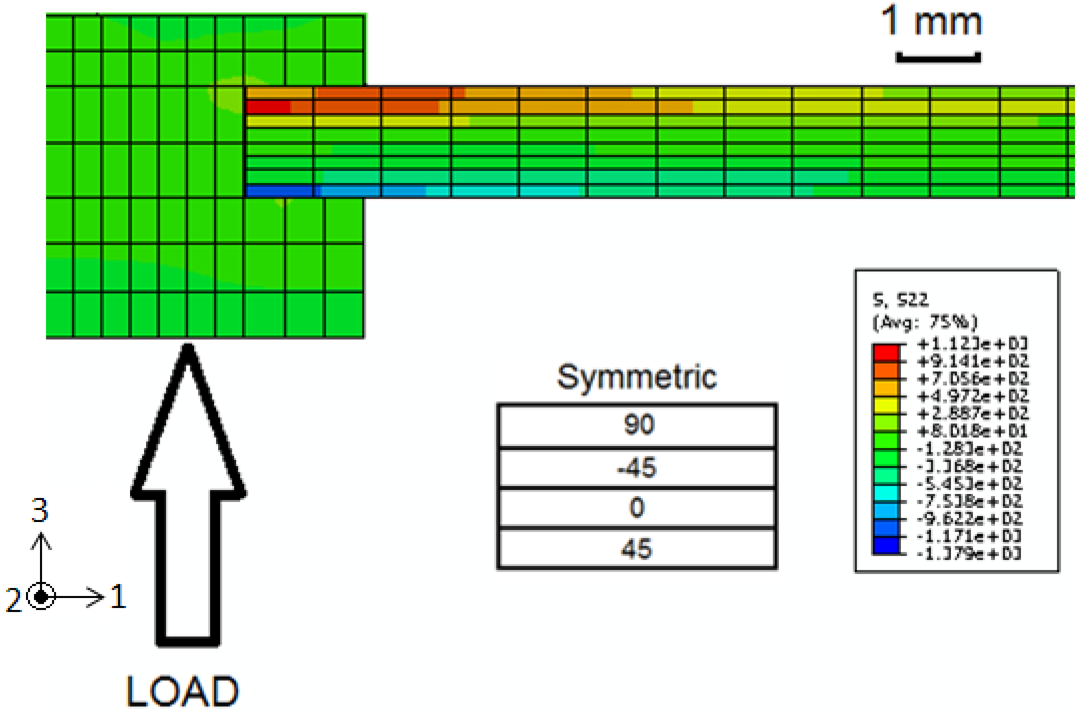
1 mm
Symmetric
90
-45
0
45
S, S22
(Avg: 75%)
+1.123e+03
+9.141e+02
+7.056e+02
+4.972e+02
+2.887e+02
+8.018e+01
-1.283e+02
-3.368e+02
-5.453e+02
-7.538e+02
-9.622e+02
-1.171e+03
-1.379e+03
3
2
1
LOAD

Figure 4.12: Contour plot of σ_{22} stress for specimen P0.19-8NT with *t/D = 0.34*. Unites of stress MPa

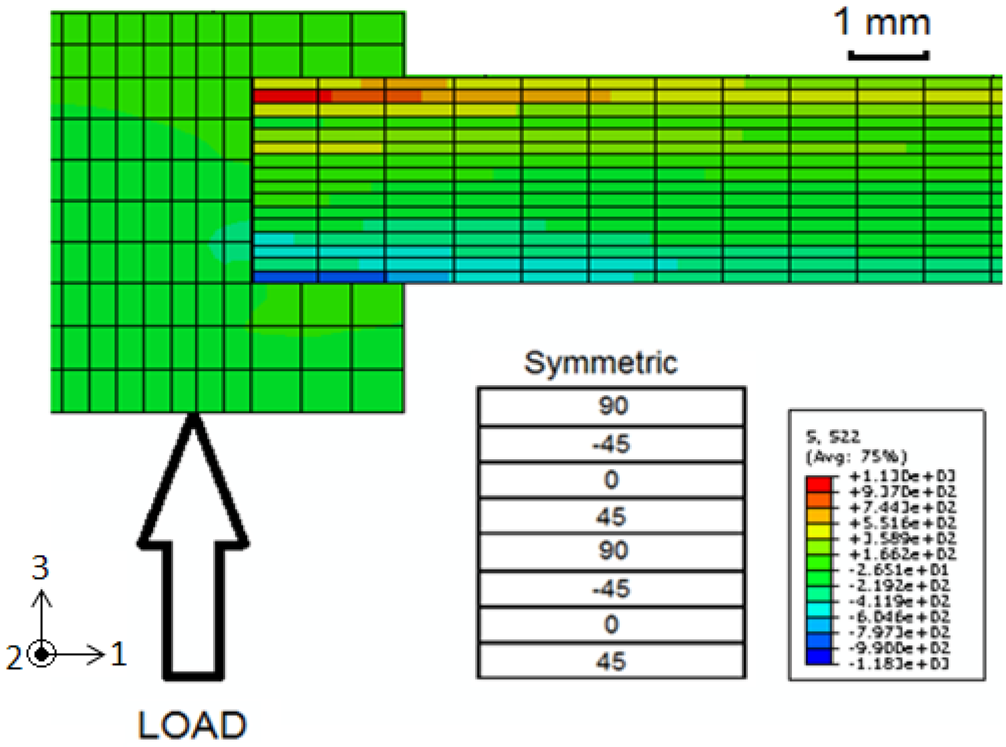
1 mm
Symmetric
90
-45
0
45
90
-45
0
45
S, S22
(Avg: 75%)
+1.130e+03
+9.370e+02
+7.443e+02
+5.516e+02
+3.589e+02
+1.662e+02
-2.651e+01
-2.192e+02
-4.119e+02
-6.046e+02
-7.973e+02
-9.900e+02
-1.183e+03
3
2
1
LOAD

Figure 4.13: Contour plot of σ_{22} stress for specimen P0.25-16NT with *t/D = 0.5*. Unites of stress MPa

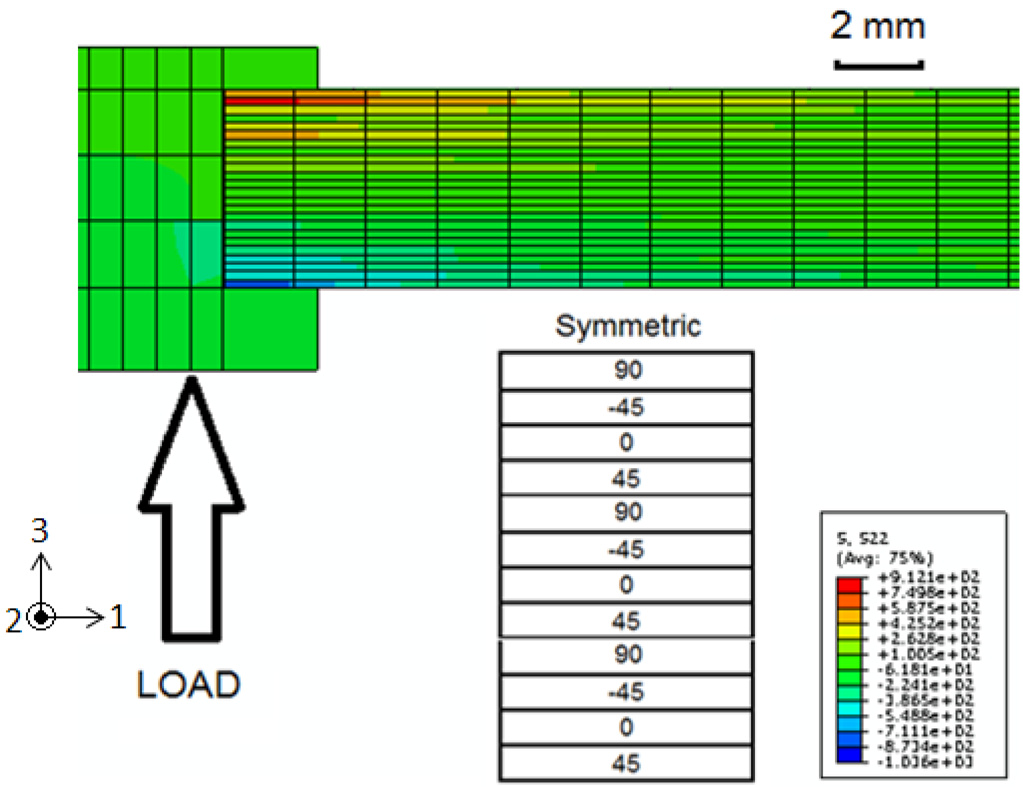
2 mm
Symmetric
90
-45
0
45
90
-45
0
45
90
-45
0
45
3
2
1
LOAD
S, S22
(Avg: 75%)
+9.121e+02
+7.498e+02
+5.875e+02
+4.252e+02
+2.628e+02
+1.005e+02
-6.181e+01
-2.241e+02
-3.865e+02
-5.488e+02
-7.111e+02
-8.734e+02
-1.036e+03

Figure 4.14: Contour plot of σ_{22} stress for specimen P0.25-24NT with *t/D = 0.76*. Unites of stress MPa

4.2.3 Interlaminar Shear Stress

Figures 4.15, 4.16 and 4.17 show the interlaminar shear stress distributions of specimens with *t/D* = 0.34, 0.5 and 0.76. The magnitude of the maximum shear stresses in the three figures was 81MPa, 86MPa and 94MPa, respectively. Two general trends were observed. The magnitude of the maximum shear stresses increased as *t/D* increased. The pull-through loading produced a maximum interlaminar shear stress at the mid-plies resembling a parabolic shape distribution through the thickness. The upper and bottom surface didn’t carry shear stresses. The magnitude of the interlaminar shear stresses decreased along the radial direction of the laminate toward the edge. For *t/D > 0.5,* maximum shear stress was observed in the area under the fastener head and dispersed towards the mid-plies at an angle of approximately 45 degree with the laminate surface. This distribution pattern represented the shear slip planes. Such distribution pattern was not obvious for *t/D* ≤ *0.5*.

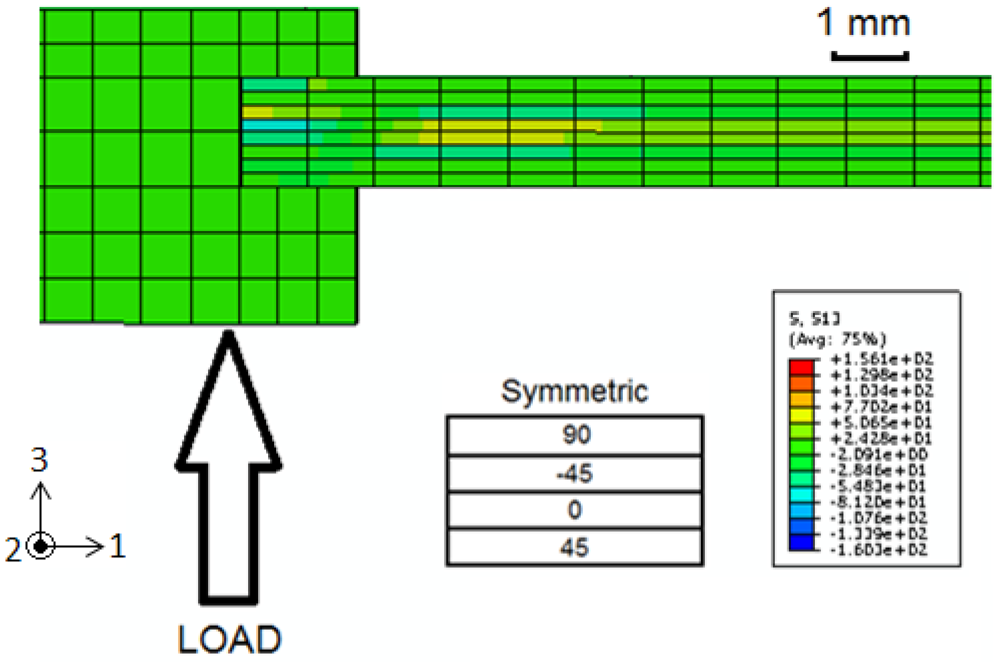
1 mm
3
2
1
LOAD
Symmetric
90
-45
0
45
S, S13
(Avg: 75%)
+1.561e+02
+1.298e+02
+1.034e+02
+7.702e+01
+5.065e+01
+2.428e+01
-2.091e+00
-2.846e+01
-5.483e+01
-8.120e+01
-1.076e+02
-1.339e+02
-1.603e+02

Figure 4.15: Contour plot of the interlaminar shear stress for specimen with *t/D* = *0.34*. Unites of stress MPa

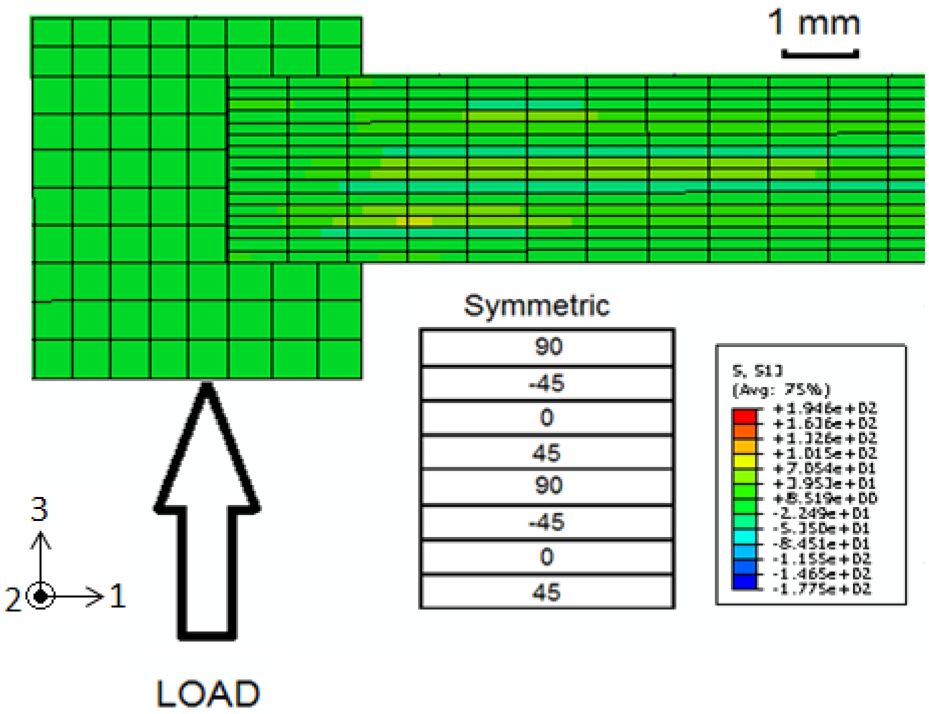

Figure 4.16: Contour plot of the interlaminar shear stress for specimen with *t/D = 0.5*. Unites of stress MPa

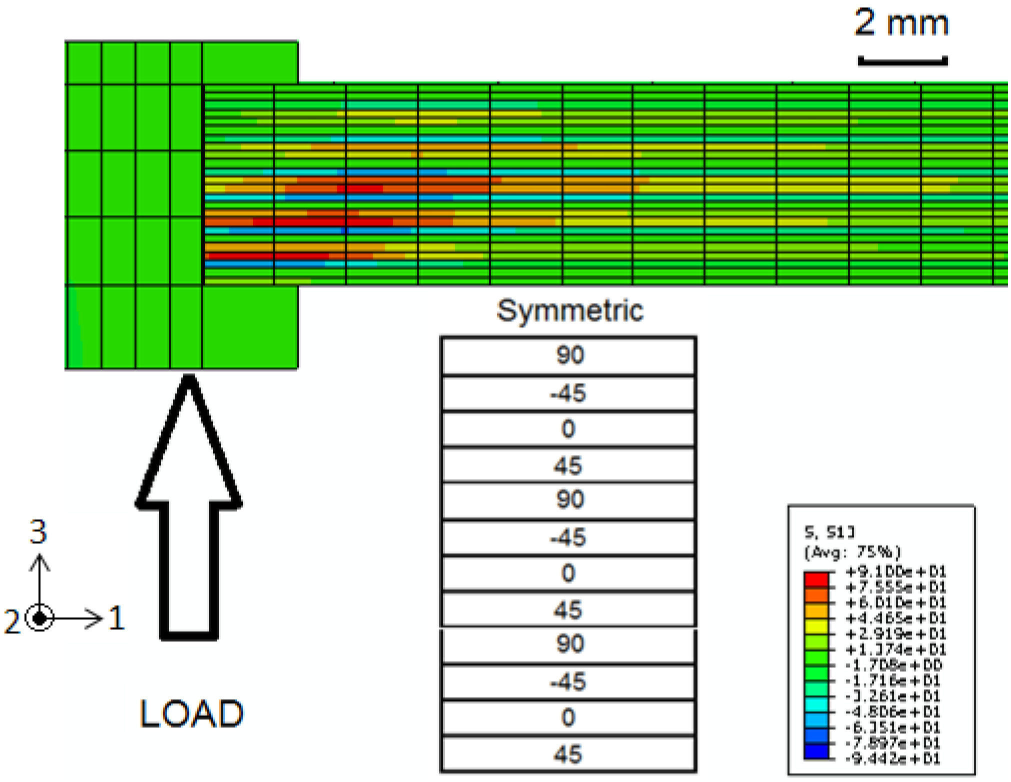

Figure 4.17: Contour plot of the interlaminar shear stress for specimen with *t/D = 0.76*. Unites of stress MPa

4.2.4 Maximum Principal Stress

The maximum principle stress distribution was also investigated. Figures 4.18, 4.19 and 4.20 present the maximum principle stress distributions of specimens with *t/D* = 0.34, 0.5 and 0.76 and the magnitude of the maximum principal stresses were 134MPa, 154MPa and 256MPa, respectively. For specimen with *t/D= 0.34*, the critical region under compression was located under the edge of the fastener head. For specimen with *t/D = 0*.5, the critical region was under compression as well compared to specimen with *t/D= 0.34*. This region was under the fastener head but was horizontally shifted towards the fastener shank. For specimen with *t/D = 0.76*, the critical region shifted to the corner of the fastener head and shank and was still under compression. The different locations of the maximum principal stress resulted in different locations of the initial matrix failure.

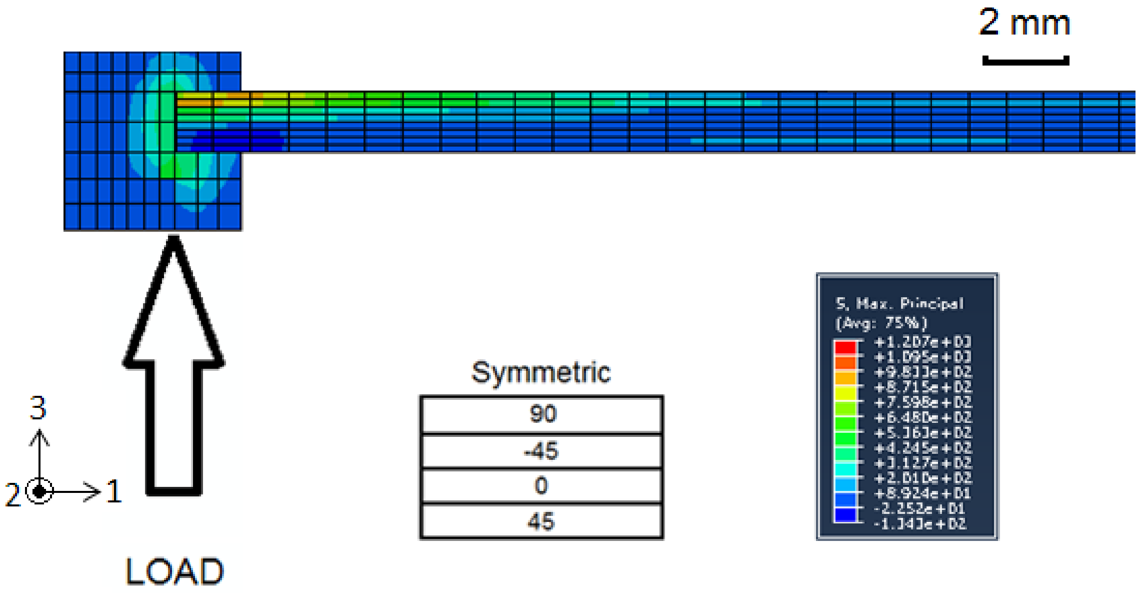
2 mm
3
2
1
LOAD
Symmetric
90
-45
0
45
S, Max. Principal
(Avg: 75%)
+1.207e+03
+1.095e+03
+9.833e+02
+8.715e+02
+7.598e+02
+6.480e+02
+5.363e+02
+4.245e+02
+3.127e+02
+2.010e+02
+8.924e+01
-2.252e+01
-1.343e+02

Figure 4.18: Contour plot of the maximum principle stress distribution for specimen with *t/D = 0.34*. Unites of stress MPa

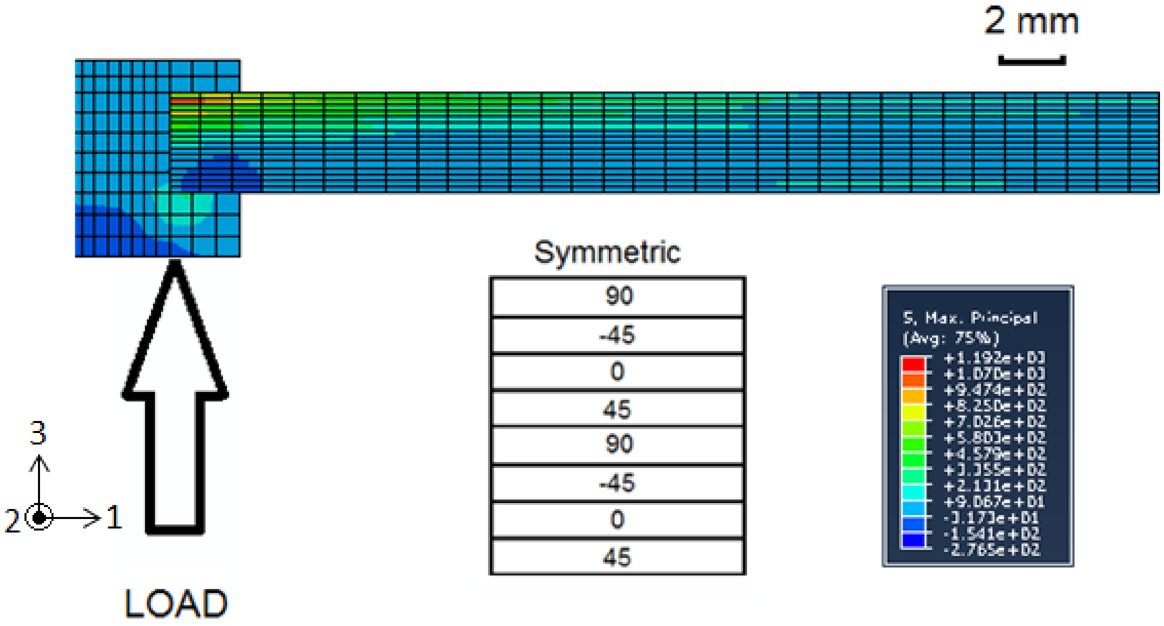

Figure 4.19: Contour plot of the maximum principle stress distribution for specimen with *t/D = 0.5*. Unites of stress MPa

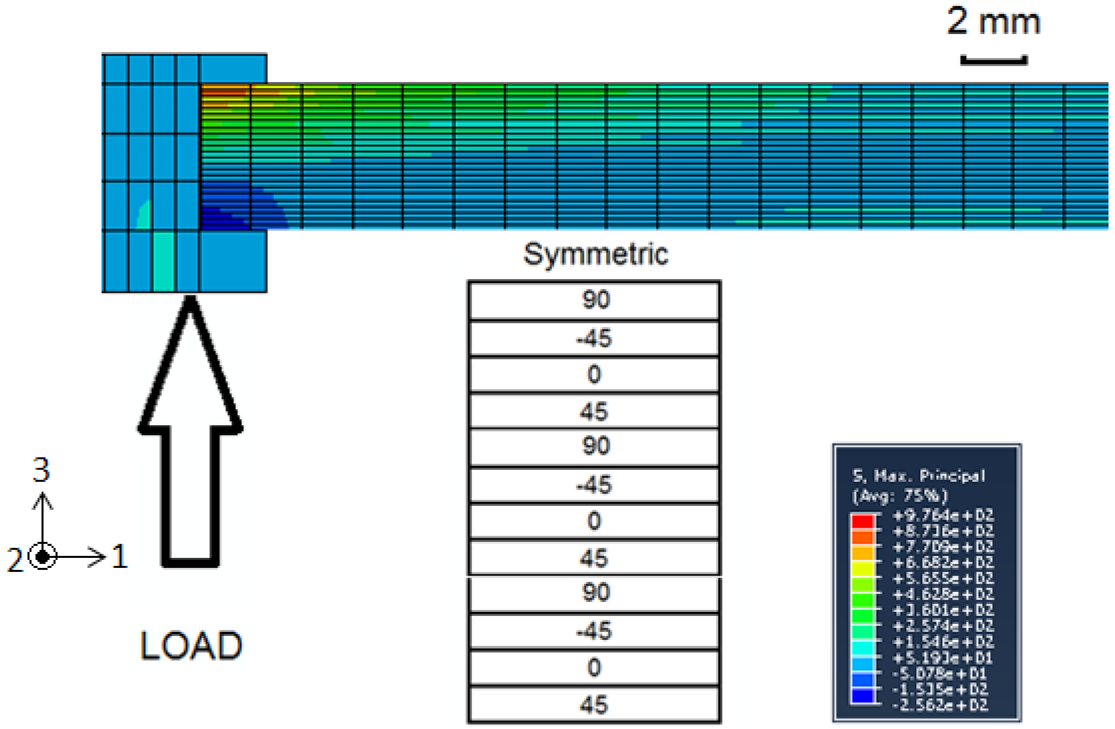

Figure 4.20: Contour plot of the maximum principle stress distribution for specimen with *t/D = 0.76*. Unites of stress MPa

Finite element models provided a better understanding of the fastener pull-through mechanisms. The experimental testing scenario was simulated with numerical models under the same loading condition. Three important stress components σ_{11}, σ_{22} and τ_{13} were investigated and their distributions were analyzed. Two general trends of the distributions were summarized as follows:

1. Fibre direction and transverse stresses decreased as *t/D* increased.
2. Interlaminar shear stress increased as *t/D* increased.

The following section will discuss the failure mode using the results from both experimental testing and numerical models.

4.3 FAILURE MODE ANALYSIS

The failure mode of the specimens was determined by two methods: visual inspection and analysis of results from numerical model. Results from both methods were compared and discussed.

4.3.1 Specimen Inspection

Both external and internal specimen damage inspections were conducted. A number of specimens were unloaded from selected points along the load-displacement curve in order to study the progression of damage. The selected points shown in Figure 4.21 corresponded to: before the failure load (point A), right after the failure load (point B), after the maximum load (point C) and after a load drop of 30% of maximum load (point D). The specimens were then cross sectioned through the center of fastener hole and polished for visual and microscopic inspections.

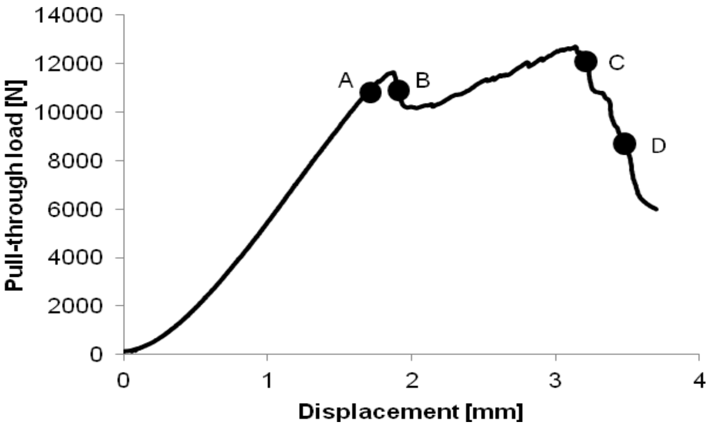

Figure 4.21: Points selected along the load-displacement curve (P0.19-24LT) for interrupted pull-through tests and specimen damage inspection

Visual examinations (Figure 4.22) showed that a fastener head indentation on the surface was visible at all selected points. At points A and B, the damage was limited to a minor indentation under the protruding fastener head. There was no visible damage found on the back side of the specimen. However, at point C, the fastener head penetrated into the surface plies of the specimens. A volcano shape bulge appeared around the fastener hole on the back side. At point D, the fastener head was embedded in the specimen and plies on the back side began to separate in the form of interlaminar cracking.

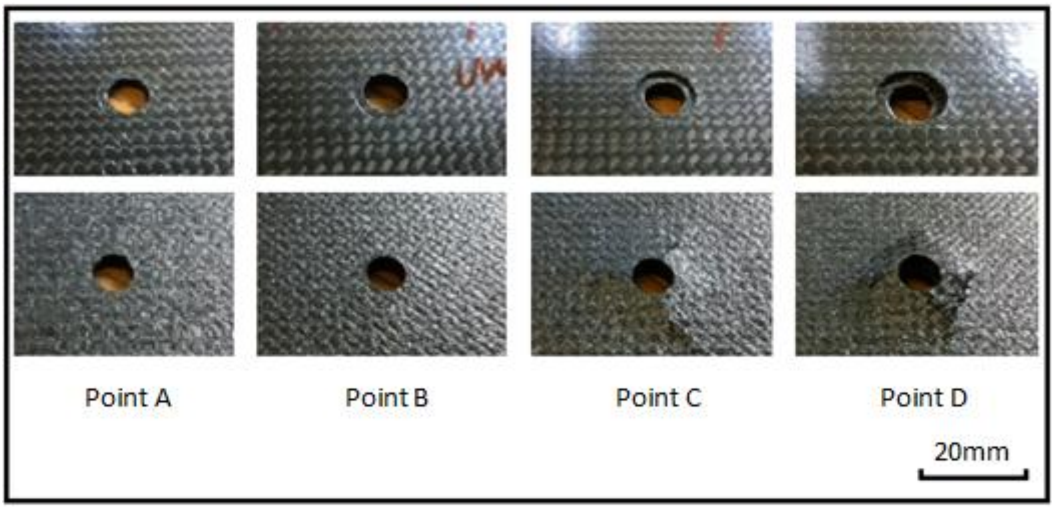

Figure 4.22: Photos of surface damage of selected points from specimen series P0.3-24LT, contact area under fastener head (top) and damage near fastener hole on the opposite side of the contact surface (bottom)

No visible damages were found due to machining. However, risk of having voids at or near the fastener hole boundary may increase stress concentration factor and thus initiate matrix cracking or delamination. Specimens containing voids at or near that region may experience earlier initial sub-critical failure. Figure 4.23 shows a void that was drilled through during machining.

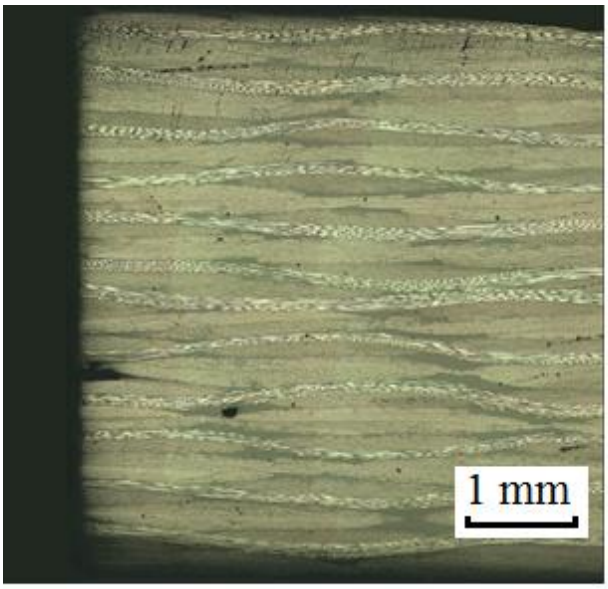

Figure 4.23: Voids at and near fastener hole boundary, right hand side of the fastener hole

Microscopic images showed that the damage was axi-symmetric near the fastener hole. No major damage was observed prior to the failure force. Fibre tows under the protruding head were bent in the immediate vicinity of the fastener head (Figure 4.24). Minor intralaminar delaminations were also found. Numerical analysis (Section 4.2.4) showed that the region under the fastener head was subjected to the maximum compressive principle stress and the parabolic distributed maximum interlaminar shear stress started from the plies under the upper surface.

After the first failure load, a major delamination near the transverse centreline was observed for specimens with $t/D > 0.5$. This delamination was caused by interlaminar shear stresses generated by the pull-through force. It started from the edge of fastener head projection and extended in the radial direction away from the fastener hole. The crack was generally discontinued and connected by intralaminar cracking as shown in

Figure 4.25. Numerical analysis (Section 4.2.3) showed that the maximum interlaminar shear stresses were found in the mid-plies for all configurations. However, at the failure load, the maximum interlaminar shear stresses of thin specimens *(t/D < 0.5)* were much smaller than the specimens with *t/D > 0.5*. Both experimental and numerical results indicated that the interlaminar cracking was the mode of failure.

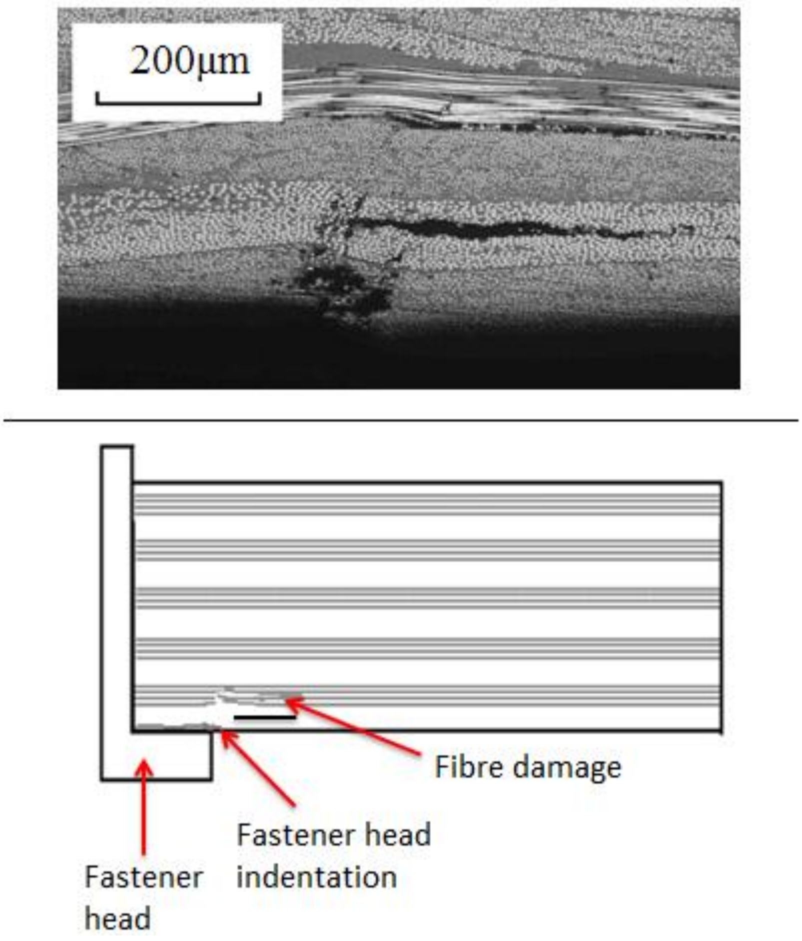

Figure 4.24: (Top) Micrograph scratch of specimen (Test ID 3) unloaded prior to the failure force (point A in Figure 4.22). (Bottom) A schematic description of the damage at point A

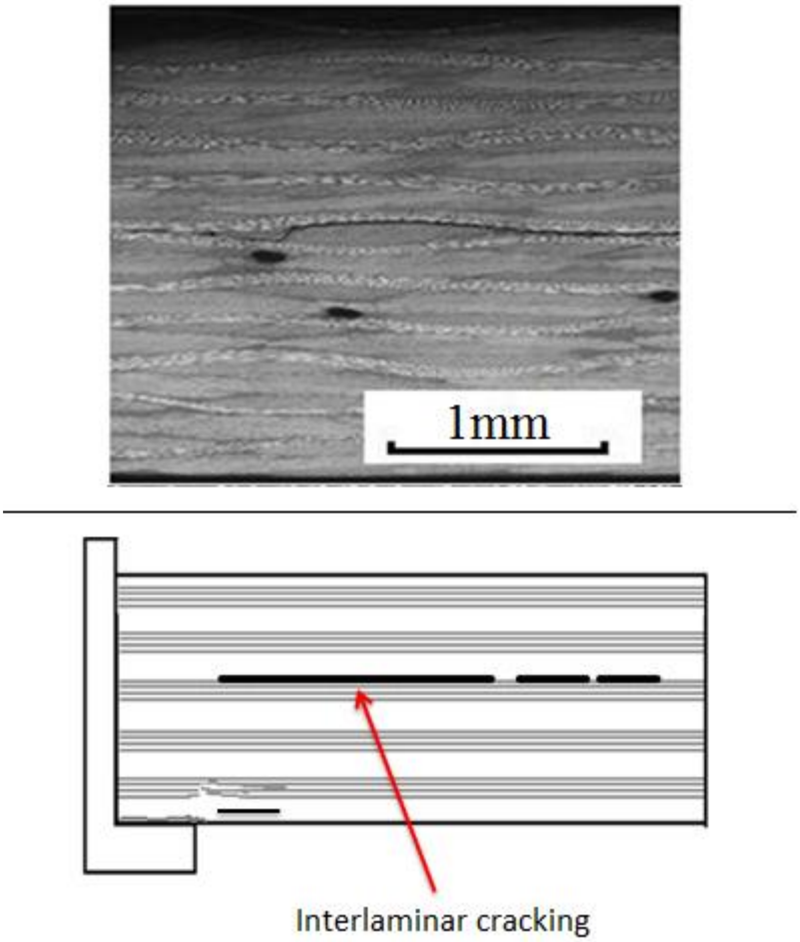

Figure 4.25: (Top) Micrograph of specimens (P0.19-24LT) unloaded right after the initial failure load (point B in Figure 4.22). (Bottom) A schematic description of the damage at point B

The image of a specimen unloaded instantaneously after maximum load drop (point C) in Figure 4.26 showed a complete through thickness damage. A conical damage zone was identified at this point. The intralaminar crack across thickness was initiated at the resin rich region near the fastener head outer edge. When the crack was impeded from propagating through the thickness by on-axis plies, another appeared on the opposite side of the ply. The crack reoriented at interfaces between plies of different orientation and grew along this fibre direction interface and as a result, created a delamination type failure mode. This through thickness and in-plane cracking network created a “staircase” appearance of fractures as mentioned in the literature [2]. In addition, a number of inter- and intralaminar cracks appeared along the edge of the fastener hole. Numerical analysis showed a similar maximum interlaminar shear stress network (Figure 4.27). The interlaminar shear stress governed the growth of delamination along the interface between on and off-axis. The intralaminar cracking was governed by the combination effect of fibre direction stresses σ_{11}, and interlaminar shear stress τ_{13}.

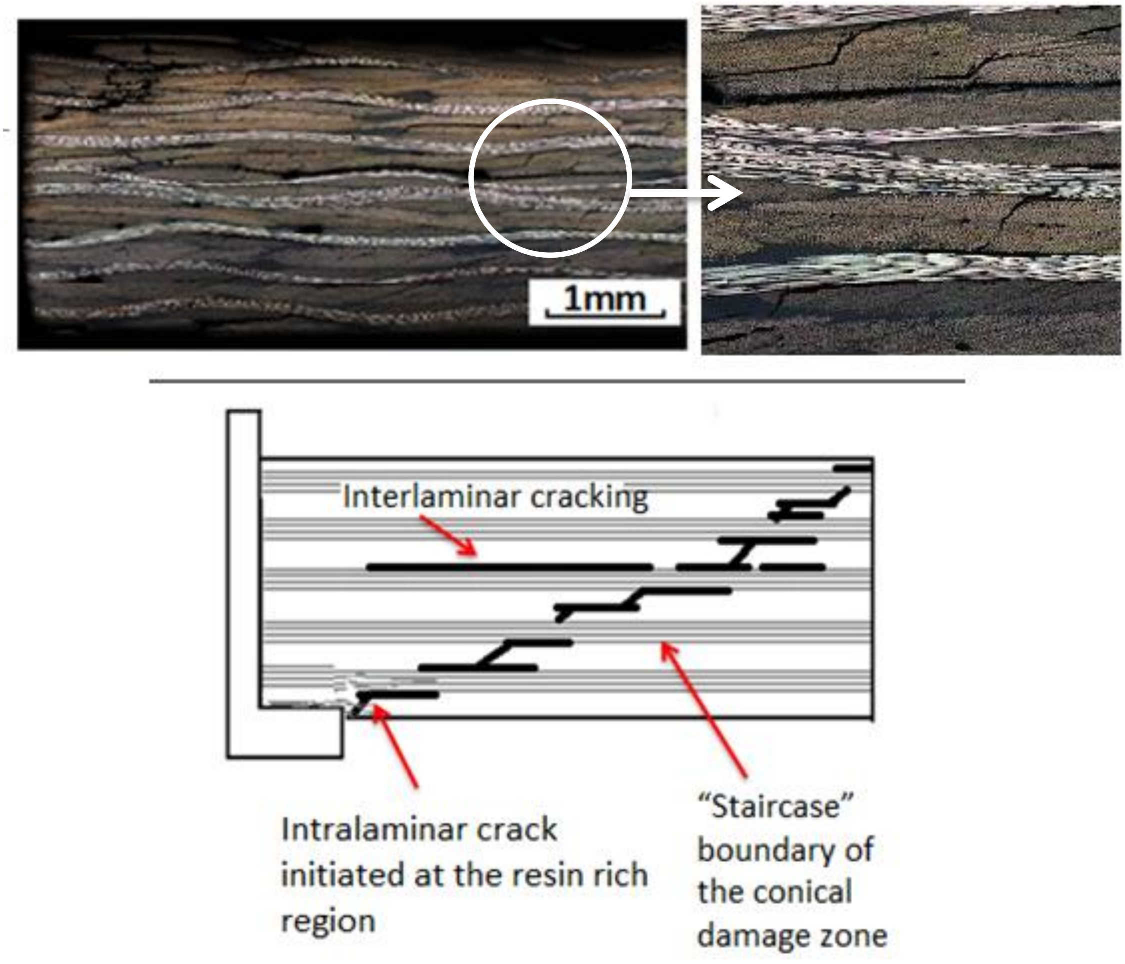
1mm
Interlaminar cracking
Intralaminar crack initiated at the resin rich region
“Staircase” boundary of the conical damage zone

Figure 4.26: (Top) Micrograph of specimen (P0.3-16LT) unloaded after maximum failure load (point C in Figure 4.23). (Bottom) A schematic description of the damage at point C

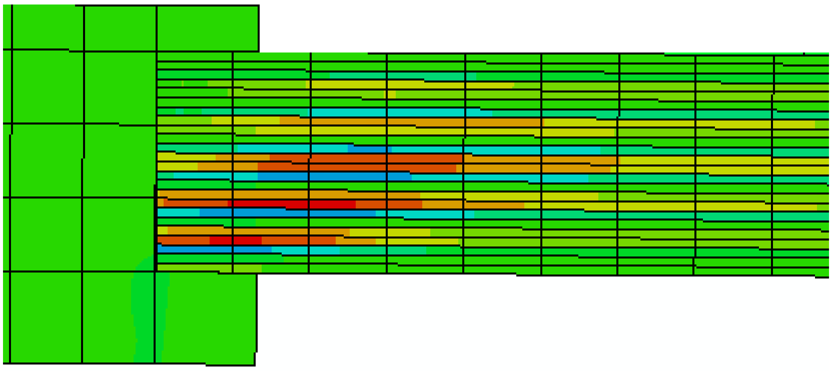

Figure 4.27: “Staircase” interlaminar shear stress distribution

At Point D, the fastener head was embedded in the specimen. The upper plies failed by the shear force as the fastener head penetrated into the surface, and plies beside the embedded zone were unveiled (Figure 4.28).

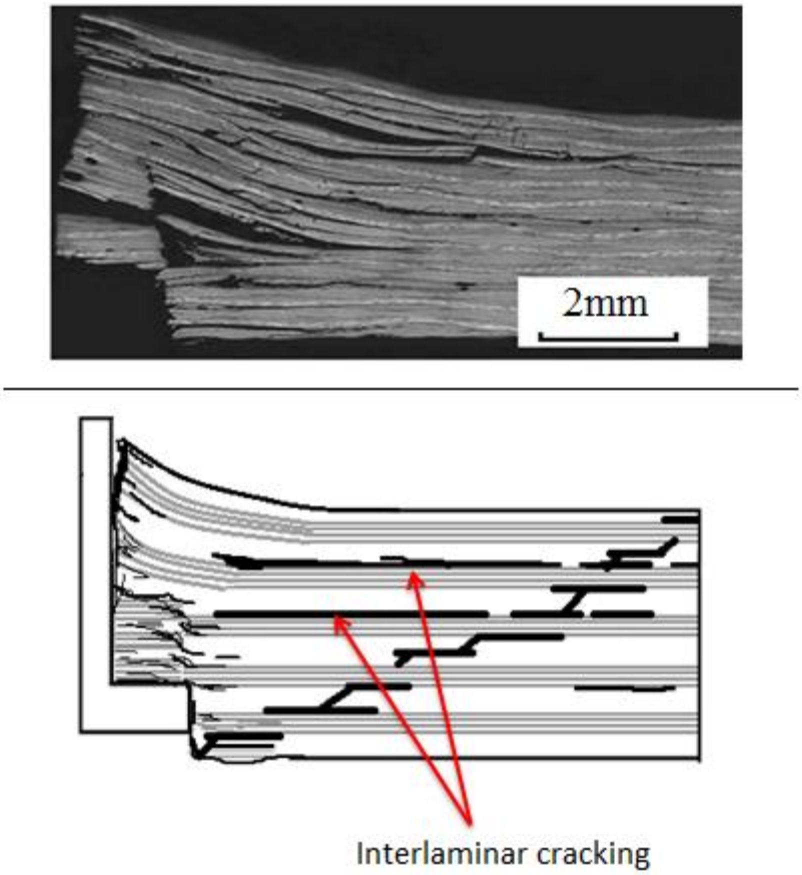

Figure 4.28: (Top) Micrograph of specimen (P0.3-24LT) unloaded from where load dropped 30% after maximum failure load (point D in Figure 22). (Bottom) A schematic description of the damage at point D

4.3.2 Numerical Analysis

During the experimental tests, a major delamination in the mid-plies was detected at failure load except for thin specimens. As mentioned in the numerical result in Section 4.2, compared to thick specimens, the interlaminar shear stress was smaller in thin specimens, but the fibre direction and transverse stresses were larger. In this section, maximum σ_{11}, σ_{22} and τ_{13} were extracted from the numerical models and compared with the corresponding experimentally determined strength of the laminar. Comparison results are presented in Figure 4.29, 4.30 and 4.31.

Figure 4.29 presents the comparison between the maximum fibre direction stresses from numerical models and the measured fibre direction strength. Specimens had fibre direction tension or compression failure when $t/D \leq 0.34$. Specimens had fibre direction compression failure only when $0.34 < t/D \leq 0.67$.

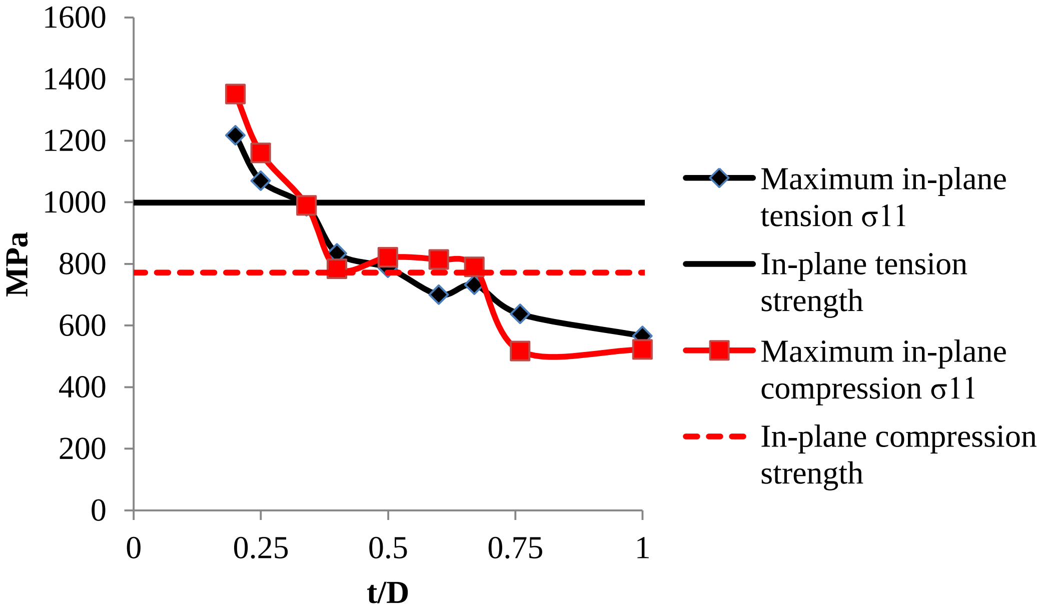

Figure 4.29: Comparison between the maximum fibre direction stresses from the numerical models and the corresponding measured specimen strength

Figure 4.30 presents the comparison between the maximum transverse stresses of numerical models and the measured transverse strength. The result indicates that specimens with $t/D \leq 0.5$ failed due to either transverse tension or compression. Specimens with *t/D* ranged from 0.5 to 0.67 failed due to tension only (Figure 4.30).

Figure 4.31 presents the comparison between the maximum interlaminar shear stresses of numerical models and the measured short beam shear strength. The result indicates that the specimens failed due to interlaminar shear stress for specimens with $t/D \geq 0.67$.

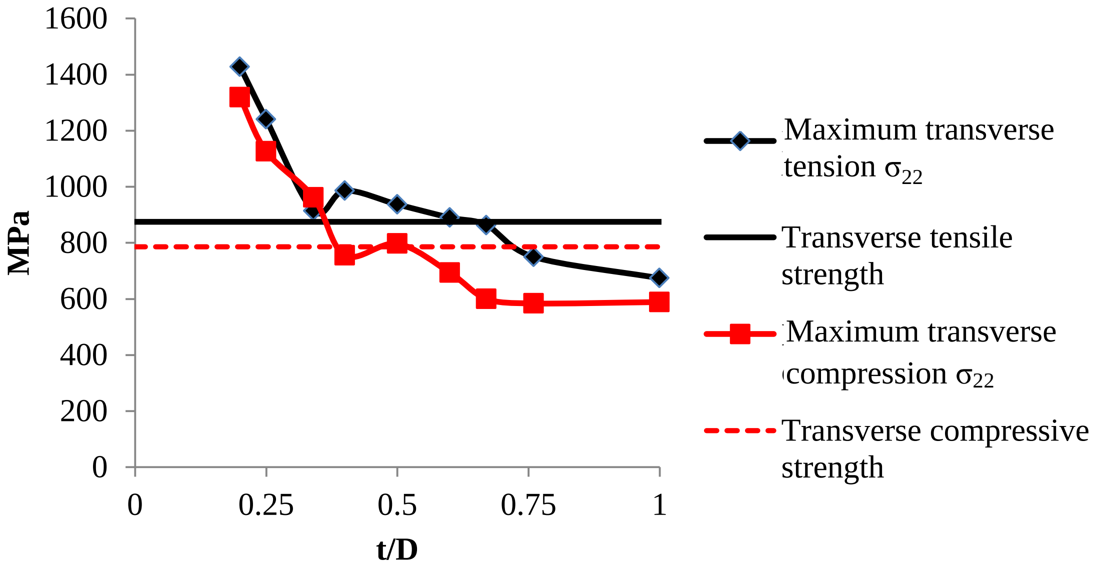

Figure 4.30: Comparison between the maximum transverse stresses from numerical models and the measured specimen strength

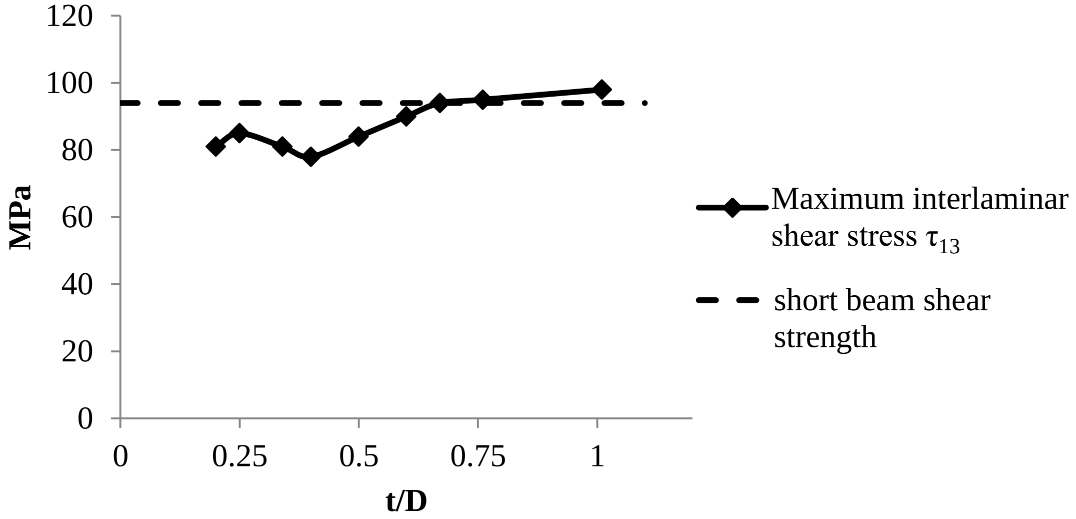

Figure 4.31: Comparison between the maximum interlaminar shear stresses of numerical models and the measured specimen strength

Based on the comparison results, the *t/D* value could be divided into three domains. At failure load, specimens failed due to stresses σ_{11} and σ_{22} when *t/D* ranged from 0 to 0.34. Specimens failed due to fibre direction or transverse compression for $0.34 < t/D < 0.6$. Specimens failed due to interlaminar shear stresses only when *t/D* was larger than 0.6. At the domain of *t/D* value ranged from 0.34 to 0.6, all types of stresses σ_{11}, σ_{22} and τ_{13} were very close to or slightly above its corresponding experimentally determined strength. The failure mode transitioned from fibre direction or transverse fibre failure to delamination within this domain. This supported the finding from Section 4.1.1 load-displacement behaviour, where $t/D = 0.5$ was the transition point. The failure of the composite laminate joint could be initiated by either fibre direction/transverse compression or interlaminar shear stress. This finding explained the variability in the load-displacement behaviours for specimens with $t/D = 0.5$ (Section 4.1.1).

Results from this section indicate the failure mode for specimens with different *t/D* range.

The failure mode is compressive or tensile fibre failure for specimens with $t/D < 0.5$. The failure mode is delamination for specimens with $t/D > 0.5$. Since $t/D = 0.5$ is the transition point between these two failure modes, the failure mode of the specimens with $t/D = 0.5$ can be either one of the two failure modes. The semi-empirical equation for the composite laminate pull-through strength will predict the strength based on the failure mode. The following section analyzed the effectiveness of each joint characteristic factor in order to simplify the prediction.

4.4 EVALUATION OF THE FACTORS INFLUENCING LAMINATE PULL-THROUGH STRENGTH

Testing results showed that both the pull-through failure load and maximum load were sensitive to the laminate thickness but not to the fastener shank diameter (Figure 4.32 and Figure 4.33). Two reasons can explain this trend. First, according to the ASTM standard, the fixture clearance hole corresponding to a 5/16” shank diameter fastener was larger than the for the 3/16” and 1/4” fasteners. Additional testing indicated that when the same fixture configuration was used for specimen series with increased fastener shank diameter, the pull-through failure load increased slightly while the corresponding displacement at failure decreased. Second, although the diameter of the fastener increased, the difference between the fastener head diameter and the shank diameter remained the same. As mentioned previously, the damage of the cross-section was axi-symmetric. In the axi-symmetric plane, the length of the contact edge between the fastener head and the laminate remained the same. As a result, even though the total actual contact area between the fastener head and the laminate increased, the net effect of fastener head diameter was not significant.

There was no clear evidence that the clamping torque influenced the specimen failure force (Figure 4.34 and Figure 4.35). An increase in fastener clamping torque increases the bearing strength by restrain delamination on the loaded side of the hole. However, the clamping torque does not affect the stress components responsible to the failure modes; the effect of clamping torque level on fastener pull-through strength was considered to be negligible.

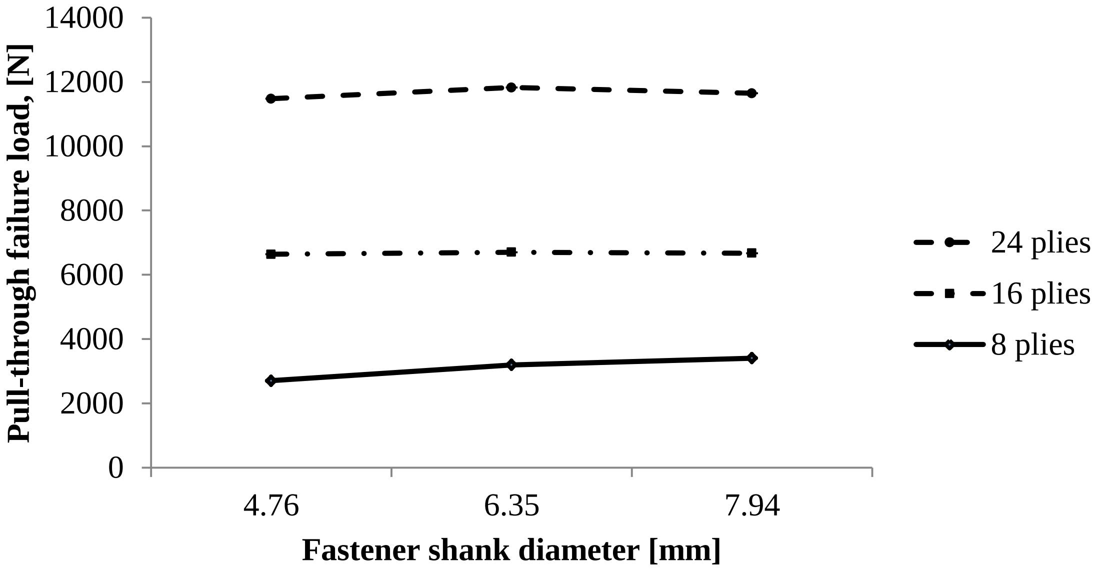

Figure 4.32: Effect of specimen thickness and fastener shank diameter on pull-through failure load

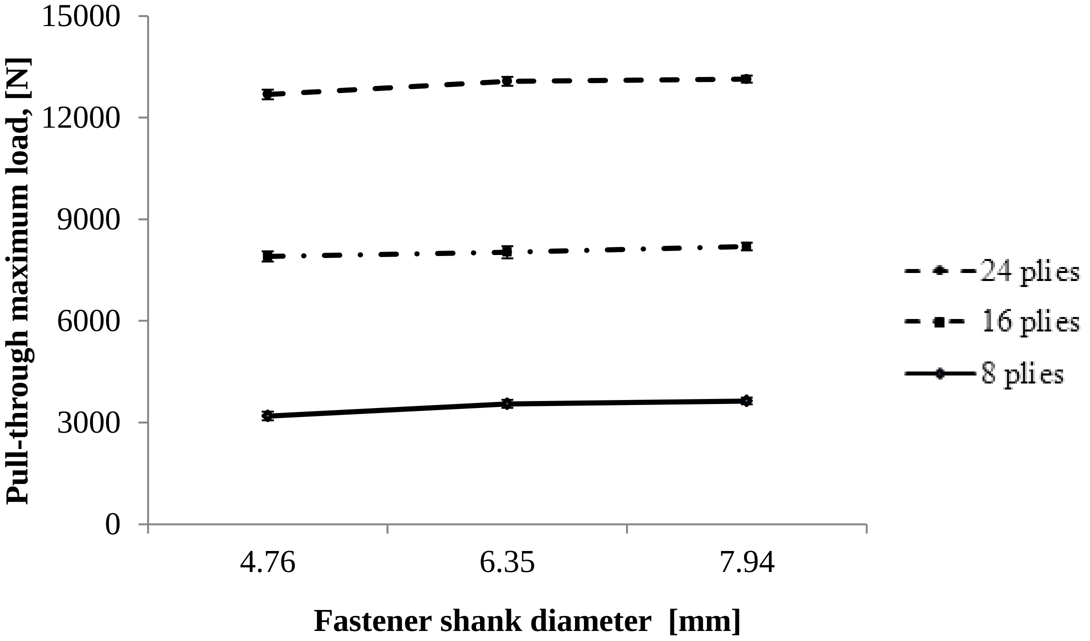

Figure 4.33: Effect of specimen thickness and fastener shank diameter on pull-through maximum load

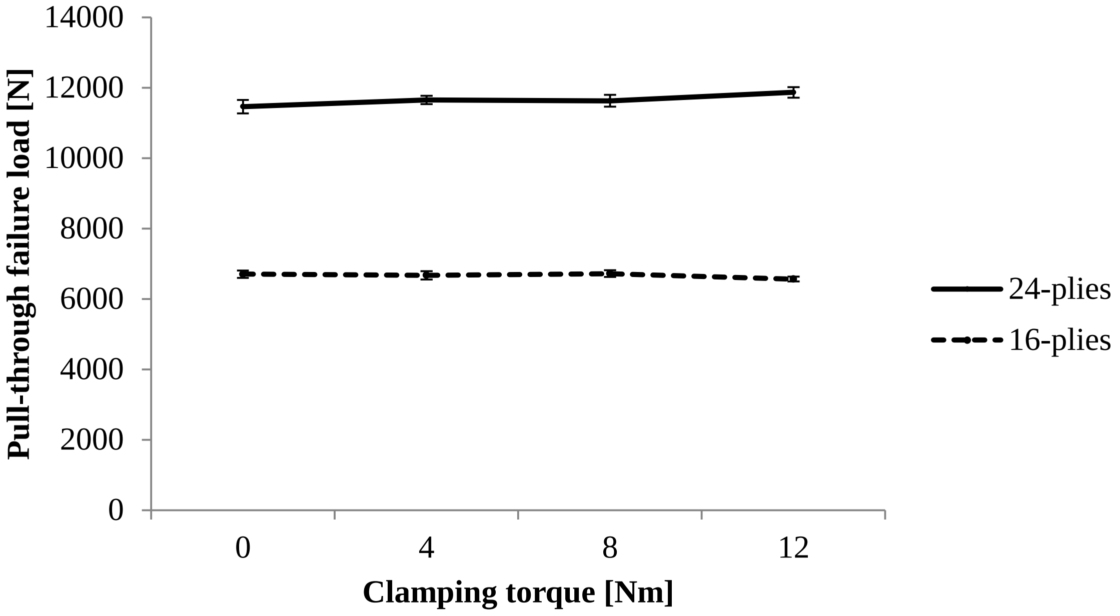

Figure 4.34: Effect of fastener clamping torque on pull-through failure load

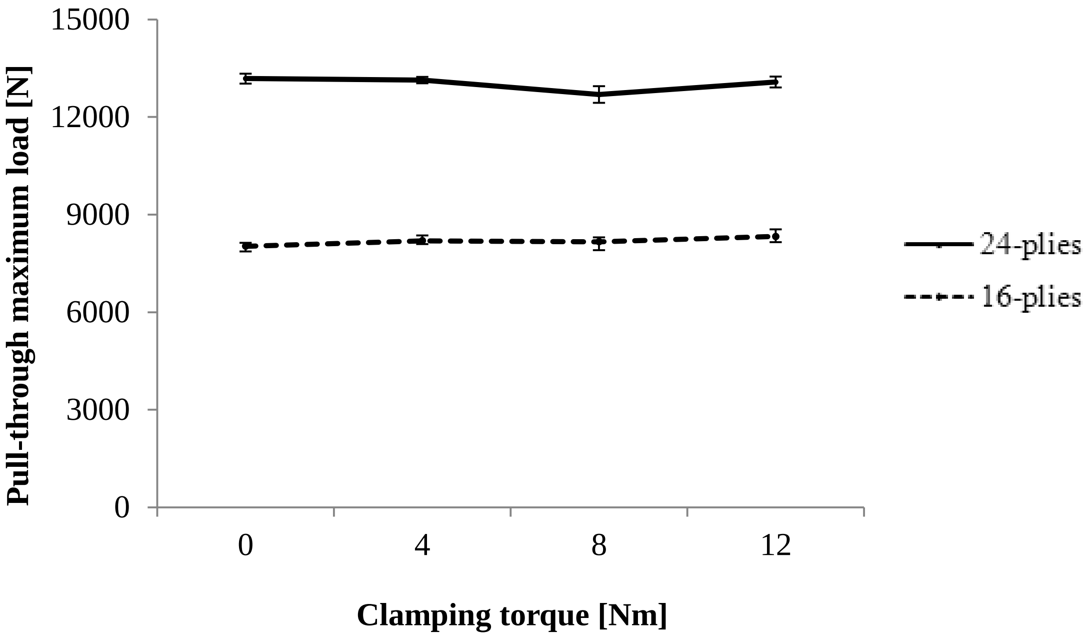

Figure 4.35: Effect of fastener clamping torque on pull-through maximum load

4.5 SEMI-EMPIRICAL EQUATION OF FASTENER PULL-THROUGH STRENGTH

Measuring fastener pull-through resistance requires a large number of tests since no robust predictive tools are available. Therefore, a semi-empirical equation for predicting fastener pull-through load was developed.

Various failure modes were observed for different range of t/D. The semi-empirical equation had the following assumptions:

- Failure load influenced by laminate thickness and fastener shank diameter only;
- Failure due to tension or compression when $t/D < 0.5$;
- Failure due to interlaminar shear stress when $t/D > 0.5$;
- Failure mode is either tension & compression failure or delamination, or combination of the two at $t/D = 0.5$.

4.5.1 Failure load prediction for t/D > 0.5

The shear stress in the cross section adjacent to the fastener head was parabolically distributed. Moreover, the first major delamination always appeared in the interfaces between on and off axis in the mid-plies. As a result, the maximum shear stress was calculated under the assumption of that the stress is uniform along the tangential direction at each ply (Figure 4.36).

Figure 4.36 shows that two sections are separated by a distance δx and the shear forces are F and F+δF while the bending moments are M and M+δM. f and f+δf are the normal stresses on an element of Area δA. There is a difference in longitudinal forces equal to δf * δA and this summed over the area *A* must be in equilibrium with the transverse shear stress *τ* on the longitudinal plane of area z * δx.

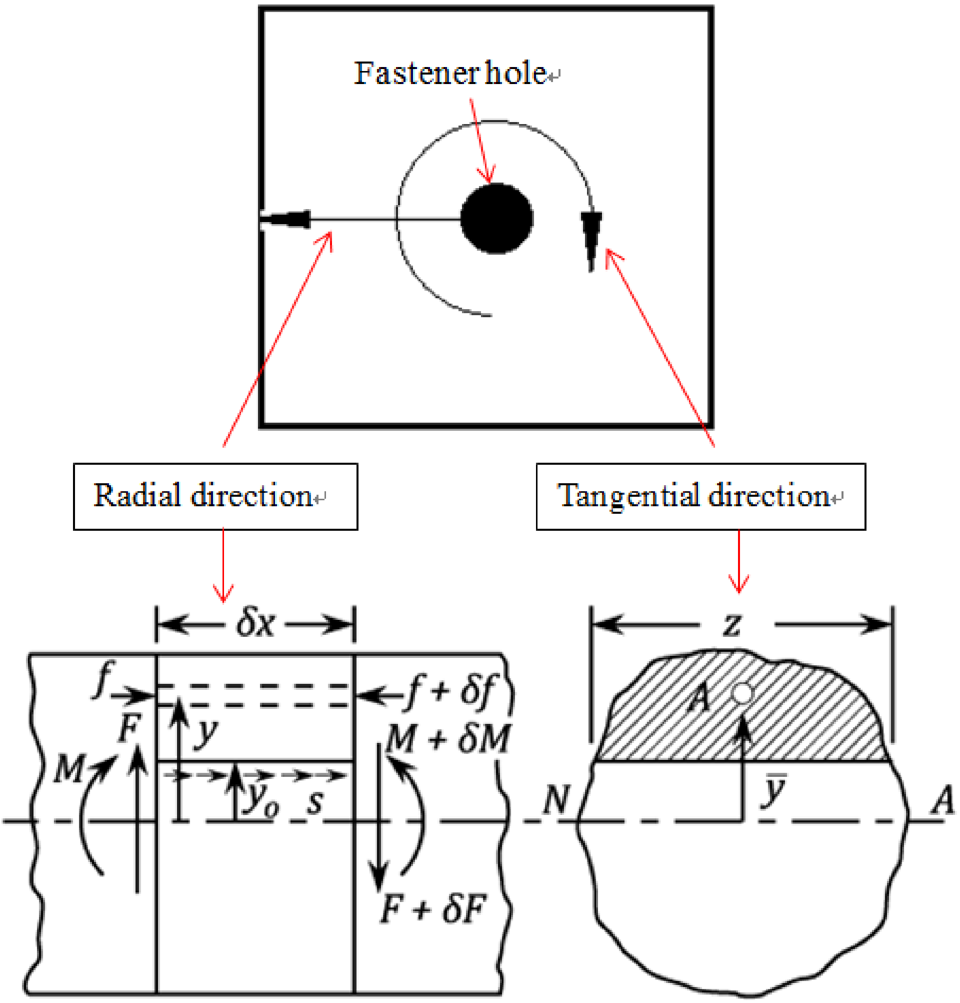
Fastener hole
Radial direction
Tangential direction
δx
f
F
y
M
y_0
s
f + δf
M + δM
F + δF
z
A
N
$\bar{y}$
A

Figure 4.36: Calculation of shear stress distribution in the laminate cross section [25]

Let:

- "τ" be the shear stress at a distance "y_0" from the Neutral Axis.
- "z" be the width of the cross section at "y_0". In this case, "z"= 2*radius*PI.
- "$\bar{y}$" be the distance of the centroid of "A" from the Neutral Axis.
- "A" be the area which its centroid has a distance "$\bar{y}$" to the neutral axis.
- "P" be the failure force of fastener pull-through.

So, the shear stress at "$\bar{y}$" is:

$$\tau\, z\, \delta x = \int \delta f * \delta A \tag{4.1}$$

$$f = \frac{M\, y}{I} \tag{4.2}$$

$$f + \delta f = \frac{(M + \delta M)\, y}{I} \tag{4.3}$$

Substituting equation 4.2 and 4.3 into the equation 4.1:

$$\tau = \left(\frac{\delta M}{\delta x}\right)\left(\frac{A\,\bar{y}}{z\, I}\right) = F * \frac{A\,\bar{y}}{z\, I} \tag{4.4}$$

The cross section along the tangential direction at a radius can be treated as rectangular section. The momentum of inertia "I" is $\frac{b\,d^3}{12}$.

The maximum shear stress at the neutral axis of rectangular section and given by:

$$\tau = \frac{3\,F}{2\,b\,d} \tag{4.5}$$

For the pull-through specimens:

$$\tau_{max} = \frac{3\,P}{2\,Pi\,D_{fastener\ head}\,t}; \tag{4.6}$$

$$P = \frac{2\,Pi\,D_{fastener\ head}\,t\,\tau_{max}}{3} \tag{4.7}$$

where τ_{max} is the failure shear stress obtained from short beam test $\tau_{13max.}$ The equation was calibrated by experimental and numerical results. A function F in terms of "*t/D*" was defined. F $(\frac{t}{D})$ is the ratio of pull-through strengths from experimental results over numerical models (Figure 4.37).

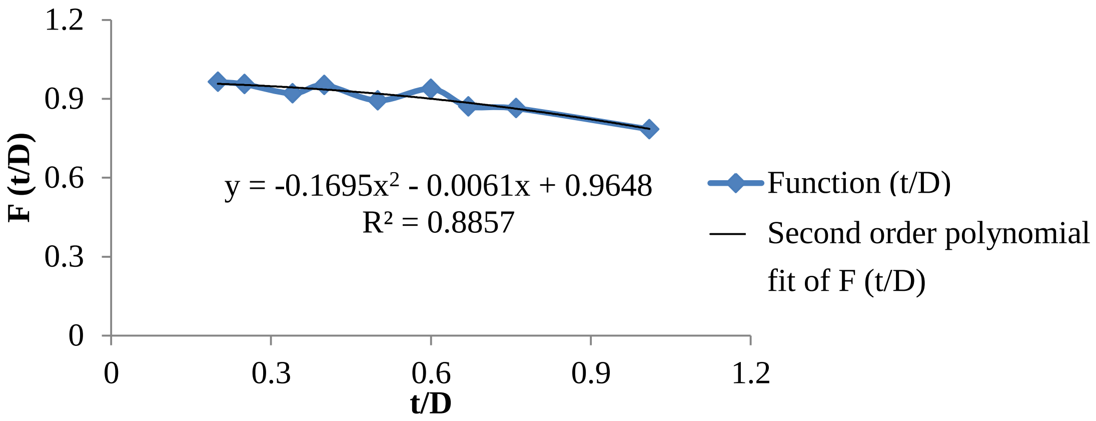

Figure 4.37: Second order polynomial fit of function "F (t/D)". F $(\frac{t}{D})$ is the ratio of pull-through strengths from experimental results over numerical models

The semi-empirical equation for laminate bolted by mechanical fastener under pull-through load is:

$$\text{Pull through failure load} = \frac{2\,Pi\,D_{fastener\ head}\,t\,\tau_{max}}{2.9 - 0.018\,\frac{t}{D} - 0.51\,\left(\frac{t}{D}\right)^{2}}$$

Where

Laminate thickness "t", fastener shank diameter "D" and fastener head diameter "$D_{fastener\ head}$" are in millimeter;

This Document Provided by the Abbott Aerospace Technical Library ABBOTTAEROSPACE.COM

Pull through failure load is in Newton;

Interlaminar shear strength “τ_{max}” is in MPa.

The comparison between the model prediction and the actual test data is shown in Figure 4.38. The maximum error was 1050 (N) for a specimen of “t/D = 0.6” and the average error was 3%.

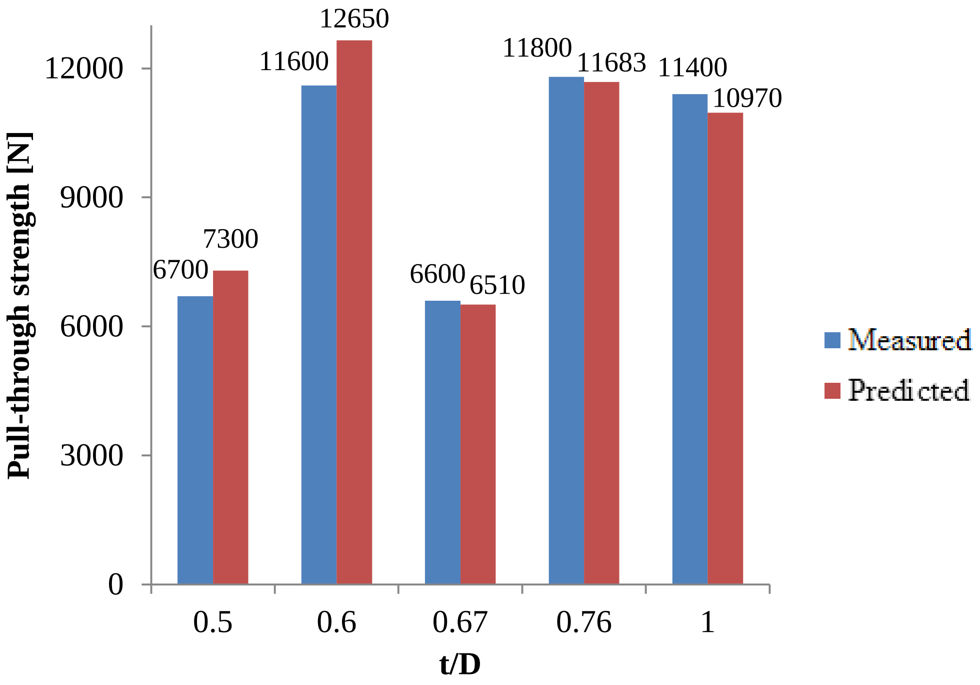

Figure 4.38: Comparison between the pull-through failure load semi-empirical model prediction and the experimental data

4.5.2 Failure Load Prediction of Specimens with “t/D” = 0.5

The failure mode at *t/D = 0.5* was complicated. Both maximum interlaminar shear stress and maximum flexure stresses were exceeded the corresponding failure strength. As discussed in Section 4.1.1, the failure mode could either fibre failure or delamination. The load-displacement curves could be either similar to $t/D > 0.5$ or $t/D < 0.5$.

Using semi-empirical equation to predict the failure load at the failure mode transition point is unreliable under this circumstance. Researchers need to be aware of that the failure mode is uncertain. For the failure load at t/D = 0.5, using average value from experimental testing and taking the standard deviation into consideration are recommended.

4.5.3 Failure Load Prediction of Specimens with t/D < 0.5

The failure mode analysis showed that the failure mode was compressive or tensile fibre failure for specimens with $t/D < 0.5$. However, the causes of this failure mode and prediction of the pull-through strength are complicated. Similar to the bulging of the pressurized fuselage surface caused by biaxial or internal pressure loads, a non-linear out-of-plane deformation on the specimen laminate surface was resulted from the fastener pull-through load. This deformation induced both flexure and membrane stresses (Figure 4.39). Due to relatively large deformation of the laminate surface for specimens with $t/D < 0.5$, the bulging effect needs to be considered when predicting the pull-through strength. Both flexure and membrane analysis need to be performed. The semi-empirical equation for specimens with $t/D < 0.5$ remains one of the future works.

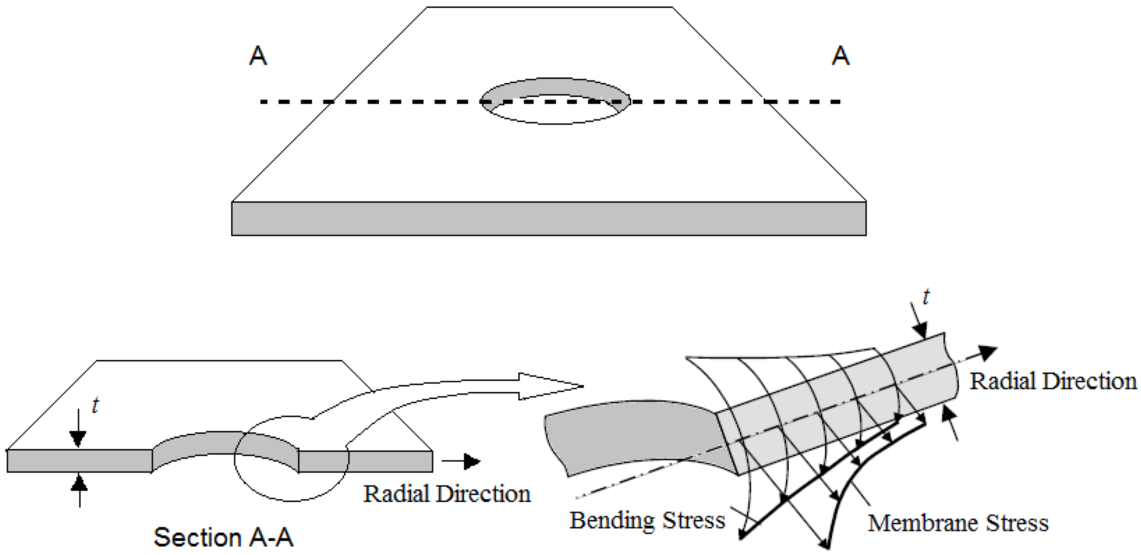
A
A
t
Radial Direction
Section A-A
t
Radial Direction
Bending Stress
Membrane Stress

Figure 4.39: Stresses induced by bulging effect near the fastener hole boundary [35]

4.6 SUMMARY

In this chapter, both experimental and numerical simulation results of the fastener pull-through failure of bolted composite joint were presented and discussed. A new parameter of the ratio between laminate thickness and fastener shank diameter t/D was introduced. Based on t/D value, the load-displacement behaviour of the specimens was categorized in three types (Type I: $t/D < 0.5$; Type II: $t/D > 0.5$; Type III: $t/D = 0.5$). Visual inspection of the failed specimen and numerical models showed that the failure mode for specimens with Type I load-displacement behaviour was the in-plane tensile fibre failure and/or compressive fibre failure; the failure mode for specimens with Type II load-displacement behaviour was a delamination type failure; and the failure mode for specimens with Type III load-displacement behaviour was at the transition point between failure modes of Type I and Type II. Further analysis indicated that the primary factor affecting pull-through strength was the laminate thickness, whereas the effect of fastener shank diameter and clamping torque were limited. Based on these findings, a semi-empirical equation for predicting the fastener pull-through failure strength was developed for specimens with Type II load-displacement behaviour. The average error was 3%.

Chapter 5

Conclusions and Future Work

5.1 CONCLUSIONS

In this thesis, the effect of laminate thickness, fastener size, fastener head geometry and clamping torque on pull-through failure load of a carbon fibre epoxy out-of-autoclave plain weave fabric laminate was investigated. A comprehensive analysis for the failure mechanisms was conducted and a semi-empirical equation was derived to predict the pull-through failure load for thick specimens as a function of the laminate thickness and fastener diameter. A new parameter "*t/D*" was introduced, which was the indicator for load-displacement behaviour and failure mode. Figure 5.1 concludes the findings in terms of "*t/D*" range.

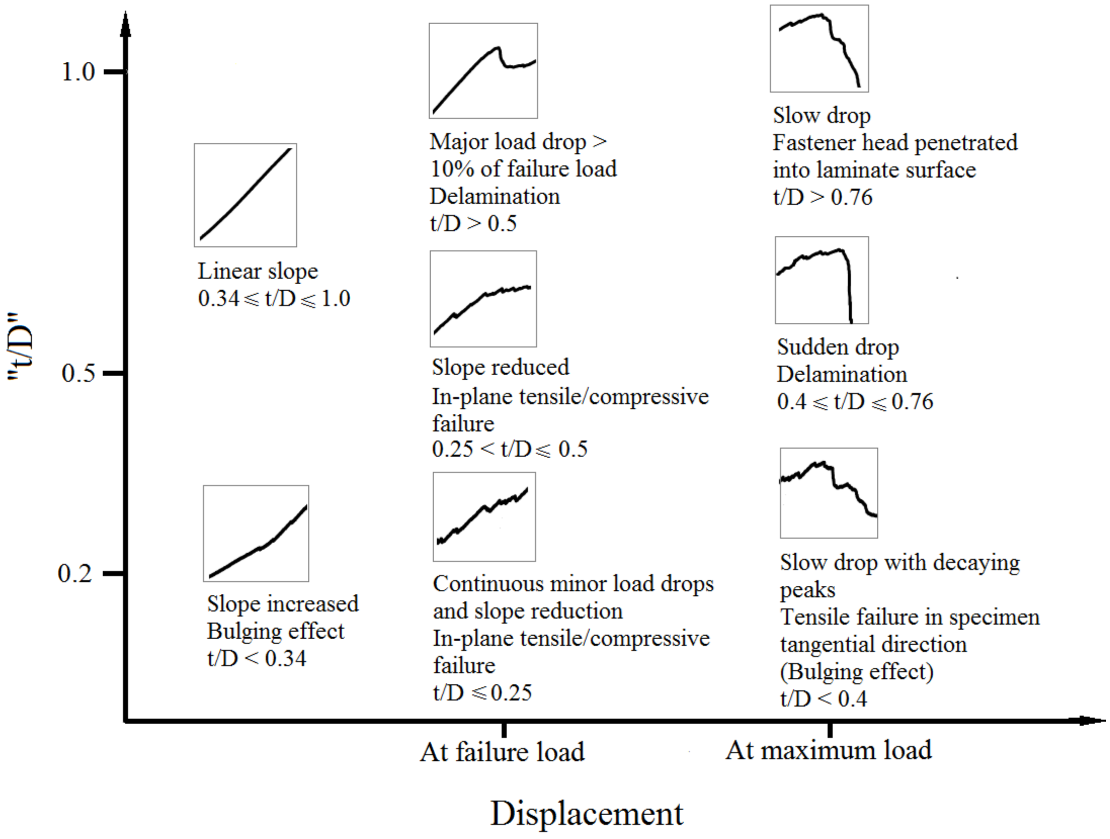
1.0
0.5
0.2
"t/D"
Major load drop > 10% of failure load
Delamination
t/D > 0.5
Slow drop
Fastener head penetrated into laminate surface
t/D > 0.76
Linear slope
0.34 ≤ t/D ≤ 1.0
Slope reduced
In-plane tensile/compressive failure
0.25 < t/D ≤ 0.5
Sudden drop
Delamination
0.4 ≤ t/D ≤ 0.76
Slope increased
Bulging effect
t/D < 0.34
Continuous minor load drops and slope reduction
In-plane tensile/compressive failure
t/D ≤ 0.25
Slow drop with decaying peaks
Tensile failure in specimen tangential direction
(Bulging effect)
t/D < 0.4
At failure load
At maximum load
Displacement

Figure 5.1: Summary of load-displacement behaviours and failure modes depend on *t/D*

The following conclusion can be drawn from this work for protruding fasteners used with out-of-autoclave fabric laminates:

- The pull-through failure load is more sensitive to laminate thickness
- The fastener size has a limited effect on the pull-through failure load
- The effect of clamping torque on pull-through failure load is not significant
- The magnitude of the load drop after failure load depends on the ratio of laminate thickness to fastener shank diameter “t/D”.

When “t/D” > 0.5

- Interlaminar and intralaminar delamination is the main failure mode.
- A major delamination is formed in the mid plies after failure load.
- The shear stress is the main cause of the delamination.

5.2 RECOMMANDATIONS FOR FUTURE WORK

Based on the results of this study, the following guidance and suggestions are established. It is the hope that these suggestions will provide insights and assist the researchers on future tests.

1. Interlaminar shear stress distributions are the key on this topic.
2. “t/D” is the most important parameter when examining the bolted joint.
3. Failure mode and load-displacement behaviour are not stable at “t/D = 0.5. Therefore, most tests are needed for a robust result.
4. Clamping torque has very limited effect. When focusing on the pull-through load,

its effect can be negligible. However, it is unclear if clamping torque will affect pull-through strength when combining with other parameters.

5. Testing fixture design is critical. Experience from this work suggests that designing two-piece loading yoke and connects via ball joint. The purpose is to align the fastener and testing machine cross head. Second, the aerospace grade fasteners require a special torque wrench. The accessibility of such tool for installing specimens needs to be considered while designing the fixture.
6. Do not use washer under fastener head as it will result inaccurate load-displacement behaviours as well as the false failure mode.

As an extension to this work, several issues are worth to be investigated in the future.

1. Confirm the ultimate failure mode for specimens of “t/D < 0.5” by both flexure and membrane analysis.
2. Develop a semi-empirical equation for “t/D < 0.5”
3. Perform a progressive failure analysis using numerical method and compare with the results from microscopic inspections.
4. Investigate the 100˚ tension and 130˚ countersunk fastener following the same methodology presented in this work.
5. Investigate the pull-through behaviours using tape prepregs and different layup patterns.

Reference

1. ASTM D 7332/D 7332M – 07. 2007. “Standard Test Method for Measuring the Fastener Pull-Through Resistance of a Fiber-Reinforced Polymer Matrix Composite”

2. Banbury, A. and Kelly, D.W. 1999. “A study of fastener pull-through failure of composite laminates,” Composite Structures., 45 (1999) 241-254.

3. Waters, Jr W.A and Williams, J.G. 1985. “Failure Mechanisms of Laminates Transversely Loaded by Bolt Push-Through,” NASA Technical Memorandum 87603.

4. Chen, W.H and Lee, S.S. 1995. “Numerical and Experimental Failure Analysis of Composite Laminate with Bolted Joints Under Bending Load,” Journal of Composite Materials., 29(2): 15-36.

5. Rubin, A.M. 1991. “Evaluation of Multilevel Delaminations Induced During Aircraft Composite Structures Assembly,” presented at 8th International Conference on Composite Materials, July 1991.

6. Kelly, G. and Hallstrom, S. 2005. “Strength and Failure Mechanisms of Composite Laminates Subject to Localized Transverse Loading,” Composite Structures., 69 (2005) 301-314. conical

7. Elder, D.J., Verdaasdonk, A.H. and Thomson, R.S. 2008. “Fastener Pull-Through in A Carbon Fibre Epoxy Composite Joint,” Composite Structures., 86 (2008) 291-298.

8. Sihn, S., Iarve, E.V. and Roy, A.K. 2006. “Asymptotic Analysis of Laminated Composites with Countersunk Open- and Fastened-Holes,” Composite Science and Technology., 66 (2006) 2479-2490.

9. Cole, R.T., Bateh, E.J. and Potter, J. 1982. “Fasteners for Composite Structures,” Composites., July 1982.

10. Starikov, R. and Schon, J. 2001. “Quasi-static Behaviour of Composite Joints with Countersunk Composite and Metal Fasteners,” Composites., Part B 32 (2001) 401-411.

11. Plinger, D.W. 1996. “Bolted Joints in Composite Overview,” presented in AGARD conference, September 2-3, 1996.

12. Rose, D., Rother, M. and Schelling, H. 1987. “Typical Joints in A Wing Structure,” agard conference proceedings No. 427, April 27-29, 1987.

13. Madan RC.1991. “Influence of low-velocity impact on composite structures,” composite materials: Fatigue and fracture (Third Volume), ASTM STP 1110, O'Brien TK, editor. Philadelphia: American society for testing and materials 1991:457-75.

14. Williams JG, Anderson MS, Rhodes MD, Stavrnes Jr JH, Stroud WJ. 1980. “Recent developments in the design, testing and impact damage tolerence of stiffened composite panels, fibrous composites in structural design,” Proceedings of Fourth Conference on Fibrous Composites in Structural Design. New York: Plenum press 1980; 259-91.

16. Konish HJ, Swellow JL, Cruse TA. 1972. “Experimental investigation of fracture in an advanced fibre composite,” Journal of Composite Materials., 6(1972) 14-24.

17. Abaqus 6.10 Documentation, Dassault Systèmes, 2010

18. Micheal C, Y. Niu, Composite airframe structures: Practical design information and data, Second Edition, Hong Kong, China. Conmilit Press, 1992.

19. Banbury, A. and Kelly, D.W. 1999. “A study of fastener pull-through failure of composite laminates, Part 2: failure prediction” Composite Structures., 45 (1999) 255-270.

20. A. Nanda Kishore, N. Siva Prasad, 2012. “An Experimental Study of Flat-Joggle-Flat Bonded Joints in Composite Laminates,” International Journal of Adhesion and Adhesives, 35 (2012) 55-58

21. Paton, R., Hou, M. and Beehag, A. “A Breakthrough in the Assembly of Aircraft Composite Structures,” presented in 25th International Congress of the Aeronautical Science, 3-8 September 2006.

22. McCarthy, M. “Bolted Joints in Composite Aircraft Structures,” COMPOSIT Workshop on Joining and Assembling Technologies, 11 April 2004, Centro Ricerche Fiat, Turin, Italy.

23. Vasiliev, V. and Morozov, E. Mechanics and Analysis of Composite Materials, Elsevier, New York, 2001.

24. Tarnopol, S. and Iu, M. Static Test Methods for Composites, Van Nostrand Reinhold Co, New York, 1985.

25. Ashbee, K. Fundamental Principles of Fiber Reinforced Composites, Lancaster, Technomic Pub. Co, 1989.

26. Raton, B. Finite Element Modelling of Composite Materials and Strucutures, CRC Press, Cambridge, England, 2000.

27. Gibson, R. Principles of Composite Material Mechanics, New York, McGraw-Hill, 1994.

28. Montgomery, D. Design and Analysis of Experiments, Second Edition, New York, John Wiley, 2001.

29. Boll, D., Bascom, W. and Weidner, J. 1986. “A Microscopy Study of Impact Damage of Epoxy-Matrix Carbon-Fibre Composite,” Journal of Materials Science., 21 (1986) 2667-2677

30. Lawlor, V., Stanley, W. and McCarthy, M. “Characterisation of Damage Development in Single-shear Bolted Composite Joints,” Journal of Plastics, Rubber and Composites, 31 (1996) 126-133

31. Thoppul, S., Finegan, J. and Gibson, R., 2009. “Mechanics of Mechanically Fastened Joints in Polymer-Matrix Composite Structures – A review,” Composites Science and Technology, 69 (2009) 301-329

32. Chen, W., Shiaw, S. and Yeh, J. 1994. “Three-dimentional Contact Stress Analysis of a Composite Laminate with Bolted Joint,” Composite Structures., 30 (1995) 287-297

33. Chang, F., Scott, R. and Springer, G. 1984. “Failure of Composite Laminates Containing Pin Loaded Holes - Method of Solution”, Journal of Composite Materials., 18(1984) 255-278

34. P. Pedersen, Elasticity – Anisotropy – Laminates 2nd ed, Technical University of Denmark. Dept. of Solid Mechanics, FAM., DTU, 1998

35. Federal Aviation Administration. Bulging Factor Solutions for Cracks in Longitudinal Lap Joints of Pressurized Aircraft Fuselages., Springfield, 2004. pp.1-3, 2010

36. ASTM D 5687/D 5687M – 95. 2002. “Standard Guide for Preparation of Flat Composite Panels with Processing Guidelines for Specimen Preparation”

37. Park, C. and Grandt, A., 2007, “Effect of Load Transfer on the Cracking Behaviour at a Countersunk Fastener Hole,” International Journal of Fatigue., 29 (2007) 146-157

38. Caprino, G., Langella, A. and Lopresto, V., 2002, “Elastic Behaviour of Circular Composite Plates Transversely Loaded at the Centre,” Composite., Part A 33 (2002) 1191-1197

39. Running, D., Ligon, J. and Miskioglu, I., 1999, “Fastener Design for Transversely Loaded Composite Plates,” Journal of Composite Materials., 33 (1999) 928-940

40. Chang, F.K. and Chang, K.Y., 1987, “Post-Failure Analysis of Bolted Composite Joints in Tension or Shear-Out Mode Failure,” Journal of Composites Materials., 21 (1987) 809-833

41. Caprino, G., Langella, A. and Lopresto, V., 2003, "Prediction of the First Failure Energy of Circular Carbon Fibre Reinforced Plastic Plates Loaded at the Centre," Composite., Part A 34 (2003) 349-357

42. Dano, M-L., Gendron, G. and Picard, A., 2000, "Stress and Failure Analysis of Mechanically Fastened Joints in Composite Laminates," Composite Structures., 50 (2000) 287-296

43. Aslan, Z., Karakuzu, R. and Okutan, B., 2003, "The Response of Laminated Composite Plates Under Low-Velocity Impact Loading," Composite Structures., 59 (2003) 119-127

44. Ireman, T., 1998, "Three-Dimensional Stress Analysis of Bolted Single-Lap Composite Joints," Composite Structures 43 (1998) 195-216

45. Chaudhuri, R. and Seide, P., 2010, "Interlaminar Shear Stresses Around an Internal Part Through Hole in a Stretched Laminated Composite Plate," Composite Structures., 92 (2010) 835-843

46. Sen, F., Sayman, O. and Ozcan, R., 2010, "Failure Response of Single Bolted Composite Joints Under Various Preload," Indian Journal of Engineering & Material Science., 17 (2010) 39-48

47. Kermanidis, T., Labeas, G. and Tserpes. K., 2000, "Finite Element Modeling of Damage Accumulation in Bolted Composite Joints under Incremental Tensile Loading," European Congress on Computational Methods in Applied Sciences and Engineering., Barcelon, 11-14 September, 2000

48. Kumar, S., Sivashanker, S. and Bag, A., 2005, "Failure of Aerospace Composite Scarf-joints Subjected to Uniaxial Compression," Materials Science and Engineering., A 412 (2005) 117-122

49. Lowson, M. V., "The future aerospace use of advanced Materials," In Proc. Royal Aeronautical Sot. ConJ Aerospace Applications of Advanced Materials, March 1989.

50. Waszczack, J. and Cruse, T., "Failure Mode and strength predictions of anisotropic bolt bearing specimens", Journal of Composite Materials., 5 (1971) 421-433.

51. De Jong, T., "Stress around pin-loaded holes in elastically orthotropic or isotropic plates." Journal of Composite Materials., 11 (1977) 313-325.

52. Soni, S. R., "Failure analyses of composite laminates with a fastener hole," Journal of Composite Materials., ASTM STP749, (1981) 145-64.

53. Ramkumar, R., "Bolted joint design," Test methods and design allowables for fibrous composites. ASTM STP734 (1981) 376-95.

54. Wong, C. and Matthews, F., "A finite element analysis of single and two hole bolted joints in fibre reinforced plastic," Journal of Composite Materials.,15 (1981) 481-91.

55. Erikson, L., "Contact stresses in bolted joints of composite laminates," Composite Structures., 6 (1986) 57-75.

56. Konish, H., Swellow, J. and Cruse, T., "Experimental investigation of fracture in an advanced fibre composite," Journal of Composite Materials., 6 (1972) 114-124.

57. Boll, D., Bascom, W. and Weidner, J., "A microscopy study of impact damage of epoxy-matrix carbon-fibre composites," Journal of Materials Science., 21 (1986) 2667-2677.

58. Clark, G., "Modelling of impact damage in composite laminates," Composite., 20 (1989) 209-214.

59. Ye, L., "The role of matrix resin in delamination onset and growth in composites," Composite Science Technology., 33 (1988) 257–277

60. Elber, W., "Failure mechanics in low-velocity impacts on thin composite plates," NASA technical paper 2152 (1983).